The microstructure-processing-property relationships in an Al matrix composite system reinforced by Al-Cu-Fe alloy particles

by

Fei Tang

A dissertation submitted to the graduate faculty

in partial fulfillment of the requirements for the degree of

DOCTOR OF PHILOSOPHY

Major: Materials Science and Engineering

Program of Study Committee:
Iver E. Anderson, Major Professor
Bulent Biner, Co-major Professor
Scott Chumbley
Vinay Dayal
Alan Russell
Dan Sordelet

Iowa State University

Ames, Iowa

2004

Graduate College
Iowa State University

This is to certify that the doctoral dissertation of

Fei Tang

has met the dissertation requirements of Iowa State University

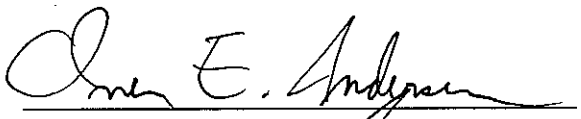

Major Professor

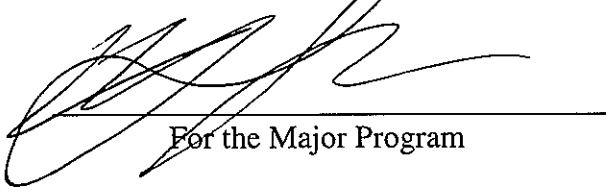

For the Major Program

TABLE OF CONTENTS

ABSTRACT

Metal matrix composites (MMC), especially Al matrix composites, received a lot of attention during many years of research because of their promise for the development of automotive and aerospace materials with improved properties and performance, such as lighter weight and better structural properties, improved thermal conductivity and wear resistance. In order to make the MMC materials more viable in various applications, current research efforts on the MMCs should continue to focus on two important aspects, including improving the properties of MMCs and finding more economical techniques to produce MMCs.

Solid state vacuum sintering was studied in tap densified Al powder and in hot quasi-isostatically forged samples composed of commercial inert gas atomized or high purity Al powder, generated by a gas atomization reaction synthesis (GARS) technique. The GARS process results in spherical Al powder with a far thinner surface oxide. The overall results indicated the enhanced ability of GARS-processed Al and Al alloy powders for solid state sintering, which may lead to simplification of current Al powder consolidation processing methods. Elemental Al-based composites reinforced with spherical Al-Cu-Fe alloy powders were produced by quasi-isostatic forging and vacuum hot pressing (VHP) consolidation methods. Microstructures and tensile properties of Al/Al-Cu-Fe composites were characterized. It was proved that spherical Al-Cu-Fe alloy powders can serve as an effective reinforcement particulate for elemental Al-based composites, because of their high hardness and a preferred type of matrix/reinforcement interfacial bonding, with reduced strain concentration around the particles. Ultimate tensile strength and yield strength of the composites were increased over the corresponding Al matrix values, far beyond typical observations. This remarkable strengthening was achieved without precipitation hardening and without severe strain hardening during consolidation because of the matrix choice

(elemental Al) and the "low shear" consolidation methods utilized. This reinforcement effectiveness is further evidenced by elastic modulus measurements of the composites that are very close to the upper bound predictions of the rule of mixtures. The load partitioning measurements by neutron diffraction showed that composite samples made from GARS powders present significantly higher load transfer efficiency than the composites made from commercially atomized powders. Also, the composite samples made from GARS powders show a higher strengthening effect and ductility than the samples made from commercial purity powders. The higher load transfer efficiency and higher strength and ductility may result from an enhanced inter-particle bonding strength, promoted by the "clean" interfaces between particles. Further analysis of the load sharing measurements and the calculated values of the mismatch of coefficient of thermal expansion (CTE) and the geometrically necessary dislocation (GND) effects suggest that these strengthening mechanisms can be combined to predict accurately the strength of the composites.

By neutron diffraction measurements, it also was found that the composites consolidated from Al and $Al_{63}Cu_{25}Fe_{12}$ quasicrystal alloy reinforcement powders have compressive residual stress in the Al matrix, contrary to the tensile residual stress in typical Al/SiC composites. The compressive stress state is promoted by several factors, including the volume expansion of the reinforcement particles caused by a solid-state diffusional phase transformation of the quasicrystal phase to a lower density crystalline ω phase and the stiffness mismatch between the matrix and reinforcement phases. This compressive residual stress persists in spite of a CTE mismatch factor that acts in opposition on cooling from the consolidation temperature. The composites made by the quasi-isostatic forging process exhibited higher tensile strengths and much higher compressive residual stresses than the composites made by the VHP process. Annealing experiments indicated that this strengthening was probably due to an enhanced dislocation density in the Al matrix of the forged samples.

GENERAL INTRODUCTION

Introduction

Modern composite material, which is a combination of two or more distinct material phases, is usually produced to achieve a particular balance of properties for a given range of applications. As a major type of composite material, metal matrix composite (MMC) material typically has a fiber or particulate phase that is stiffer and stronger than the continuous matrix phase. As early as the late 1970s, efforts were started on developing discontinuously reinforced MMC material, chiefly Al alloys, using SiC whisker reinforcements [1]. The principal motivation of these efforts was to significantly extend the structural efficiency of the Al alloys by achieving high specific modulus and specific strength. But the high cost of the whiskers and difficulty in avoiding whisker damage and health hazards during consolidation led to the concept of particulate reinforcements [2]. Particulate-reinforced MMC material provides essentially isotropic properties, with a balance of enhanced strength and stiffness, and reasonable ductility. Additional functional properties for which the MMC may be developed, including high thermal or electrical conductivity (or conversely electrical and/or thermal insulation), good wear resistance, controlled coefficient of thermal expansion (CTE), and/or environmental resistance. The balance of properties obtained in these composites typically can not be obtained in any related monolithic material.

The motivation for the development and application of the MMCs is not only for their improved properties and performance, such as lighter weight and better strength, but also from the pressures imposed by legislative, economic, or environmental concerns. For example, there are legislated financial penalties for failure to comply with corporate average

fuel economy requirements for lighter, more fuel-efficient automobiles [3]. Motivated by this concern, the Partnership for a New Generation of Vehicles (PNGV) was created in 1993 between the U.S. federal government and the U.S. Council for Automotive Research, which represents Chrysler Corporation, Ford Motor Corporation, and General Motors Corporation, and also involves federal agencies, national laboratories, universities, and suppliers. The goal of the program was to develop a vehicle with up to three times the fuel economy of conventional mid-sized sedans, while improving recyclability and maintaining comparable performance, utility, safety, and ownership cost standards. Achieving this goal will require significant improvements in powertrain efficiency and a weight reduction of up to 40 percent, which is about 590 kg for a conventional average six-seat sedan [3]. Therefore, it is obvious that extensive weight reduction and use of lightweight materials, such as MMC materials, is desired and necessary in automotive parts production.

Metal-matrix composites are currently in service using materials based on alloys of aluminum, titanium, iron, cobalt, copper, silver, and beryllium. By far the most widely produced MMCs are based on aluminum alloy matrices, and these are in current use for automotive and rail ground transportation, thermal management and electronic packaging, and aerospace and recreational applications [1, 3-5]. Usually MMCs are more expensive on a per-pound basis relative to the material displaced in applications, but an overall cost reduction often results when MMCs are put into service because of improved system performance. Moreover, novel or simplified processing methods are being developed for producing MMCs to reduce costs by eliminating processing steps [1, 6, 7]. Therefore, in order to make the MMC materials more viable in various applications, current research efforts on the MMCs should continue to focus on improving the properties of MMCs and on finding more economical techniques to produce MMCs.

In spite of at least three decades of research conducted on metal matrix composites, including mechanical properties, microstructural analysis, fracture behavior and matrix/reinforcement interface characterization, the complexities of processing these dissimilar materials systems has prevented realization of ultimate composite material design goals. In other words, there is still a major difficulty in obtaining optimum interaction between matrix and reinforcement and ensuring sufficient wetting or compatibility of the reinforcement elements without excessive chemical or mechanical degradation of their properties. The production cost of current MMCs, such as Al/SiC MMC, is still a strong barrier to realization of extensive applications. The research on developing affordable or cost-effective processing techniques similar to those usually carried out for unreinforced alloys is still much needed [1, 3-7]. In addition, basic understanding of strengthening mechanisms in MMCs is also need to be explored and refined for the purpose of the theoretical prediction and development of more advanced composite materials.

Research Objectives

The basic research goal focuses on developing understanding of pure Al metal matrix composite (MMC) design and synthesis, especially for particulate reinforcement by spherical Al-Cu-Fe quasicrystal (QXL) particles, as an ideal example of composite processing simplification. It will emphasize the correlation of the processing, microstructure and mechanical behavior of the model composites, and improved understanding of the effects of the size distribution of the reinforcements, the reinforcement/matrix interfacial behavior and the purity of powders. Analysis issues will include the internal residual stresses and processing techniques on the mechanical properties and strengthening mechanisms of an Al MMC material system.

Pure Al powders were chosen as the matrix material to avoid the complications of matrix heat treatment effects at this stage of the research on basic strengthening mechanisms and interface effects in an Al matrix composite. A powder metallurgy processing technique (solid state sintering) is proposed for producing the composites because it offers better microstructural control than a liquid phase route and employs lower temperatures that offer better control of interface kinetics. The approach also makes it possible to employ alloy compositions and microstructural refinements that are only available via rapidly solidified powders. In order to find a simplified and relatively low cost powder processing method for composites, the effects also were studied of metal powder surface chemistry, especially oxide layer thickness and purity, on the solid state sintering kinetics and on the microstructures and properties of the resulting composite materials.

Dissertation Organization

To support the positions in this introduction, there is an extensive review of research literature that is close related to the dissertation study topics. The subsequent chapters are arranged in such a way that five individual published or submitted research papers are each presented as a separate chapter. The first paper (chapter 2) presents results and discussion of metal powder surface chemistry effects on the solid state sintering kinetics, matrix/reinforcement particle interface bonding, and tensile properties of composites made by quasi-isostatic forging. The second paper (chapter 3) reports the microstructures and tensile properties of Al/AlCuFe alloy composites consolidated by quasi-isostatic forging with two kinds of metal powders that have different oxide and impurity surface layers. The third paper (chapter 4) presents the tensile properties of the composites with several volume fractions of reinforcement particles made by vacuum hot pressing (VHP). By neutron diffraction measurement of the load partitioning between Al matrix and reinforcement phase, a hybrid

strengthening model is proposed to predict the tensile properties of the composite material. In the fourth paper (chapter 5), the effects of consolidation techniques, including quasi-isostatic forging and VHP, on the residual stresses and tensile strength of the composites are presented. The fifth paper (chapter 6) reports the neutron diffraction measurements of the residual stresses in the Al matrix and of the load partitioning between different phases in the composites. The mechanisms of the compressive residual stresses formed in the Al matrix were analyzed. Finally, these chapters are followed by a general conclusion. The references for each paper and manuscript are at the end of the chapter in which they are cited.

Literature Review

1. Tensile properties of Al matrix composites

Discontinuous particulate reinforced aluminum (PRA) matrix composites have experienced a recent resurgence of interest. Although initial efforts to develop PRA composites were directed toward aerospace applications, critical applications have now been implemented in the automotive and transportations industries, as well as in the electronics fields. They are also being considered in the manufacturing and robotics industries. PRA is a class of MMC material with an attractive balance of specific stiffness and strength and a host of other properties, including good wear resistance, thermal conductivity, and low thermal expansion, all of which makes them good multifunctional light weight materials. PRA materials may also exhibit near-isotropic properties when compared to their continuously reinforced counterparts, and are easier to process using standard metallurgical processing such as powder metallurgy, rolling and extrusion [4, 5].

However, in order to apply the PRA systems in relatively high temperatures, it is also necessary to design the system component phases for retention of their high strength at elevated temperature. One common approach to retention of strength at high temperature is to use ceramic or refractory phases for reinforcement particulate. Reasonable tolerance of impact and toughness are also needed for many applications. Although a large number of literature references covering both theoretical and experimental aspects are available on the mechanical behavior of PRA composites, especially reinforced by SiC, current PRA properties are still not as high as they could be, according to the prediction of various theories.

Table 1. The calculated yield strength gain from dislocations due to the differential thermal contraction on cooling from a typical consolidation temperature of pure aluminum and the ceramic reinforcement, assumed average particle size is 10μm and the aspect ratio is 1. The considered volume fraction of ceramic phase is 20 vol.% [3].

Ceramic Species	Δσ (MPa)
Al_2O_3	34.37
SiC	38.69
TiB_2	38.69
AlN	39.29
CrN	41.13
Si_3N_4	40.38
Fused Silica	42.57
Graphite	42.57

Table 2. The predicted overall increase in yield strength of Al alloy based MMC with 20 vol.% SiC and experimentally measured values [3].

Particle Size (μm)	Predicted Δσ (MPa)	Experimentally Determined Δσ (MPa)
0.5	98.72	60
10	61.75	34
70	34.8	27
250	19.55	10

By comparing the theoretically predicted increase in yield strength with experimentally measured values in table 1 and table 2, it becomes evident that the predicted yield strength is larger than the experimentally determined improvement and the improvement is not large. Based on this, end users in a structural application may not be ready to pay a significantly increased price for discontinuously reinforced MMCs in comparison with their unreinforced counterparts, if the reinforcing provides only a 30-50% improvement in yield strength and UTS. Most currently competitive MMCs' benefit/cost ratios are still very low which makes these MMCs not commercial viable. The two main reasons for a low Q/C ratio are the nature of the discontinuous reinforcement, which enables only a modest improvement of mechanical properties over the unreinforced matrix, and the existing technological barriers. From table 2, in order to achieve a significant improvement in valuable mechanical properties, ceramic particles with an average particle size of less than 2-3 μm should be used and / or a higher volume fraction of ceramic phase should be introduced in the metal matrix. Such composites are, however, difficult to manufacture, making clear necessary further development of processing technologies and new types of composites to make this possible.

The other primary disadvantage of current PRAs is that they suffer from low ductility, inadequate fracture toughness and inferior fatigue crack growth performance compared to that of the constituent matrix material [8-11]. Figure 1 (a) shows the composite tensile ductility (normalized by the ductility of the unreinforced alloy) as a function of the reinforcement volume fraction for a number of commercially available Mg-based MMCs and PRA materials [11]. Despite the experimental scatter, the figure shows that the ductility of these composites is significantly reduced as compared to the unreinforced counterparts. Figure 1(b) from reference [12] shows the same trend of decrease of fracture strain with an increase of weight percent of SiC particulates.

The dominant factor in controlling the elastic modulus of PRA composites is the volume fraction of reinforcement, and it is relatively insensitive to the particle distribution. There are several models proposed for predicting the elastic modulus of metal matrix composites. The iso-strain model, also known as the rule of mixtures, gives the upper bound of elastic modulus and the Iso-stress model gives the lower bound. There is also a Halpin-Tsai model specifically proposed for discontinuously reinforced composites which can provide a value that is between the upper and lower bound values. The equations for the three kinds of models are shown in table 3.

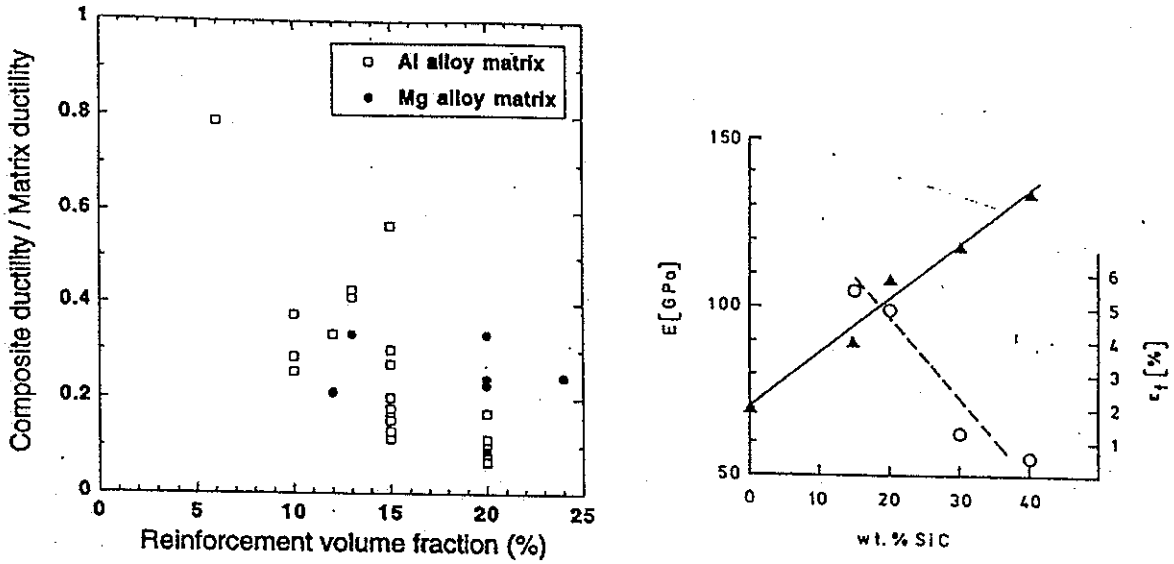

Fig. 1. (a) Experimental values of the composite tensile ductility (normalized by the ductility of the unreinforced alloy subjected to the same thermo-mechanical treatments) as a function of the reinforcement volume fraction [11], (b) Young's modulus and fracture strain vs. amount (weight percent) of SiC particulates of extruded material [12].

The equations in Table 3 for upper and lower bound of the elastic modulus of the composites were derived from variational energy principles of classical elasticity theory. The upper

bound of a composite elastic modulus is determined by the principle of minimum potential energy. For the case in which the Poisson's ratio value of the matrix is equal to that of the reinforcement, $\nu_m = \nu_r$, the expression for the upper bound of elastic modulus become the rule of mixtures expression $E_c = V_r E_r + V_m E_m$. The lower bound of elastic modulus is determined by the application of the principle of minimum complementary energy.

Table 3. Equations for elastic modulus [13-15].

Iso-strain model (Rule of mixtures) Upper Bound	Iso-stress model Lower Bound	Halpin-Tsai equation
Appropriate for continuous reinforcement		Appropriate for discontinuous reinforcement
$E_c = V_r E_r + V_m E_m$	$1/E_c = V_r/E_r + V_m/E_m$	$E_c = \frac{E_m(1+\xi\eta V_r)}{1-\eta V_r}$ $\eta = \frac{(E_r/E_m)-1}{(E_r/E_m)+\xi}$ $\quad \xi = 2S$

E_c: elastic modulus of composite material — E_m: elastic modulus of matrix material

E_r: elastic modulus of reinforcement material — V_r: volume fraction of reinforcement

V_m: volume fraction of matrix — S: particle aspect ratio

The Halpin-Tsai equations, which are an approximate representation of more complicated micromechanics results, were developed by an interpolation procedure. The procedure of this interpolation enables the generalization of usually limited, although more exact, micromechanics results and it is simple, so it can be readily used in the design process. Some physical insights into the Halpin-Tsai equations can be gained by examining their behavior for the ranges of values of ζ and η. ζ can range from 0 to ∞. When ζ=0, $1/E_c = V_r/E_r + V_m/E_m$, which is the lower bound of a composite material modulus. When $\zeta = \infty$, $E_c = V_r E_r + V_m E_m$, which is upper bound of a composite material modulus. Thus ζ is a measure of the reinforcement of the composite material. For small values of ζ, the fibers are not very

effective, whereas for large values of ζ, the reinforcements are extremely effective in increasing the composite stiffness above the matrix stiffness [16].

Figure 2 gives some experimental results for elastic modulus of Al/SiC composites with different Al alloys matrix [9, 12, 17-20]. Compared with upper bound values by the rule of mixtures, the experimental values are apparently much smaller. Halpin-Tsai equations gives a relatively good prediction if assume $\zeta = 2$, i.e. aspect ratio S = 1.

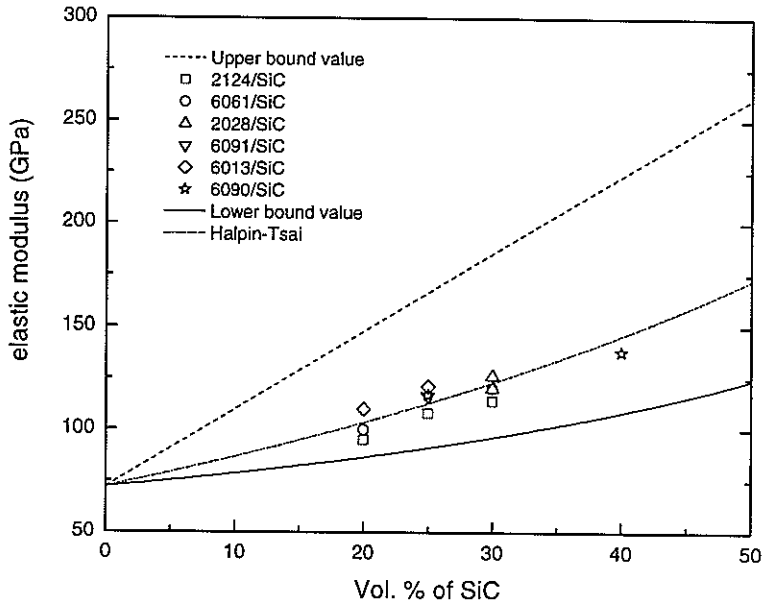

Fig. 2. Elastic modulus of SiC reinforced composites with different Al matrix compared with three prediction models [9, 12, 17-20].

2. Deformation and fracture of Al MMC

In particulate composites, fracture initiation is associated with particle fracture, interfacial matrix failure, and inclusion fracture, depending on the particular composite and matrix

condition. Preferential void nucleation has been observed in regions of high volume fraction of particulate, suggesting that local plastic constraints are important [21]. R.J.Arsenault, et al. showed that in PRA composites containing a high volume fraction of particles and whiskers, the deformation is highly localized. There are manifestations of three distinct localized deformation mechanisms : (a) there are very narrow "necks" in fracture samples; (b) the dislocation density is confined to a small region very close to the fracture surface; (c) slip line generation is confined also to a localized region. Finite element method studies also showed that deformation is more severe in reinforcement cluster regions of the matrix than in the remainder of the matrix [22].

Flom and Arsenault found a higher SiC particle concentration on the fracture surface than in the matrix, whereas other work has found a lower concentration, or the same density as in the matrix [23]. Many of the fracture studies show that the damage associated with fracture is highly localized at the fracture interface, with little evidence of general voiding away from the fracture. This raises the possibility that plastic strain tends to localize at a relatively early stage of the deformation. S.F. Corbin and D.S.Wilkinson did a microstructural study designed to observe flow at low strains (i.e. below 0.2% plastic strain) and reveals that deformation develops inhomogeneously in the composites. The onset of plastic flow appears to be associated with regions of the microstructure, which are relatively particle free [24].

D.J.Lloyd showed that the tensile elongation of a 6061Al/SiC composite is very sensitive to heat treatment, decreasing with increasing strength and decreasing work hardening rate [25]. But the tensile fracture mode is also very dependent on the reinforcement particle distribution that is strongly influenced by many aspects of the processing route. It is suggested that fracture initiates in the clusters of reinforcement particles present after fabrication. In these clusters, due to elastic misfit and the plastic constraint of the particles, the matrix between the particles is subjected to high triaxial stress that results in fracture of the matrix ligaments

between the particles. Fracture of the matrix in the clusters, together with any fracture of the particles within the cluster, allows a crack to grow through the cluster and to link by fast fracture through the matrix to adjacent clusters resulting in macroscopic fracture. These clusters in a sense limit the volume fraction of reinforcement that can be used. In powder processed MMC, size matching is important because clusters will be more probable if the particle size difference of matrix and reinforcement powder is large.

The geometry of the reinforcement particulate in metal-matrix composites has been shown to markedly affect matrix deformation behavior [26]. Studies of the constitutive behavior of composite materials by the finite element method showed that the stress fields that were developed in response to external loads can vary significantly with the geometry of the reinforcing phase. This has, in turn, been shown to alter fracture behavior especially near the matrix/reinforcement interface, where stress concentrations at sharp corners of the reinforcements give rise to intense localized plastic flow. Due to the complexity of the stress fields, dislocation glide, void nucleation, and crack growth in the matrix during plastic deformation proceeds differently from those processes commonly dominant in monolithic materials.

J.Llorca, S.Suresh, et al. analyzed the overall constitutive response of the composite and the evolution of matrix failure by finite element models [27]. The results showed that sharp corners of reinforcement particles act to limit ductility in two ways. The stress concentration at a corner site promotes early void nucleation and for a given aspect ratio, the constraint is higher with a sharp corner than with a rounded corner. The constraint on plastic flow for the particulate reinforced and sphere reinforced composites is much less than for the whisker reinforced composites. S.G.Song and N.Shi et al. also studied the particle shape effects on the fracture and ductility of a spherical and an angular particulate-reinforced 6061-Al composite containing 20 pct. Vol. Al_2O_3 [28]. The result shows that the spherical particulate composite

exhibited a slightly lower yield strength and work hardening rate but a considerably higher ductility than the angular counterpart. Experimental evidence has shown that in some composites, voids nucleate preferentially at the sharp corners of ceramic reinforcements [29-32]. These voids frequently lead to premature failure of the composite. A feasible way to improve ductility, therefore, is to use spherical reinforcements to reduce stress concentrations and, thereby, bring about a change in the stress and strain distribution throughout the composite.

Lots of research has identified the following general trends associated with MMC reinforcement particle fracture [23, 33, 34].

(1) The propensity for particle fracture increases with increasing reinforcement concentration.

(2) The propensity for particle fracture increases with increasing overall plastic strain.

(3) In the same tensile test specimen, larger reinforcement particles fracture more easily than smaller ones.

(4) Regions of the composite with clustered reinforcement particles exhibit a greater degree of particle fracture than regions where the local concentration of the particles is reduced.

(5) Cracks within the reinforcement are usually oriented normal to the loading axis for uniaxial tension, and parallel to the loading axis for uniaxial compression.

(6) The tendency for reinforcement failure depends on such factors as the reinforcement geometry and shape, matrix and reinforcement composition, interface properties, and thermomechanical processing techniques (such as extrusion).

(7) Defects that are introduced to the reinforcing phase during processing may serve as preferential nucleation sites for failure during subsequent mechanical loading.

(8) The damage introduced in the composite as a consequence of particle fracture can also trigger or influence other failure modes. Sharp microcracks that develop as a result of particle

fracture can enhance localized ductile plastic flow within the matrix, thereby promoting such additional failure mechanisms as ductile separation by void growth or shear banding.

(9) Experiments show that particle fracture (a) decreases the overall stiffness, flow strength, and ductility of the composite, (b) decreases the total life in low-cycle fatigue, and (c) increases the apparent crack propagation rates in high-cycle fatigue.

Considering all different factors it is clear that the fracture process in particle reinforced composites is quite complex, and a quantitative understanding is lacking. It is also apparent that different composites may be dominated by different fracture processes, but to maximize ductility for a particular volume fraction, the composite should have [35, 36]:

(1) Uniform particle distribution.

(2) A fine uniform particle size distribution.

(3) A high interfacial strength.

(4) Control of particle shape, probably spherical

(5) A ductile matrix.

3. Strengthening mechanisms of MMC

Strengthening mechanisms of composites have been studied extensively in recent years. Several mechanisms and models have been suggested to explain the strength of metal matrix composites [12, 16, 37-40].

(1) Load transfer from the matrix to the particles, i.e., the continuum shear lag model.

(2) High dislocation densities produced on cooling from high temperatures due to the large difference between the coefficient of thermal expansion (ΔCTE) of the matrix and that of the particles.

(3) Residual elastic stresses also caused by the large difference in the CTE.

(4) Internal stress gradients exist across the matrix during loading due to constraints from the reinforcements. This constraint induces strengthening to the composites.

(4) Grain and subgrain strengthening.

(5) Orowan strengthening.

(6) Matrix and interfacial strengthening due to solution and precipitation.

(7) Strengthening arising from constrained plastic flow and triaxiality in the ductile matrix owing to the presence of a brittle reinforcement (back stress).

(8) Work hardening.

The continuum shear lag model was developed to predict the strength of composites originally by Cox [41]. The model centers on the transfer of tensile stress from matrix to a fiber by means of interfacial shear stresses. For the aspect ratio typically used in particle reinforced MMCs, the continuum shear lag model underestimates the strength. Nardone and Prewo have suggested that better agreement is obtained if the equation is modified to allow for whisker or fiber end loading effects which give the following equation for strength prediction [37].

$$\sigma_{cy} = \sigma_{my}\left[\frac{1}{2}V_r(s+2)+V_m\right] \quad \text{..... (1)}$$

where s is the aspect ratio of the reinforcement, σ_{cy} and σ_{my} represent the yield strength of composite and matrix material respectively. V_r and V_m represent the volume fraction of reinforcement and matrix respectively. The theoretical prediction by means of this model is closer to the experimental results when the aspect ratio is small. The difficulty with this continuum approach is that it ignores the influence of particles on the micromechanics of deformation, such as the very high work hardening at low strains, and modifications in microstructures, such as grain size and dislocation density [42].

A model to predict the yield strength of a particle-reinforced MMC by considering the dislocation density due to mismatch between thermal expansion coefficients (ΔCTE) of particle and matrix was built up by R.J.Arsenault et al [43]. It is proposed that the high matrix dislocation density caused by ΔCTE should account for the observed strengthening, where the increase in dislocation density ($\Delta\rho$) due to thermal mismatch is proportional to

$$\Delta\rho \propto \frac{V_i \varepsilon}{b(1-V_i)} \frac{1}{t} \quad \text{..... (2)}$$

where b is the Burger's vector, ε is the thermal misfit strain prior to plastic relaxation, V_i of the reinforcement volume fraction, and t is the smallest reinforcement dimension. Then the yield strength increase of composite compared with unreinforced matrix is

$$\Delta\sigma_y = \alpha\mu b\sqrt{\Delta\rho} \quad \text{..... (3)}$$

where α is a constant, which is 1.25 for Al. μ is the shear modulus of the matrix. While dislocation density and elastic misfit strengthening models are in agreement with the general trends of the strengthening results, they are not sufficiently detailed to account for particle size and distribution variations, and how the different microstructural factors interact. For Al-Cu-Fe quasicrystal reinforcement with a CTE which is close to the CTE of Al matrix, this model is not verified also.

In powder processed composites, the grain size can be extremely small and significantly contribute to the strength, whereas in melt processed MMCs the grain size more closely approaches unreinforced alloys. Orowan strengthening is not a major factor with the 5μm and larger reinforcement particles usually used, but particles of this size can result in quench

hardening and enhanced work hardening because of elastic misfit back stress hardening [38, 44, 45]. Particle shape, in terms of aspect ratio, will influence composite strength, but for the typical aspect ratio range of up to 2:1, it is not expected to be a major factor. The predominant direct strengthening factor is the volume fraction of reinforcement. Powder processed material tends to give somewhat higher strengths than melt processed composites, probably because of additional strengthening from oxide dipersoids, and the somewhat finer grain size.

An experiment for measuring direct load transfer from Al matrix to SiC reinforcement was done by L.Huan, J.B.Li, et al [46]. They measured the bearing stresses of the aluminum matrix in a SiC_p/6061Al composite by an X-ray stress analysis technique. They showed that the actual bearing stresses of the matrix and reinforcement in 20 Vol.% SiC_p/6061Al composites were 75.9% and 196.6% of the average applied stress and the actual bearing stress of the reinforcement was 1.59 times higher than that of the matrix. This load transfer from matrix to reinforcements was caused by the significant difference between the elastic modulus of the two phases. The neutron diffraction technique is also used more and more in load partitioning and internal stress measurement in different kinds of composite materials, primarily due to its greater penetration of the testing materials [47-51]. Other resulting advantages of neutron diffraction include: the ability to study systems containing heavy elements and/or large diameter fibers or particles; the ability to study and separate subsurface micro- and macrostress gradients; and the ability to achieve bulk volume averaging in samples such as tensile test specimens. Another important aspect is that neutron scattering cross sections vary randomly across the periodic table rather than increasing systematically with atomic number as do x-ray scattering factors [52]. This means that light elements often scatter as strongly as heavy elements.

Povirk et al. [53] and Arsenault et al. [54] studied residual stress on the uniaxial response in tension and compression of the Al/SiC composites. The results show that the yield strength of the composites is asymmetric in terms of tension and compression. The results were explained by the effect of the residual stress acting to increase the yield strength in compression and reduce the yield strength in tension. Sun et al. [55] studied the residual stress in Al/SiC composites by x-ray diffraction and proved that the residual stresses in the particulate reinforced composites are hydrostatic by both experiments and mathematical analysis.

The extent of strengthening is also dependent on the matrix alloy microstructure, being lowest in over aged material. The studies of C.W.Wong et al. on Al-Cu/SiC MMC showed that there are solute rich zones in the near vicinity of SiC particulates and that the nucleation of secondary phases was enhanced both at and in the near vicinity of SiC particulates [56]. The result of ageing studies revealed accelerated ageing kinetics for the Al-Cu/SiC composites. This is caused by the increase in heterogeneous nucleation sites around SiC particles where a high dislocation density usually exists due to the large ΔCTE between Al and SiC. A finer SiC particulate size and a higher weight percent of SiC particulates can both produce a larger surface area for nucleation of strengthening precipitates in the metallic matrix, which leads to accelerate the ageing kinetics [57, 58]. Because of the difficulty of controlling the aging condition and microstructures of the metal matrix and the highly complex relationships between microstructures and mechanical performance of MMC [17, 59, 60], the initial stage of this proposed research on Al/QXL composites will use pure Al matrix. The choice of pure Al matrix can also avoid the complications of strengthening mechanisms from both reinforcement particles and precipitate phases, and thus, separate the different effects that will normally be added together.

4. Interface of MMC

The ability to achieve any strengthening in a composite is dependent on the ability to transfer stress from the matrix to the stronger reinforcing particles. This is dependent on achieving a strong interfacial bond between the matrix and the reinforcement. If the interfacial bond is weak the interface will fail before any effective stress transfer to the particle can occur, and no strengthening is achieved [15]. Not all combinations of reinforcement and matrix are compatible with melt phase processing and others cannot be processed by solid state processing into commercially useful composites. In some composites, the coupling between the reinforcement and the matrix is poor and adhesion promoters are needed. In others, excessive interfacial reactivity, especially in liquid phase processing, can lead to a brittle layer around the reinforcement. An interface with a metallic bond is more ductile than ionic or covalent bonds, and is desirable in metal matrix composites, if possible.

Several drawbacks of conventional composite materials such as low temperature ductility and poor toughness hinder their wide range of application. The causes for the remarkable drop in ductility and toughness of such composites are believed to be related to the structure at the interface region and the processing factors [8, 21]. The major problems encountered during the molten phase fabrication ceramic particle-reinforced aluminum matrix composites are the reactivity of ceramics with molten aluminum at higher processing temperatures and the poor wettability of ceramics by Al at lower processing temperature. The reaction between ceramics and liquid aluminum during processing can cause significant degradation in the properties of the composites [15]. In this dissertation, because the chosen Al based quasicrystal powder can have very good metallic bonding with the aluminum matrix, it provides an excellent basis to overcome the chemical and mechanical degradation problem.

Depending on the materials and the degree of bonding achieved, the interface can be one of two kinds [61]:

(1) Reversible bond only, generally physical

There is no chemical interaction between the two materials on either side of the interface. There is an attractive force binding the two, due to Van der Waals forces. This "physical bond" is established in a reversible manner. The resulting bond energy is relatively low and is temperature independent. This type of bond is reversible, since the physical act of separating the two surfaces after contact can be made without significant additional energy losses, bond strengths being low. Reversibility of bonding at the interface has indeed been observed in polymer matrix composites [62] and in Al/SiC bonds formed by deformation and shear in the solid state.

(2) Chemical or metallurgical bonds

On the basis of sessile drop experiments and experience in metal matrix composites processing, it has become clear that in interfaces separating a metal from another material, a stronger chemical bond can be established, resulting from chemical interaction across the interface. Such bonds generate a work of adhesion (by definition, the energy liberated on their formation from two free surfaces) that is temperature dependent. These chemical bonds are typically an order of magnitude higher in heat of formation than physical bonds and, therefore, have much higher interfacial strength. In practical terms, their importance translates into the observation noted above that one of the two methods of improving wettability in metal matrix composites solidification processing is to 'add something to the fiber or the matrix that will promote reactions between the two'. These are irreversible bonds in the sense that once established, they can not be broken without also damaging adjoining material on either side of the interface.

Microscopic investigations of interfaces are now possible with advanced high resolution transmission electron microscopy, and recent results are reviewed by Ruhle and Evans [63]. These include recent investigations of metal/oxide interfaces, for which it was shown by Mader that oxides produced by internal oxidation display a layer of oxygen anions along their low energy facets with the metal matrix [64]. Almost all interface research in the MMC field found in the literature was focused on Al/SiC interface composition and structure analysis, including both physical and chemical types of interfaces. A similar study about the bonding strength and interface microstructure of Al/Al-Cu-Fe quasicrystal has not been reported, providing motivation for this aspect of the study.

5. Al-Cu-Fe quasicrystal and quasicrystal reinforced composites

The discovery in 1984 of an icosahedral phase in an Al-Mn alloy by Shechtman et al. [65] has encouraged an extensive body of theoretical and experimental studies on this family of materials with a quasicrystal lattice. This new type of phase with a crystallographically forbidden symmetry is characterized as a quasiperiodic crystal or a quasicrystal [66]. Since that time, many other alloy systems that form quasicrystalline phases were discovered. A thermodynamically stable quasicrystalline phase with sharp Bragg peaks was first reported by Tsai et al. in the ternary Al-Cu-Fe system [67]. These stable icosahedral phases can be produced by conventional solidification and by melt-quenching, as well as by mechanical alloying, and shows sharp Bragg peaks after annealing [68, 69].

The Al-Cu-Fe system was first studied in detail by Bradley and Goldschmidt in 1939 [70]. They reported that the system included fourteen single-phase areas after slow cooling. The icosahedral phase was designated as the Ψ-phase, close to a composition of $Al_{65}Cu_{23}Fe_{12}$, and was reported to be an unknown phase. Tsai et al. reported that a stable quasicrystalline phase was formed in the composition range from 16 to 24 at% Cu and 11 to 17 at% Fe [67]. On the

other hand, Faudot et al. established that: (1) additional phases, especially β phase (a cubic Al-Cu-Fe solid solution, $Al_5(Cu,Fe)_5$), formed on quenching, but were eliminated after annealing, and (2) the formation of a single i-phase can be obtained after annealing for the compositions from $Al_{64}Cu_{24}Fe_{12}$ to $Al_{61.75}Cu_{25.5}Fe_{12.75}$. For the composition $Al_{62}Cu_{25.5}Fe_{12.5}$, the XRD lines are narrow for a range of annealing temperatures (800°C to 600°C). This result shows that around this composition there exists a single phase domain where the i-phase is perfect and remains stable at 600°C [71]. D.Gratias et al. performed a study of the phase diagram of Al-Cu-Fe in the vicinity of the icosahedral phase and showed that this phase extends at high temperature (680°C) over a concentration range defined by a narrow triangle with vertices 62.4-24.4-13.2, 65-23-12 and 61-28.4-10.6 (respectively in Al, Cu and Fe contents) centered around the composition $Al_{62.3}Cu_{24.9}Fe_{12.8}$ [72]. F.W.Gayle, et al., also determined isothermal sections of the Al-Cu-Fe equilibrium phase diagram at 700°C and 800°C in the region of 50 to 75 at. pct Al and 0 to 25 pct Fe using SEM/EDS techniques [73]. The icosahedral phase has equilibrium phase fields with four distinct phases at 700°C and 720°C (β-Al(Cu, Fe), λ-$Al_{13}Fe_4$, ω-Al_7Cu_2Fe, and liquid) and three phases at 680°C (β, ω, λ) and 800°C (β, λ and liquid).

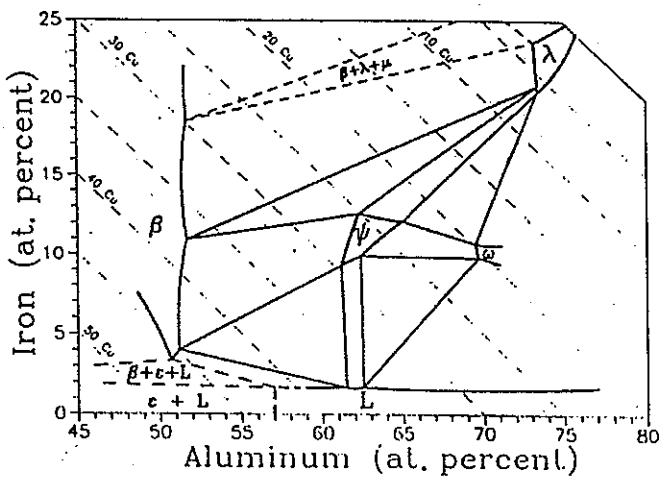

Fig.3. Isothermal section of Al-Cu-Fe ternary phase diagram at 700°C [73].

S.M.Lee, et al. studied the solidification sequence of the icosahedral quasicrystal forming Al-Cu-Fe alloys as functions of cooling rate during solidification [74]. For a moderate cooling rate regime, the i-phase is formed by a peritectic reaction. For a high cooling rate regime, where large undercooling of the liquid is obtainable, the i-phase is formed directly from the undercooled melt, without the formation of the primary λ ($Al_{13}Fe_4$) or β (Al(Cu, Fe)) phases. Because the β-phase is always mixed with the i-phase in the as-cast or as-quenched states and disappears after annealing at 873 K [71], P.Ochin, et al. investigated the influence of the cooling rate on the respective volume fractions of the i- and β-phases for two compositions $Al_{63}Cu_{25}Fe_{12}$ and $Al_{63}Cu_{24.5}Fe_{12.5}$ in the as-quenched state [75]. It was found that the higher the cooling rate, the less the β-phase will grow, and the β/i phase ratio will decrease. So even for this stable icosahedral phase, ultrafast cooling from the melt provides the most reliable method of preparation by suppressing segregation during cooling through successive high temperature transformations.

It is well known that quasicrystal alloys have very high hardness and high modulus [76, 77]. The original metastable quasicrystals were initially prepared by very rapid solidification processes, such as melt spinning. Now, experiments show that thermodynamically stable Al-Cu-Fe quasicrystal powder can be produced by gas atomization and can retain its high hardness at elevated temperature [78]. According to the results of a recent microhardness test, the Vickers microhardness value of $Al_{64}Cu_{22}Fe_{14}$ quasicrystals particles in a pure Al matrix composites is about 890 [79]. U.Koster also reported a Vickers microhardness of 1000 of the same quasicrystal (QXL) compound in monolithic form [80]. The elastic modulus of this quasicrystal material, from a very recent report, is 181 GPa [81]. The Al-Cu-Fe quasicrystal sample for this elastic modulus measurement was made by hot isostatic pressing (HIP) of gas atomized powder and was fully dense. The fully dense QXL sample illustrated the capability of local interparticle diffusion and bonding between QXL particles at temperatures only slightly above the range used for PRA consolidation. The spherical shape

of atomized quasicrystal particles can also improve the ductility of a composite because of the relatively low level of strain concentration, compared to fragmented SiC. Therefore, Al-Cu-Fe quasicrystals, produced by gas atomization, may act as a very good reinforcement particulate for Al MMC materials.

Table 4. Properties of Pure Al, Al-Cu-Fe quasicrystal and SiC.

	Elastic modulus (GPa)	Density (g/cm^3)	Coefficient of thermal expansion ($\times 10^{-6}$ K^{-1})
Pure Al	70	2.7	23.6
$Al_{63}Cu_{25}Fe_{12}$	181[81]	4.7	14-19[82]
SiC	400-450	3.2	3.8

Quasicrystals were firstly used as an intrinsic strengthening phase in 1987 when a well-controlled homogeneous dispersion of nanocrystalline quasicrystals was achieved within an aluminium solid solution matrix by a precipitation process in an Al-Li-Cu-Mg alloy [83]. A first approach for commercial application as reinforcement was made in 1989 with a new type of maraging steel [84], where particles with an icosahedral structure were found to precipitate under controlled annealing conditions. A further successful attempt at hardening of Al-alloys by such phases with aperiodic structure was reported in 1992 for Al-Mn-Ce melt-spun ribbons [85] with tensile strengths exceeding 1 GPa. The microstructure of this alloy was characterized by a fine dispersion of spherical quasicrystalline particles, 50 - 100 nm in diameter surrounded by an Al-matrix with a 5-15 nm grain size. Upon the substitution of other lanthanides and transition metals for Ce and Mn, respectively, this microstructural concept was later extended to other alloy systems such as Al-(V,Cr)-(Fe, Co, Ni) and Al-Mn-(Y, La, Nd, Gd) [86, 87]. Since the practical use of melt-spun ribbons for mechanical applications is obviously limited, there have been a number of investigations to produce such Al-based composites in form of bulk samples. Mainly these attempts were done by powder

metallurgical methods, where powders were synthesized by gas atomization or solid state reaction and were compacted using hot pressing and/or hot extrusion [87-90].

F.Schurack et al. produced a Al matrix composites reinforced by extrinsic Al-Mn-Ce and Al-Cu-Fe quasicrystal particles. The quasicrystal powders were synthesized by milling of elemental powder mixtures or arc-melted prealloys using a planetary ball mill. Large (up to 10 mm diameter) irregular shape quasicrystal powders were hot extruded with pure Al powder to form the bulk sample. Compression tests on the composite samples showed yield strength of about 400 MPa, ultimate tensile strength of 565 MPa and a ductility of up to 19% fracture strain as optimum mechanical properties [91].

6. Powder metallurgy technologies of Al MMC

A wide variety of fabrication techniques have been explored for metal matrix composites. These include powder metallurgy, molten metal methods, semisolid casting, pressure infiltration and spray deposition [4, 15, 92]. For molten metal methods, extrinsic ceramic particulates have been incorporated into molten matrix alloys, but it had limited success because most metals do not wet ceramic particles, and these results in rejection of the particles from the melt [93]. In general, molten aluminum does not wet most ceramic particles at typical casting temperatures and the molten metal methods attempt to improve this wetting behavior [61].

The powder metallurgy processing technique is attractive for several reasons [15, 94, 95]. This approach offers microstructural control of the phases that is absent from the liquid phase route. Powder metallurgy processing employs lower temperatures and, therefore, theoretically offers better control of interface reaction kinetics. The powder metallurgy processing approach also makes it possible to employ matrix alloy compositions and microstructural refinements that are only available via the use of rapidly solidified powders. Because of their

basis as a powder, these composites have been deformation processed after powder consolidation to develop the best properties. The composites behave in a manner similar to new high strength aluminum alloys made by the powder metallurgy technique: i.e. the previous particle oxide skins must be broken up by metal working before the true properties of the matrix metal and, hence, the composite can be achieved. The most common primary breakdown process has been extrusion. Other metal working processes such as rolling, forging, shear spinning and swaging have also been demonstrated. The ceramic reinforcements give rise to dulling of the machine tools that decreases the machinability of these composites. Unfortunately, for current particulate reinforced aluminum (PRA) [24, 25], a considerable amount of complexity and cost is added [6] by the need for extensive hot deformation of the blended powder compact to mitigate the deleterious effects of the oxide coating on the prior particle boundaries of the Al alloy powders. The Al oxide coating on most commercially atomized powders is a severe barrier to sintering, especially solid state sintering, and unless thoroughly distributed in the microstructure of an Al MMC, it can significantly reduce ductility and fatigue strength [6, 96-98]. So ideally, "clean" aluminum and quasicrystal powders are needed to circumvent the need for conventional processing procedure. The gas atomization reaction synthesis (GARS) technique is a patented method invented in Ames Lab [99]. By this method, much less oxidized low cost powders can be produced. Because of much lower impurity and oxidation level on the GARS powder surface, the composite material produced by GARS powders should have better Al/QXL interface bonding and ductility. Previous studies [98, 100-104] give a thorough discussion of the results of an extensive study of the surface reactions promoted during the gas atomization process. The prior study compared the surface oxide characteristics of different types of gas atomized Al powders, especially the differences between physisorbed and chemisorbed moisture contents of the oxide, and concluded that the high purity powders from the GARS process exhibit far less chemisorbed hydrogen in the oxide coating. In-situ characterization of sintering behavior of die pressed commercial pure Al and GARS pure Al powders has

been done by electromagnetic acoustic transducer (EMAT) technology recently by J.C.Foley et al. [100, 105, 106]. The results also shows that the commercial pure Al powder compact showed no sintering, but the GARS Al powders showed very significant sintering in the 500°C furnace with a flowing nitrogen atmosphere.

Further, the SiC particulate can add a material cost penalty, typically 2 to 4 times the cost of the Al alloy powder, and can present an extreme problem for conventional Al recycling methods. These disadvantages in processing and material cost and the lack of effective recyclability motivate the development of alternatives for both reinforcement materials and Al matrix powder processing techniques [6].

In the powder metallurgy method, it is important to achieve an initial homogeneous mixture of reinforcement and matrix powders. To achieve this, the sizes of the matrix and reinforcement powders need to be carefully chosen so that agglomerates are not left after blending, and carry over into the final product. The appropriate size ratio will depend on the blending process used, but in one case a SiC/Al particle size ratio of 0.7:1 gave a more uniform reinforcement distribution than a ratio of 0.3:1 [96]. Size ratio of Al and SiC powders has effect on the green strength of CIPped Al/SiC sample, which was shown by M.D.Weber and R.J.Fields et al [97]. Samples with size ratio of 0.69 were significantly stronger than those with size ratio of 4.8 for a given SiC concentration or relative density. Their results also showed that there is a green strength maximum between 10% and 18% SiC, which is due to the connectivity of the brittle SiC phase and the formation of a SiC skeletal structure when the volume fraction of reinforcement reaches 15% to 17%. The reinforcement skeletal structure formation can be explained by percolation theory.

In a typical powder composite consolidation approach, vacuum hot pressing consolidates the composite to over 95% dense and in a near-net shape, and can be carried out below the

solidus of the alloy, or in the liquid-solid region. The kinetics of densification are higher using liquid phase sintering, but it has the disadvantage that reaction can more readily occur between the reinforcement and the liquid phase to form undesirable intermetallics at the ceramic particle interface. Liquid phase sintering will also degrade the microstructure of a rapidly solidified alloy powder, and generate coarse intermetallic phases typically in the melted and resolidified regions. Completely solid state consolidation enables advantage to be taken of the supersaturated metastable alloy compositions that can be obtained by the rapid solidification atomization and ribbon casting processes [15].

Vacuum hot pressing is a form of uniaxial hot pressing which involves radial constraint from the die wall, with the radial stress generated at the die wall being proportional to the pressure applied via an effective Poisson's ratio υ. Only the uniaxial pressure is controlled during processing and the shear is nonzero. Unconstrained uniaxial compression (sinter forging) produces a large shear component [94]. Ceracon processing, which is a type of quasi-isostatic forging developed by Ceracon Inc., involves consolidation of a porous metal perform to theoretical density under quasi-isostatic conditions. During processing, a granular ceramic medium transfers pressure from an advancing ram of a press to a P/M perform. This process differs from true iso-static pressing, in which a fluid medium is used to transfer pressure to the powder. Isostatic pressing (granular forge) is a hybrid between hot isostatic pressing and uniaxial hot pressing. The difference in the axial and radial stresses introduces a shear level between hot isostatic pressing and forging. Thus, there is shear to disrupt packing irregularities and interparticle films, but the negative aspect is the anisotropic dimensional change. The benefit with dimensional change of uniaxial hot pressing is that the radial dimensions are determined by the tooling and only the height strain leads to variation in the final height [94]. In order to get good bonding between matrix and reinforcement particles, the uniaxial or iso-static pressure used in current composites processing are quite high so that some degradation of the reinforcement occurs when it is applied at room temperature before

sintering. By choosing quasicrystal reinforcement materials that are more compatible with Al matrix, it is possible to improve the reinforcement matrix bonding while decreasing the pressure applied during sintering. Lower pressure will be used in vacuum hot pressing procedure to produce the Al/quasicrystal composites that shows the same microstructure and tensile properties as those consolidated at very high pressure.

References

1. D.B.Miracle, S.L.Donaldson, Composites, ASM Handbook, Vol. 21, 10th edition, ASM International, Materials Park, Ohio, 2001.
2. A.P.Devecha, S.G.Fishman, S.D.Karmarkar, "Silicon carbide reinforced aluminum-a formable composite," JOM, Vol. 33, No. 9, 1981, p. 12-17.
3. V.M.Kevorkijan, "Aluminum composites for automotive applications: a global perspective," JOM, Vol. 51, No. 11, 1999, p. 54-58.
4. J.E.Allison, G.S.Cole, "Metal-matrix composites in the automotive industry: Opportunities and Challenges," JOM, Vol. 45, No. 1, 1993, p. 19-24.
5. B.Maruyama, W.H.Hunt, "Discontinuously reinforced aluminum: current status and future direction," JOM, Vol. 51, No. 11, 1999, p. 59.
6. I.E.Anderson, J.C.Foley, J.F.Flumerfelt, "Simplified aluminum powder metal processing routes for automotive applications," Proceedings of the first international conference on powder metallurgy aluminum & light alloys for automotive applications, Nov. 10-11, 1998, Dearborn, Michigan, edited by W.F.Jandeska and R.A.Chernenkoff, published by MPIF, p. 75.
7. F.Tang, I.E.Anderson, S.B.Biner, "Solid state sintering and consolidation of Al powders and Al matrix composites," Journal of Light Metals, Vol. 2, No. 4, 2002, p. 201-214.
8. A.B.Pandey, N.Chawla, "The fracture toughness and fatigue behavior of DRA," JOM, Vol. 51, No. 11, 1999, p. 69.

9. T.S.Srivatsan, J.Mattingly, "Influence of heat treatment on the tensile properties and fracture behavior of an aluminum alloy-ceramic particle composite," Journal of Materials Science, Vol. 28, 1993, p. 611-620.
10. P.M.Bronsveld, P.Bruinsma, J.T.De Hosson, M.A.Sargent, W.H.M.Alsen, "Microstructural analysis of hot isostatically pressed Al-SiC," Materials Science and Engineering A, Vol. A135, 1991, p. 77-81.
11. J.L.Lorca, C.Gonzalez, "Microstructural factors controlling the strength and ductility of particle-reinforced metal-matrix composites," Journal of the Mechanics and Physics of Solids, Vol. 46, No. 1, 1998, p.1-28.
12. D.L.McDaniels, "Analysis of stress-strain, fracture, and ductility behavior of aluminum matrix composites containing discontinuous silicon carbide reinforcement," Metallurgical Transactions A, Vol. 16A, No. 6, 1985, p. 1105-1115.
13. John C. Halpin, Primer on composite materials analysis, Technomic Publishing Company, 1992, p.161.
14. A.K.Kaw, Mechanics of Composite Materials, CRC Press LLC, 1997, p.145.
15. D.J.Lloyd, "Particle reinforced aluminum and magnesium matrix composites," International Materials Reviews, Vol. 39, No. 1, 1994, p.1-23.
16. R.M.Jones, Mechanics of Composite materials, Taylor & Francis Inc., 1999, p.137.
17. T.S.Srivatsan and R.Annigeri, "The quasi-static and cyclic fatigue fracture behavior of 2014 aluminum alloy metal-matrix composites," Metallurgical and Materials Transactions A, Vol. 31A, No. 3, 2000, p. 959.
18. N.Chawla, U.Habel, Y.L.Shen, C.Andres, J.W.Jones, J.E.Allison, "The effect of matrix microstructure on the tensile and fatigue behavior of SiC particle-reinforced 2080 Al matrix composites," Metallurgical and Materials Transaction A, Vol. 31A, 2000, p.531.
19. M.G.McKimpson, E.L.Pohlenz, S.R.Thompson, "Evaluating the mechanical properties of commercial DRA," JOM, Vol. 45, No. 1, 1993, p. 26.
20. M.M.Schwartz, Composite Materials: Properties, Nondestructive Testing, and Repair,

Volume I, 1997, Prentice-Hall Inc., p.169.

21. W.H.Hunt, T.M.Osman, J.J.Lewandowski, "Micro- and macrostructural factors in DRA fracture resistance," JOM, Vol. 45, No.1, 1993, p. 30-35.
22. R.J.Arsenault, N.Shi, C.R.Feng, L.Wang, "Localized deformation of SiC-Al composites," Materials_Science and Engineering A, Vol. 131, 1991, p. 55-68.
23. Y.Flom, R.J.Arsenault, "Deformation of SiC/Al composites," Journal of Metals, July 1986, p. 31-34.
24. S.F.Corbin and D.S.Wilkinson, "Low strain plasticity in a particulate metal matrix composite," Acta Metallurgica et Materialia, Vol. 42. No. 4, 1994, p. 1319-1327.
25. D.J.Lloyd, "Aspects of fracture in particulate reinforced metal matrix composites," Acta Metallurgica et Materialia, Vol. 39, No. 1, 1991, p. 59-71.
26. S.Y.Qin, C.R.Chen, G.D.Zhang, W.L.Wang, Z.G.Wang, "The effect of particle shape on ductility of SiC_p reinforced 6061 Al matrix composites," Materials Science and Engineering A, Vol. 272, 1999, p. 363-370.
27. J.Llorca, A.Needleman, S.Suresh, "An analysis of the effects of matrix void growth on deformation and ductility in metal-ceramic composites," Acta Metallurgica et Materialia, Vol. 39, No. 10, 1991, p. 2317-2335.
28. S.G.Song, N.Shi, G.T.Gray, J.A.Roberts, "Reinforcement shape effects on the fracture behavior and ductility of particulate-reinforced 6061-Al matrix composites," Metallurgical and Materials Transactions A, Vol. 27A, No. 11, 1996, p. 3739-3746.
29. T.Christman, A.Needleman, S.Nutt, S.Suresh, "On microstructural evolution and micromechanical modeling of deformation of a whisker-reinforced metal-matrix composite," Materials Science & Engineering A, Vol. A107, No. 1-2, 1989, p. 49-61.
30. M.Manoharan, J.J.Lewandowski, "Crack initiation and growth toughness of an aluminum metal-matrix composite," Acta Metallurgica, Vol. 38, No. 3, 1990, p. 489-496.

31. T.L.Dragone, W.D.Nix, "Geometric factors affecting the internal stress distribution and high temperature creep rate of discontinuous fiber reinforced metals," Acta Metallurgica et Materialia , Vol. 38, No. 10, 1990, p. 1941-1953.

32. S.R.Nutt, A.Needleman, "Void nucleation at fiber ends in Al-SiC composites," Scripta Metallurgica, Vol. 21, No. 5, 1987, p. 705-710.

33. W.M.Zhong, G.L'Esperance, M.Suery, "Effect of thermomechanical processing on the microstructure and mechanical properties of Al-Mg (5083) / SiC_p and Al-Mg (5083) / $Al_2O_{3\,p}$ composites, Part 3: Fracture mechanisms of the composites," Materials Science and Engineering A, Vol. 214, 1996, p 104-114.

34. J.C.Lee, K.N.Subramanian, "Failure behaviour of particulate-reinforced aluminuim alloy composites under uniaxial tension," Journal of Materials Science, Vol. 27, 1992, p. 5453-5462.

35. N.Chawla, C.Andres, J.W.Jones, J.E. Allison, "Effect of SiC Volume Fraction and Particle Size on the Fatigue Resistance of a 2080 Al/SiC_p Composite," Metallurgical and Materials Transactions A, Vol. 29, No. 11, 1998, p. 2843.

36. V.K.Varma, S.V.Kamat, Y.R.Mahajan, V.V.Kutumbarao, "Tensile behaviour of powder metallurgy processed (Al-Cu-Mg)/SiC_p composites," Materials Science and Technology, Vol. 17, 2001, p. 93.

37. V.C.Nardone, K.M.Prewo, "On the strength of discontinuous silicon carbide reinforced aluminum composite," Scripta Metallurgica, Vol. 20, 1986, p. 43-48.

38. R.J.Arsenault, N.Shi, "Dislocation generation due to differences between the coefficients of thermal expansion," Materials Science and Engineering A, Vol. 81, No. 8, 1986, p. 175-187.

39. F.Bonollo, R.Guerriero, E.Sentimenti, I.Tangerini, W.L.Yang, "Effect of quenching on the mechanical properties of powder metallurgically produced Al-SiC (particles) metal matrix composites" Material Science and Engineering A, Vol. 144, 1991, p. 303-309.

40. T.W.Clyne, P.J.Withers, An Introduction to Metal Matrix Composites, Cambridge University Press, Cambridge, 1993, 261.

41. H.L.Cox, "The elasticity and strength of paper and other fibrous materials," Brit. J. Appl. Phys. Vol. 3, 1952, p. 73-79.

42. M.Gupta, M.K.Surappa, "Processing-microstructure-mechanical properties of Al based metal matrix composites synthesized using casting route," Key Engineering Materials, Vols. 104-107, 1995, p. 259-274.

43. R.J.Arsenault, L.Wang, C.R.Feng, "Strengthening of composites due to microstructureal changes in the matrix," Acta Metallurgica et Materialia, Vol. 39, No. 1, 1991, p. 47-51.

44. M.Taya, K.E.Lulay, D.J.Lloyd, "Strengthening of a particulate metal matrix composite by quenching," Acta Metallurgica et Materialia, Vol. 39, No. 1, Jan, 1991, p. 73-87.

45. P.J.Withers, W.M.Stobbs, O.B.Pedersen, "Application of the Eshelby method of internal stress determination to short fibre metal matrix composites," Acta Metallurgica, Vol. 37, No. 11, 1989, p. 3061-3084.

46. L.Huan, J.B.Li, Z.Q.Kang, Z.G.Wang, "Relative load-bearing capacity of two constituents in a SiC_p/6061Al composites," Journal of Materials Science Letters, Vol. 15, 1996, p. 616-619.

47. P.J.Withers, A.P.Clarke, "A neutron diffraction study of load partitioning in continuous Ti/SiC composites," Acta Materialia, Vol. 46, 1998, p. 6585-6598.

48. A.J.Allen, M.A.M.Bourke, S.Dawes, M.T.Hutchings, P.J.Withers, "The analysis of internal strains measured by neutron diffraction in Al/SiC metal matrix composites," Acta Matallurgica et Materialia, Vol. 40, 1992, p. 2361-2373.

49. P.J.Withers, "Neutron strain measurement of internal strain in metal and ceramic matrix composites," Key Engineering Materials, Vols. 108-110, 1995, p. 291-314.

50. L.Ryelandt, C.Salmon, F.Delannay, "Neutron diffraction analysis of the evolution of phase stresses during plastic straining of aluminum matrix composites reinforced with a

continuous, random planar network of fibers," Materials Science Forum, Vols. 347-349, 2000, p. 486-491.

51. G.Albertini, G.Bruno, A.Carrado, F.Fiori, M.Rogante, F.Rustichelli, "Determination of residual stresses in materials and industrial components by neutron diffraction," Measurement Science and Technology, Vol. 10, 1999, p. R56-R73.
52. A.D.Krawitz, "Neutron stress measurements in composites," Residual Stresses in Composites, Measurement, Modeling & Effects on Thermo-Mechanical Behavior, Proceedings of a symposium sponsored by the SMD of TMS, Edited by E.V.Barrera and I.Dutta, Denver, Colorado, February 21-25, 1993, p. 161-176.
53. G.L.Povirk, S.R.Nutt, A.Needleman, "Continuum modeling of residual stresses in metal-matrix composites," Measurement, Modeling & Effects on Thermo-Mechanical Behavior, Proceedings of a symposium sponsored by the SMD of TMS, Edited by E.V.Barrera and I.Dutta, Denver, Colorado, February 21-25, 1993, p. 3-23.
54. R.J.Arsenault, M.Taya, "Thermal residual stress in metal matrix composite," Acta Metallurgica et Materialia, Vol. 35, 1987, p. 651-659.
55. Z.M.Sun, J.B.Li, Z.G.Wang, W.J.Li, "Residual stresses in silicon carbide particulate reinforced aluminum composites," Acta Metallurgica et Materialia, Vol. 40, 1992, p. 2961-2966.
56. C.W.Wong, M.Gupta, L.Lu, "Effect of variation in physical properties of the metallic matrix on the microstructural characteristics and the ageing behaviour of Al-Cu/SiC metal matrix composites," Journal of Materials Science, Vol.34, No. 7, 1999, p.1681-1689.
57. M.Gupta, F.Mohamed, E.Lavernia, T.S.Srivatsan, "Microstructural evolution and mechanical properties of SiC/Al_2O_3 particulate-reinforced spray-deposited metal-matrix composites," Journal of Materials Science, Vol. 28, No. 8, 1993, p. 2245-2259.

58. Y.Song, T.N.Baker, "Calorimetric and metallographic study of precipitation process in AA6061 and its composites," Materials Science & Engineering A, Vol. 201, No. 1-2, 1995, p. 251-260.

59. B.S.Majumdar, A.B.Pandey, "Deformation and fracture of a particle-reinforced aluminum alloy composite: part II. Modeling," Metallurgical and Materials Transactions A, Vol. 31, 2000, p. 937.

60. P.M.Singh, J.J.Lewandoski, "Effects of heat treatment and reinforcement size on reinforcement fracture during tension testing of a SiC_p discontinuously reinforced aluminum alloy," Metallurgical Transaction A, Vol. 24, 1993, p. 2531.

61. A.Mortensen, I.Jin, "Solidification processing of metal matrix composites," International Materials Reviews, Vol. 37, No. 3, 1992, p. 101-128.

62. D.Hull, An Introduction to Composite Materials, Cambridge University Press, 1981, p.3.

63. M.Ruhle and A.G.Evans, "Structure and chemistry of metal/ceramic interfaces," Materials Science and Engineering, Vol. 107, 1989, p. 187-197.

64. W.Mader, "Structure and Chemistry of Interfaces between Oxide Precipitates and a Metal Matrix," Z. Metallkd., Vol. 80, No. 3, 1989, p.139-151.

65. D.Shechtman, I.Blech, D.Gratias, J.W.Cahn, "Metallic phase long-range orientational order and no translational symmetry," Physical Review Letters, Vol. 53, No. 20, 1984, p.1951-1953.

66. D.Levine, P.J.Steinhardt, "Quasicrystals. I. Definition and Structure," Physical Review B, Vol. 34, No. 2, 1986, p. 596-616,

67. A.P.Tsai, A.Inoue, T.Masumoto, "A stable quasicrystal in Al-Cu-Fe System," Japanese Journal of Applied Physics, Part 2: Letters, Vol. 26, No. 9, 1987, p. L1505-L1507.

68. K.Hiraga, B.P.Zhang, M.Hirabayashi, A.Inoue, T.Masumoto, "Highly ordered icosahedral quasicrystal of Al-Cu-Fe alloy studied by electron diffraction and high-resolution electron microscopy," Japanese Journal of Applied Physics, Part 2: Letters, Vol. 27, No. 6, 1988, p. L951-L953.

69. N.Asahi, T.Maki, S.Matsumoto, T.Sawai, "Quasicrystallization characteristics of mechanically alloyed $Al_{65}Cu_{20}Fe_{15}$," Materials Science and Engineering A, Vol. 181/182, 1994, p. 841-844.

70. A.J.Bradley, H.J.Goldschmidt, Journal of the Institute of Metals, Vol. 65, 1939, p. 403.

71. F.Faudot, A.Quivy, Y.Calvayrac, D.Gratias, M.Harmelin, "About the Al--Cu--Fe icosahedral phase formation," Materials Science and Engineering A, Vol. 133, 1991, p. 383-387.

72. D.Gratias, Y.Calvayrac, J.Devaud-Rzepski, F.Faudot, M.Harmelin, A.Quivy, P.A.Bancel, "The phase diagram and structures of the ternary AlCuFe system in the vicinity of the icosahedral region," Journal of Non-Crystalline Solids, Vol. 153&154, 1993, p. 482-488.

73. F.W.Gayle, A.J.Shapiro, F.S.Biancaniello, W.J.Boettinger, "The Al-Cu-Fe phase diagram: 0 to 25 at. pct Fe and 50 to 75 at. pct Al – equilibria involving the icosahedral phase," Metallurgical Transactions A, Vol. 23, No. 9, 1992, p. 2409-2417.

74. S.M.Lee, H.J.Jeon, B.H.Kim, W.T.Kim, D.H.Kim, "Solidification sequence of the icosahedral quasicrystal forming Al-Cu-Fe alloys," Materials Science and Engineering A, Vol. 304-306, 2001, p. 871-878.

75. P.Ochin, A.Quivy, A.Dezellus, S.Peynot, J.P.Guibert, "Optimum quenching conditions for the formation of the icosahedral phases in Al-Cu-Fe alloys," Scripta Metallurgica et Materialia, Vol. 25, 1991, p. 1821-1826.

76. K.Urban, M.Feuerbacher, M.Wollgarten, "Mechanical behavior of quasicrystals," MRS Bulletin, Vol. 20, No. 11, 1997, p. 65-68.

77. E.Giacometti, N.Baluc, "Microindentation of Al-Cu-Fe icosahedral quasicrystal," Scripta Materialia, Vol. 41, No. 9, 1999, p. 989-994.

78. D.J.Sordelet, M.J.Kramer, O.Unal, "Effect of starting powders on the control of microstructural development of Al-Cu-Fe quasicrystalline plasma-sprayed coatings," Journal of Thermal Spray Technology, Vol. 4, No. 3, 1995, p. 235-244.

79. F.Tang, I.E.Anderson, S.B.Biner, "Processing and characterization of aluminum matrix composites with atomized reinforcement particulate and clean matrix powders," Advance in Powder Metallurgy & Particulate Materials 2000, Proceedings of the 2000 International Conference on Powder Metallurgy & Particulate Materials, sponsored by MPIF/APMI, Part 12, p. 127-140.

80. U.Koster, W.Liu, "Mechanical properties of quasicrystalline and crystalline phases in Al-Cu-Fe Alloys," Journal of Non-Crystalline Solids, Vol. 153&154, 1993, p. 446-452.

81. F.Tang, I.E.Anderson, S.B.Biner, "Microstructures and mechanical properties of pure Al matrix composites reinforced by Al-Cu-Fe alloy particles," accepted by Materials Science and Engineering A, in press.

82. P.Archambault, C.Janot, "Thermal conductivity of quasicrystals and associated processes," MRS Bulletin, Vol. 20, No. 11, 1997, p. 48-53.

83. P.Sainfort, B.Dubost, "Coprecipitation hardening in Al-Li-Cu-Mg Alloys," Journal de Physique, Vol. 48, Suppl. C3, 1987, p. 407-413.

84. A.Inoue, H.M.Kimura, T.Masumoto, M.Watanabe, F.Takahashi, A.Nagata, "High mechanical strength of quasicrystalline phase surrounded by FCC-Aluminum phase in rapidly solidified Al-Mn-Ce alloys," Materials Transactions, JIM, Vol. 33, 1992, p. 723-729.

85. M.Watanabe, A.Inoue, H.M.Kimura, T.Aiba, T.Masumoto, "High mechanical strength of rapidly solidified $Al_{92}Mn_6Ln_2$ (Ln=Lanthanide Metal) alloys with finely mixed icosahedral and aluminum phases," Materials Transactions, JIM, Vol.34, No.2, 1993, p. 162-168.

86. A.Inoue, H.M.Kimura, K.A.Sasamori, T.Masumoto, "Structure and mechanical strength of Al-V-Fe melt-spun ribbons containing high volume fraction of nanoscale amorphous particles," Nanostructured Materials, Vol. 7, No. 3, 1996, p. 363-382.

87. T.Masumoto, A.Inoue, M.Watanabe, J.Nagahora, T.Shibata, Japanese patent No.6256692, 1992 and United States Patent No. 5,458,700, 1995.

88. A.P.Tsai, K.Aoki, A.Inoue, T.Masumoto, "Synthesis of stable quasicrystalline particle-dispersed Al base composite alloys," Journal of Materials Research, Vol. 8, No.1, 1993, p. 5-7.

89. A.Inoue, H.Kimura, K.Kita, "New horizons in quasicrystals," A.I.Goldman, D.J. Sordelet, P.A. Thiel and J.M.Dubois, Editors, World Scientific, Singapore, 1997, p. 256.

90. S.B.Biner, D.J.Sordelet, B.K.Lograsso, I.E.Anderson, "Composite material reinforced with atomized quasicrystalline particles and method of making same," United States Patent No. 5,851,317, December 1998.

91. F.Schurack, J.Eckert, L.Schultz, "Processing and mechanical properties of quasicrystal-reinforced Al-Alloys," Materials Research Society Symposium and Proceedings, Material Research Society, Vol. 643, 2001.

92. C.K.Narula, J.E.Allison, "Advanced materials for automobiles," CHEMTECH, Vol. 26, No. 11, 1996, p. 48.

93. A.M.Patton, "Foundry trials of graphite-containing aluminum alloys," Journal of Institute of Metals, Vol. 100, July 1972, p.197-201.

94. R.M.German, Sintering theory and practice, John Wiley & Sons publishing, Inc., 1996, p. 326-360.

95. S.B.Biner, "Development of quasicrystal reinforced aluminum composites for industrial applications," Final Report to Center for Advanced Technology Development of Iowa State University, (July 1996).

96. J.J.Lewandowski, C.Liu, W.H.Hunt, "Processing and properties for powder metallurgy composies," edited by P.Kumar, 1987, Warrendale, PA, The metallurgical Society of AIME, p. 117-137.

97. M.D.Weber, S.Ankem, "Green strength of particle reinforced aluminum composites," Proceedings of the 2nd International Conference on Powder Metallurgy Aluminum and Light Alloys for Automotive Applications sponsored by the MPIF in cooperation with APMI International, Edited by R.A.Chernenkoff and W.F.Jandeska, Jr., November 2-3,

2000, Troy, Michigan.

98. J.F.Flumerfelt, "Aluminum Powder Metallurgy Processing," Ph.D. Thesis, Iowa State University, 1998.

99. I.E.Anderson, B.K.Lograsso, T.W.Ellis, Ames Lab, Iowa State University, US Patent No. 5,368,657, Nov. 29, 1994.

100. I.E.Anderson and J.C.Foley, "Determining the role of surfaces and interfaces in the powder metallurgy processing of aluminum alloy powders," Surface and Interface Analysis, Vol. 31, 2001, p. 599-608.

101. F.Tang, I.E.Anderson, S.B.Biner, J.C.Foley, "Tensile properties of pure Al based Al-Cu-Fe quasicrystal reinforced model MMC," Advances in Powder Metallurgy & Particulate Materials 2001, Proceedings of the 2001 International Conference on Powder Metallurgy & Particulate Materials, sponsored by MPIF/APMI, Part 9, p. 12 -25.

102. J.F.Flumerfelt, I.E.Anderson, J.C.Foley, "Consolidation of pure aluminum powders," P/M Aluminum/Mechanical Alloying, Parts 10&11 in Advances in Powder Metallurgy & Particulate Materials, 1997, eds. R.A.McKotch & R.Webb, p. 11.

103. D.Raybould, "Forming of rapidly solidified elevated temperature aluminum alloys produced by planar flow casting," Dispersion Strengthened Aluminum Alloys, Y.W.Kim and W.M.Griffith, Editors, TMS, Warrendale, PA, 1988, p. 199-215.

104. L.Ackermann, I.Guillemin, R.Lalauze, C.Pijolat, "Study of water desorption during degassing of aluminium powders," High Strength Powder Metallurgy Aluminum Alloys II, Ed. By G.J.Hildeman and M.J.Koczak, TMS, Warrendale, PA, 1985, p. 175.

105. J.C.Foley, D.K.Rehbein and D.J.Barnard, "Investigation of the sintering processing using non-contact electromagnetic acoustic transducers," Advance in Powder Metallurgy & Particulate Materials 2001, Proceedings of the 2001 International Conference on Powder Metallurgy and Particulate, sponsored by the MPIF/APMI, Part 11, p. 26-40.

106. J.C.Foley, D.J.Barnard, "Simplified powder metallurgy processing of Al-8Fe-4Ce alloys," Advances in Powder Metallurgy & Particulate Materials 2002, Proceedings of the

2002 International Conference on Powder Metallurgy and Particulate Materials held on June 16-21, 2002, in Orlando, Florida, sponsored by the MPIF/APMI, Part 1, p. 103-114.

Solid State Sintering and Consolidation of Al Powders and Al Matrix Composites

A paper published in the Journal of Light Metals [1]

F. Tang, I. E. Anderson, and S. B. Biner

Ames Laboratory, Iowa State University, Ames, IA 50011

Abstract

As an attempt to depart from conventional transient liquid phase sintering practice, solid state vacuum sintering was studied in loose powder and in hot quasi-isostatically forged samples composed of commercial inert gas atomized (CIGA) or high purity Al powder. The high purity Al powder was generated by a gas atomization reaction synthesis (GARS) technique that results in spherical powder with a far thinner surface oxide. After vacuum sintering at 525°C for up to 100 hours, SEM results showed that the GARS Al powder achieved significantly advanced sintering stages, compared to the CIGA Al powder. Tensile results from the forged samples also showed that although its UTS is lower, 95MPa vs. 147MPa, the ductility of the GARS pure Al sample is higher than the CIGA Al sample. Forging also consolidated a model powder-based composite system composed of an Al matrix reinforced with quasicrystalline Al-Cu-Fe powders, where the same powder synthesis methods were compared. Auger surface analysis detected evidence of increased matrix/reinforcement interfacial bonding in the composite sample made from GARS powder by alloy inter-diffusion layer measurements, consistent with earlier tensile property measurements. The

[1] Reprinted from Journal of Light Metals, vol. 2-4, 2002, pp. 204 -214, with permission from Elsevier.

overall results indicated the significant potential of using Al powders produced with a thin, high purity surface oxide for simplifying current Al powder consolidation processing methods.

Keywords: Aluminum; Sintering; Powder metallurgy

1. INTRODUCTION

The need for lightweight, high performance engineering materials in automotive, transportation, and defense applications has driven development of Al-based powder metallurgy (P/M) parts and Al powder processed metal matrix composites (MMC) [1, 2]. The P/M Al parts are produced conventionally from blends of elemental and pre-alloyed powders, e.g., 201Al and 601Al (Alcoa designations), that are transient liquid phase sintered (TLPS) with properties that compete successfully for modest strength applications, replacing heavier Fe-base parts. The transient aspect of this type of sintering reaction refers to the tendency for the liquid phase, typically an Al-based eutectic composition containing either Cu, Mg, or Si, to begin solid state diffusion into adjacent Al-rich powders soon after its initial formation [3]. The microstructural limit on ductility of these materials may be traced to agglomeration or "stringers" of oxide shell fragments from the prior Al particle boundaries that are not redistributed during the TLPS process [3]. The limitations on strength of these TLPS parts can be related to inhomogeneities in the distribution of the liquid phase caused by the selection of coarse elemental constituents, for example [4]. There is also the need to control part distortion by minimizing liquid fraction [3]. Alternatively, Al-based MMC components typically are made from pre-alloyed powders that are blended with ceramic particulate, e.g., SiC, and consolidated in the solid state by a complicated series of hot compaction and deformation processes [5, 6]. Such MMC components may be tailored to

have superior specific strength and stiffness, while providing better thermal and mechanical fatigue and creep resistance at higher operating temperatures than those of monolithic, ingot-processed Al alloys.

The Al oxide coating on most commercially atomized Al and Al alloy powders essentially dictates the acceptable consolidation processing techniques and properties that are described above. In general, the oxide "shell" is a severe barrier to solid state sintering and, to some extent, can limit the alloy homogenization kinetics of transient liquid phase sintered Al-based parts. In fact, the Al oxide coating on most Al and Al alloy powders delays the solid state sintering of die pressed parts to such an extent that it renders solid state sintering impractical. This problem forced the development of the current transient liquid phase sintering approach for Al P/M parts. In turn, the TLPS process immediately imposed increased process temperature control and dimensional tolerance challenges on producers of these parts (see above). Minor Al P/M part distortion typically is overcome by repressing or coining operations [3]. These complexities can be compared to the relatively simple processing of Fe-based P/M parts that use solid state sintering and have very predictable shrinkage [7]. In current practice for Al-based MMC processing, the residual Al oxide coating fragments can significantly reduce ductility and fatigue strength [8] unless thoroughly distributed in the microstructure. A considerable amount of complexity is added [8] by the need for extensive hot deformation and interparticle shear during consolidation processing of particulate reinforced aluminum (PRA) composites [5, 6], to disperse the residual oxide stringers that can decorate the prior particle boundaries of the Al alloy powders. These disadvantages in processing control and complexity of both classes of Al powder processed materials motivated the development of an alternative Al and Al alloy powder synthesis technique [8], focusing on modification of the inert gas atomization process, a versatile, high volume production process.

A previous paper [9] gives a thorough discussion of the results of an extensive study of the surface reactions promoted during a gas atomization process. The prior study compared the surface oxide characteristics of different types of gas atomized Al powders, especially the differences between physisorbed and chemisorbed moisture contents of the oxide, and concluded that the high purity powders from the GARS process exhibit far less chemisorbed hydrogen in the oxide coating. The near-complete lack of chemisorbed hydrogen on the surface of the GARS Al powder was attributed, in part, to the capability to essentially eliminate residual moisture from the atomization spray process chamber by vacuum pumping and inert gas exchange prior to atomization. This capability compares to the common practice of inert gas purging of the spray chamber and a reliance on in-process powder "gettering" of the atmosphere contaminants in the spray chamber during commercial "inert" gas atomization (CIGA). Also, during a typical CIGA process [10, 11], a small percentage of oxygen (1-2%) is added to the inert atomization gas to promote oxidation of the Al powder surfaces. The other commercial powder involved in the previous study was atomized with a reducing "flue" gas but incorporated the introduction of ambient air in the immediate zone of the atomization nozzle for promoting oxidation and for powder transport out of the spray chamber. This powder was termed "commercial air atomized" (CAA) and was characterized by the highest content of chemisorbed hydrogen on the powder surfaces [9].

Both the CIGA and CAA powders are exposed purposefully to oxygen or air to provide an oxide passivation layer to minimize explosion hazards [11], although such Al powder is generally classified by the US Bureau of Mines in a “severe” explosibility hazard class [12]. Surprisingly, multiple tests of the minimum explosive concentration (MEC) of numerous batches of GARS Al powder at a commercial laboratory (Alcoa, New Kensington, PA) concluded that this new process produced “cleaner” Al powder with a reduced explosivity rating [9]. One batch of GARS Al powder was also subject to the complete battery of explosibility tests, MEC and 5 others [13], by an industrial collaborator at an independent

testing laboratory, Chatsworth Technology Limited in Southhampton, U.K., which documented a significant reduction in the hazard class of this new type of Al powder [13]. Apparently some characteristic of the thin, high purity oxide film on GARS Al powder is responsible for this improvement in powder handling safety, but its mechanism has remained unstudied, at this time.

Of direct relevance for the current work was the characterization of surface oxide thickness on the three types of Al powders in the previous study. Auger and TEM measurements [9] of the powder surface coatings indicated that the high purity GARS Al powder has an oxide thickness of about 5nm, compared to about 12-16nm for the CIGA and CAA powders. As a direct implication of the surface oxide thickness differences, a further study [14] was performed to compare the differences in sintering kinetics that were expected. Uniaxial die pressed cylinders with a green density of about 95% were made from CAA and GARS Al powder (dia. $< 45\mu m$) and were sintered in a purged nitrogen atmosphere while monitoring the sintering process with an electromagnetically-coupled acoustic transducer (EMAT). The EMAT study [14] concluded that a sintering temperature of only 500°C for 3 hrs. would promote sintering that was readily detectable in the GARS Al, while the CAA powder compacts did not sinter effectively at those conditions. However, sintering at 550°C promoted effective sintering in compacts made from both Al powder types [14].

Thus, we chose an intermediate temperature of 525°C for the current study that involves the sintering of tap densified GARS and CIGA Al powders to compare the more ideal situation of interparticle bonding from point contacts in high vacuum. The GARS process provided powder with a "thin" surface oxide test condition and the CIGA process provided powder with a "thick" surface oxide. This test of relative sintering activity from point contacts avoids the complications from powder surface oxides that are mechanically deformed and possibly cracked during die pressing, exposing fresh Al surface in the fissures for unimpeded

sintering. Interestingly, this point contact sintering study is also a simplified simulation of the final sintering reaction in a metal injection molded part that may be made eventually from Al powders. The use of vacuum sintering also removes the possibility of any competing powder surface reactions with a selected sintering atmosphere, e.g., nitrogen [15], which may promote sintering. Actually, vacuum sintering of Al parts in "continuously operated furnaces" has also been mentioned as an "important and interesting alternative" to nitrogen sintering in an industrial publication [3], as well. The results from another type of sintering situation will also be reported to compare the relative interparticle diffusion of alloying elements in a simplified MMC microstructure consisting of an Al matrix reinforced with Al-Cu-Fe alloy particulate, where either GARS or CIGA Al powders were used for the matrix. Also, either GARS or CIGA powders of the quasicrystalline Al-Cu-Fe alloy were used for the hard reinforcement particulate. In this test, a small amount of interparticle shear is introduced from quasi-isostatic hot (550°C) forging to full density. It is anticipated that interparticle bonding will be encouraged by the nearly-isotropic deformation of the particles at this high temperature, but the effects of the oxides on the prior particle boundaries can still be studied. Actually, only the interdiffusion effects in the composite microstructures will be reported, herein. However, the effects of prior particle boundary oxides on the mechanical properties of the isolated matrix microstructures will also be reported after consolidation of the same Al powder types by the same process steps.

2. EXPERIMENT PROCEDURE

A. Powder Materials

Commercial inert gas atomization (CIGA) processed Al powders were obtained from an

outside vendor. The CIGA Al powder had been evaluated thoroughly in earlier work [11] to characterize the surface oxide properties and its nominal purity is 99.7%. A different outside vendor supplied a batch of Al-Cu-Fe quasicrystal (QXL) alloy powder, also produced by CIGA, with the same nominal purity. A patented [17] gas atomization reaction synthesis (GARS) technique was used to produce 99.99% pure Al and $Al_{65}Cu_{23}Fe_{12}$ quasicrystal powders in the Ames Laboratory with atomization parameters provided previously [16]. The bulk chemical elements in as-atomized CIGA and GARS Al powders were also measured previously and are shown in Table 1 [16]. The as-atomized size yield of the GARS powders and the as-received CIGA powders were air classified to less than 10 μm. The size distributions were measured by a laser diffraction method and are given in Figs. 1 and 2. As shown in Fig. 1, there are relatively more fine particles in the CIGA Al powder than in the GARS Al powder. The quasicrystal powders also had slight differences in their size distributions, given in Fig. 2, which will be described below.

B. Pure Al Powder Sintering

Pure Al vacuum sintering experiments were done as following: first about one gram of fine Al powder, either CIGA or high purity GARS, was placed loosely into a small high purity, hard-fired alumina mold and hand tapped to settle any excess voids. Each mold was placed in a vacuum furnace which was evacuated slowly to 10^{-7} torr and heated to 525°C. Samples were held at this temperature for 24, 48, 72, or 100 hours. The sintering temperature was monitored by a thermocouple whose measuring junction was put just above the Al powder in the alumina mold. After sintering was completed, each mold was removed and carefully inverted on a clean surface, where the powder or sintered form fell out of the mold and was recorded in a macroscopic optical picture with a digital camera.

Table 1. Bulk powder chemical elements measurement of as-atomized pure aluminum powders [15]

Element	Al	Si (wt. %)	Fe (wt. %)	Mg (wt. %)	Cu (wt. %)	C (ppmw)	O (ppmw)	N (ppmw)
GARS	Balance	0.013	0.011	0.0002	<0.02	37	598	1
CIGA	Balance	0.11	0.17	<0.004	<0.005	84	5446	52

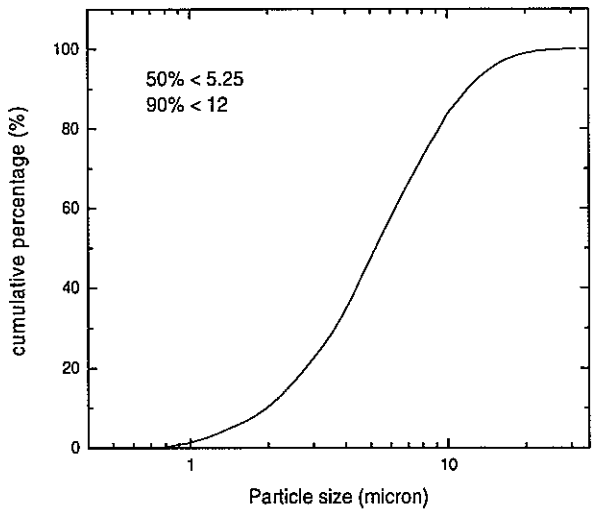

(a)

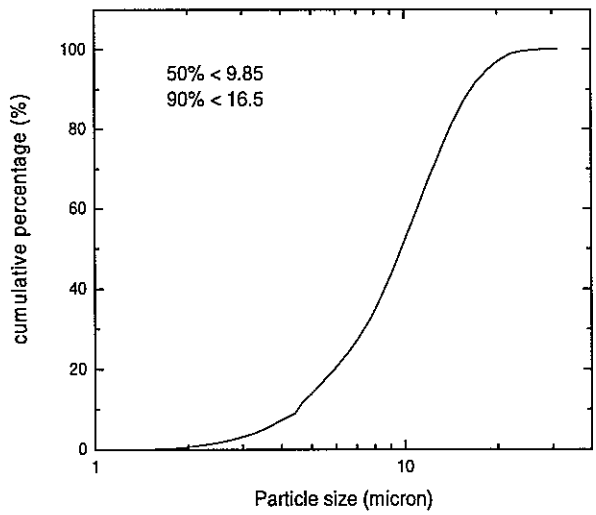

(b)

Figure 1. Size distribution of pure Al powders (a) CIGA Al powder (b) GARS Al powder.

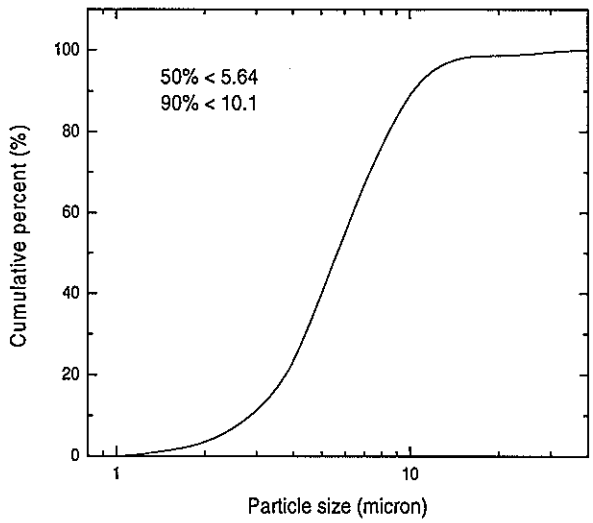

(a)

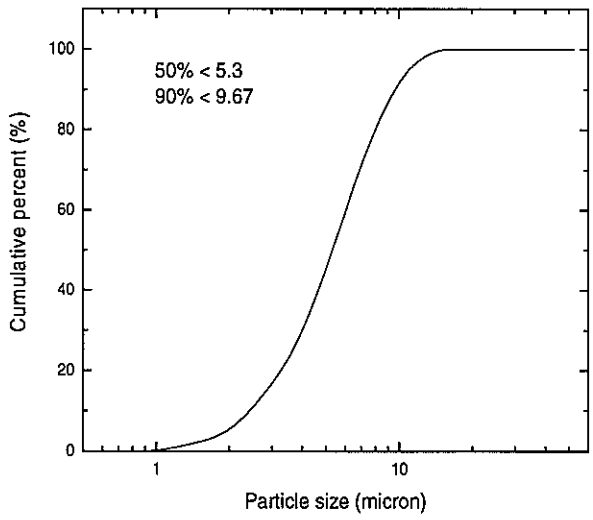

(b)

Figure 2. Size distribution of Al-Cu-Fe quasicrystal powders (a) CIGA QXL powder (b) GARS QXL powder.

C. Pure Al and Composite Materials Consolidation

Table 2 shows the nomenclature used for fully densified Al and Al/QXL composite samples. After air classification to dia. < 10μm, the quasicrystal powders were screened with a 20μm sieve to eliminate any residual large particles. Thus, the size distributions of the quasicrystal powders, given in Fig. 2, appear shifted to smaller sizes than that of the Al powders in Fig. 1. Previous work on a similar type of composite system [18] indicated that a minor population of larger QXL reinforcement particles promoted premature failure of the composite microstructure. Thus, the additional screening was performed to eliminate the residual oversize particles that are typical of the air classification process that was used. For both CIGA and GARS quasicrystal powders, 90% (cumulative volume fraction) of the quasicrystal powders size were less than 10μm and 100% of the quasicrystal powders size were less than 15 μm, as shown in Fig. 2.

Table 2. Powders used for pure Al matrix composite samples.

Sample name	Powders used
AF	CIGA Al powder (<10μm)
GF	GARS Al powder (< 10μm)
AFF	CIGA Al powder (<10μm) + CIGA quasicrystal powder (<10μm)
GFF	GARS Al powder (< 10μm) + GARS quasicrystal powder (<10μm)

For consolidation of the pure Al/QXL composite material, Al and quasicrystal powders were blended homogeneously by a high energy dynamic blending technology (HEDBT), a proprietary technique practiced by Ceracon, Inc. of Riverbank, CA. The volumetric loading of quasicrystal powders in both AFF and GFF samples was 30%. Each blended powder

sample was loaded into a cylindrical elastomeric mold and cold isostatic pressed (CIP) with a pressure of 200MPa, which was intended to produce a green density of 93% [19], based on the compressibility of pure Al powder. The green samples from CIP were forged, as described in Table 3, with a quasi-isostatic forging procedure by Ceracon. Pure Al samples were consolidated by the same CIP and forging procedures. The dimensions of the resulting pure Al and Al/QXL composite bars from forging were flattened to about 5.5 cm by 2.5 cm by 1 cm.

Table 3. Quasi-isostatic forging procedure.

Pre-heat Atmosphere	Forge Temp.	Soak at Temp.	Forge Pressure	Dwell at Pressure
99.999% Argon	550 °C	10 min	635 MPa	5 second

D. Other tests

The Archimedes technique was used to measure the density of each sample. The elastic modulus and density distribution of each sample was measured by an ultrasonic method. Tensile tests of consolidated pure Al and AL/QXL composites were performed on an Instron model 1125 tensile test machine under 1.27 mm per minute monotonic loading. Tensile sample dimensions were in 6.35 mm in diameter and 25.4 mm in uniform gauge length, according to ASTM recommendations [20]. The forged Al samples were polished and etched by Kroll's solution (1 - 3 vol.% HF, 2 - 6 vol.% HNO_3 and rest H_2O), and were observed on an AMRAY 1845 field emission scanning electron microscope (FE-SEM). Fractography of pure Al tensile samples also was performed on the FE-SEM. Average grain sizes of AF and GF elemental Al samples were measured by orientation imaging microscopy (OIM) on the FE-SEM. The grain aspect ratio of AF and GF samples were measured on two randomly chosen areas. The chemical compositions at the interface of Al matrix and

quasicrystal particles in AFF and GFF composite materials were measured with a JAMP-7830F field emission Auger microprobe. The probe size of 25 nm was used for Auger measurement.

3. RESULTS

A. Vacuum Sintering of Pure Al Powders

Fig. 3 shows a comparison of Al powder samples that were heated in vacuum at 525°C. As shown in Fig. 3a, the as-exposed CIGA Al sample poured out of the mold as loose powder particles after up to72 hours of attempted sintering. Only after 100 hours of exposure to 525°C did the CIGA Al show the fragile shape retention that indicates the early stages of sintering. In contrast, the as-exposed, high purity GARS Al sample in Fig. 3c exhibited fragile shape retention after only 24 hours of sintering. After progressively longer sintering times, 48, 72, and 100 hrs., the sintered shape gained noticeable strength and began to exhibit shrinkage, Fig. 3f, as there was a noticeably loose fit of the sintered sample in the mold.

SEM micrographs in Fig. 4 and 5 further compare the interparticle bonding of the two kinds of Al powder samples after selected sintering times. The CIGA Al powders in Fig. 4a showed essentially a complete lack of sintering, with no observable sintered neck formation, even between the finest particles. On the other hand, the GARS Al powders showed well-developed, large radius sintering necks between large and small powders in Fig. 4b. The representative micrograph of the CIGA sample in Fig. 5a shows that early-stage, sharp radius sintering necks (see lower right corner of micrograph) finally began to form between the particles after 100 hr. of exposure to 525°C. For the same sintering time in the GARS Al

sample of Fig 5b, sintered neck formation looks very extensive and some particle coalescence has begun.

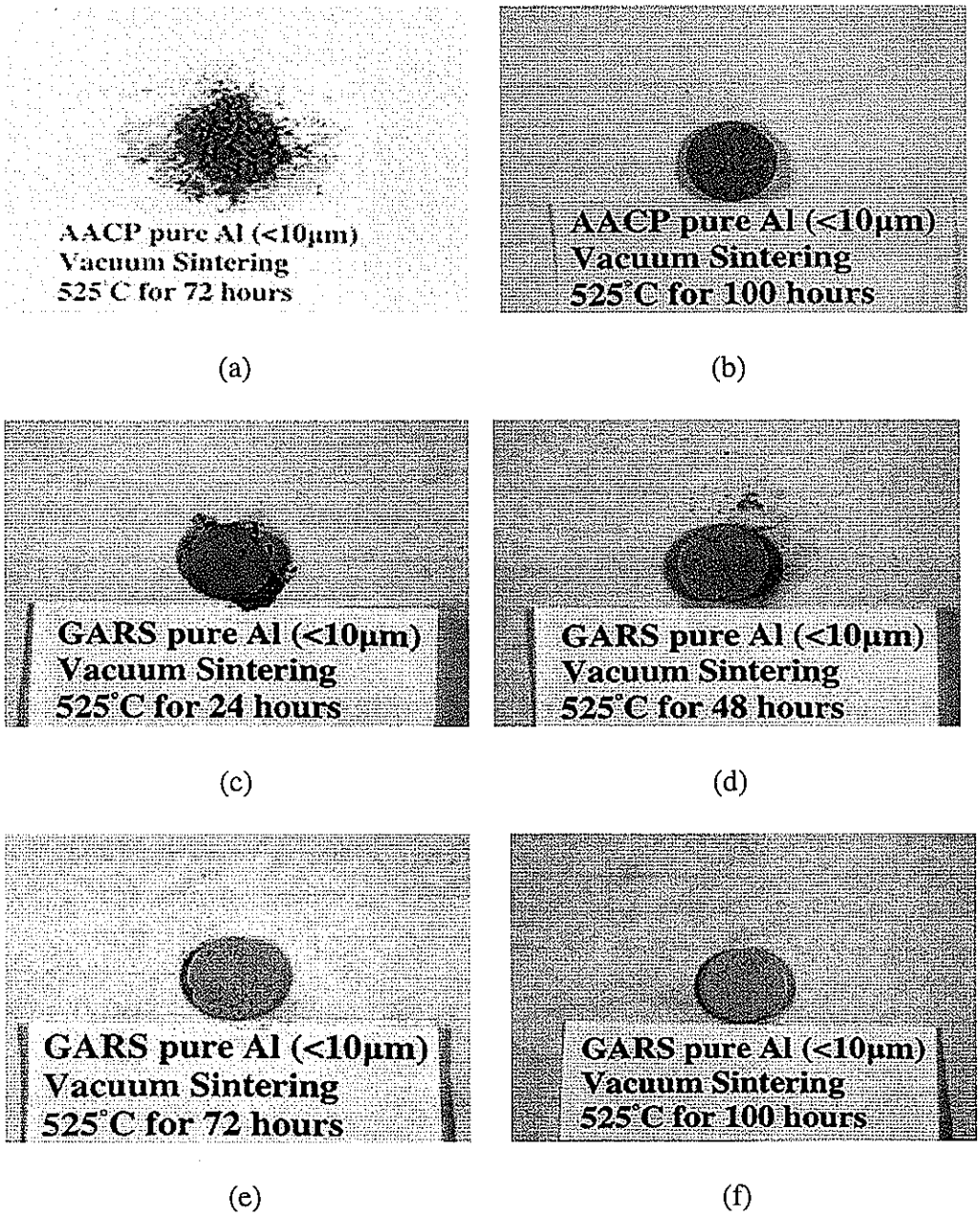

Figure 3. Micrographs of as received pure Al sintering samples vacuum sintered at 525°C. The "AACP" label on (a) and (b) is equivalent to the CIGA Al powder designation in the text.

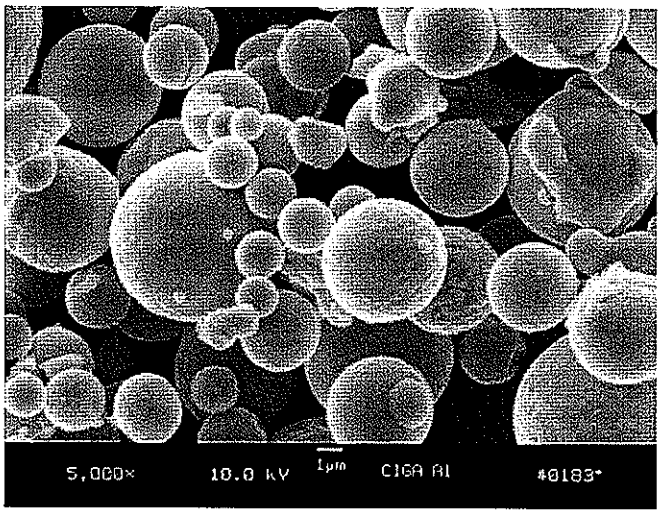

(a)

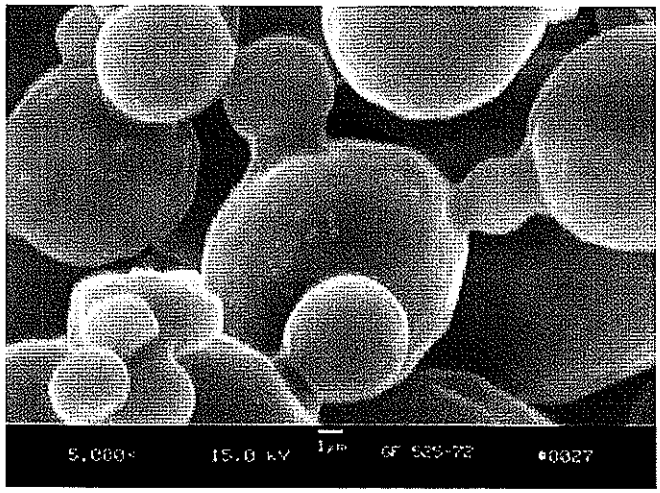

(b)

Figure 4. SEM pictures of the powders vacuum sintered at 525°C for 72 hours (a) CIGA Al powder (b) GARS Al powder.

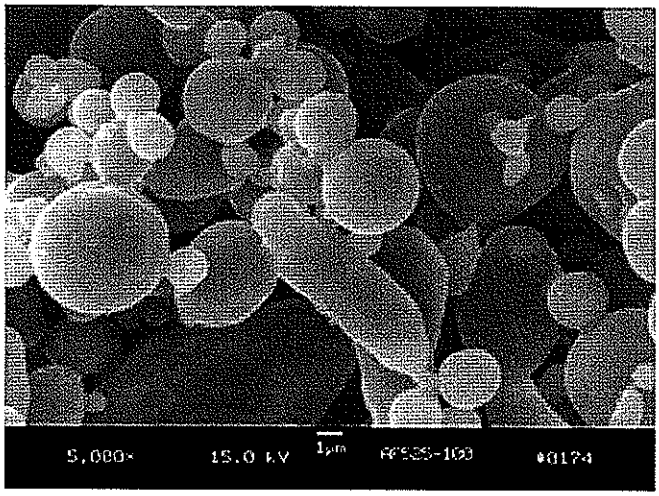

(a)

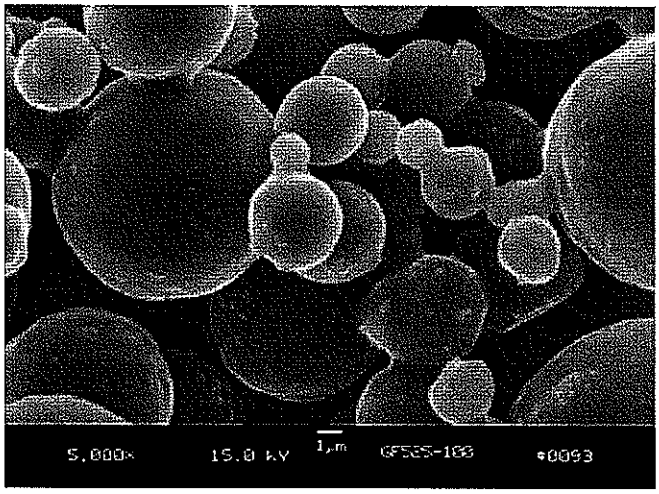

(b)

Figure 5. SEM pictures of the powders vacuum sintered at 525°C for 100 hours, (a) CIGA Al powder (b) GARS Al powder.

B. General microstructures of pure Al forging samples

The general microstructures of AF and GF Al samples after consolidation are shown in Fig. 6, where a mild etching has enhanced the light contrast of the prior particle boundary regions of both samples. The measured density in Table 4 shows that the samples are fully dense. The average grain sizes measured by OIM in the SEM indicate that the grains in both samples are still relatively small after the hot forging process, as Table 4 indicates. Also, the grain size retains the same size ranking of the original Al powders, while displaying a slightly smaller grain size than the average particle diameter of each powder particle size distribution in Fig. 1. While the as-atomized powders probably were not single crystals [21], the Al grains did not appear to grow beyond the original particle boundaries because of the remnants of surface oxide that remain, even in the GARS Al sample in Fig. 6b.

It is also somewhat apparent, especially in Fig. 6b, that the grains have a minor elongation which is normal to the forging direction (horizontal in the micrographs of Fig. 6). Although this grain elongation may cause some anisotropy of the tensile properties, the small dimensions of the forged samples permitted only longitudinal tensile sample fabrication. Computer-aided quantitative metallography also provided a measurement of the grain aspect ratio of both AF and GF samples, as shown in Table 5, which is very consistent in terms of both average values and standard deviation.

Table 4. Summary of density and grain size measurement of AF and GF pure Al sample.

Sample	Measured density (g/cm^3)	Average grain size (μm)
AF	2.7	4.3
GF	2.7	6.2

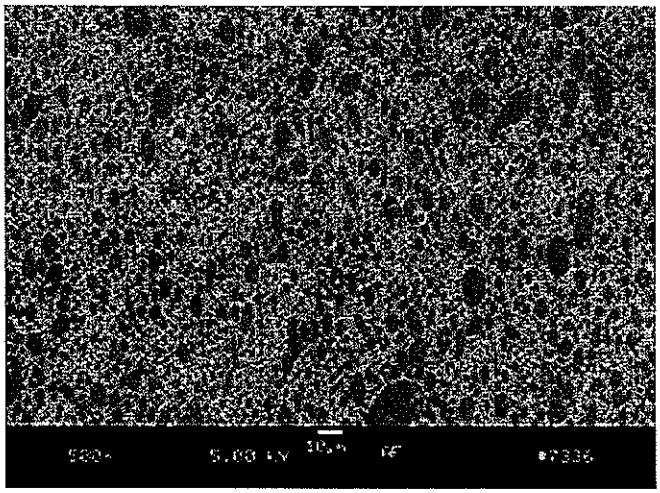

(a)

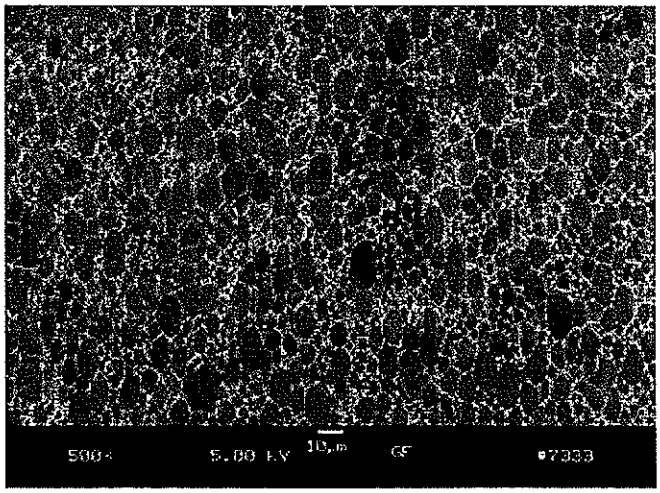

(b)

Figure 6. Microstructures of (a) AF sample and (b) GF sample.

Table 5. Measurement of grain aspect ratio of AF and GF pure Al sample.

Sample	Average aspect ratio	Standard deviation
AF	1.69	0.48
GF	1.68	0.51

C. Tensile properties of pure Al samples

An example of the tensile test behavior of the AF and GF Al samples is given in Fig. 7. A summary of tensile property measurements of the samples is shown in Table 6. The ultimate tensile strength (UTS) of the AF samples, 145 MPa, is much higher than that of the GF samples, 95 MPa. The 0.2% offset yield strength, $\sigma_{0.2}$, of the AF samples is also 35 MPa higher than that of the GF samples, as indicated in Table 6. Both the UTS and yield strength increases in the AF samples may be helped by some impurity-induced solid solution strengthening and/or precipitation hardening within the AF sample grains. In addition, the reduced grain size of the AF samples may also provide an increment of Hall-Petch strengthening (see flow stress results below). In contrast to the strength results, the tensile ductility of the AF samples is significantly lower than GF samples, when comparing both the reduction of area and the strain at the UTS point and the fracture strain. At the beginning stage of the tensile test, i.e., lower than about 0.1% strain, the stress-strain curves of the AF and GF samples are overlapped in the elastic region. But later, the AF sample shows a higher work hardening tendency than the GF sample, where the strain at UTS of AF, 6.3%, is about 6% lower than that of GF, for the samples in Fig. 7.

The fractography of AF and GF failed tensile samples are shown in Fig. 8. The fracture surface of AF shows much more fine detail, resembling small dimples, which may be caused by a combination of ductile failure of sintered regions and brittle failure of the many prior particle boundary regions. The fracture surface of GF is composed of relatively large-scale ductile shear lips, common for a high purity fcc metal and indicative of generally effective sintering of adjacent grains.

The flow stresses of AF and GF tensile samples at several different strain levels are compared in Fig. 9 to the Hall-Petch predictions from the tensile data on large-grained, high

purity Al samples from reference [22]. The comparison indicates that flow stresses of the GF samples are very consistent with linear extrapolations of the data from the former study. Apparently, a Hall-Petch relationship that uses the measured grain size in Table 4 as the dislocation barrier spacing works quite well for predicting the flow stress of the GF sample. Unfortunately, the measured flow stresses of the AF sample fell well above the predicted level for two of the same strain levels, as indicated by the arrows in Fig. 9. This behavior may indicate that the dislocation barrier spacing for the AF sample is considerably closer than the grain size measurement in Table 4, perhaps because of a higher impurity concentration within the Al grains.

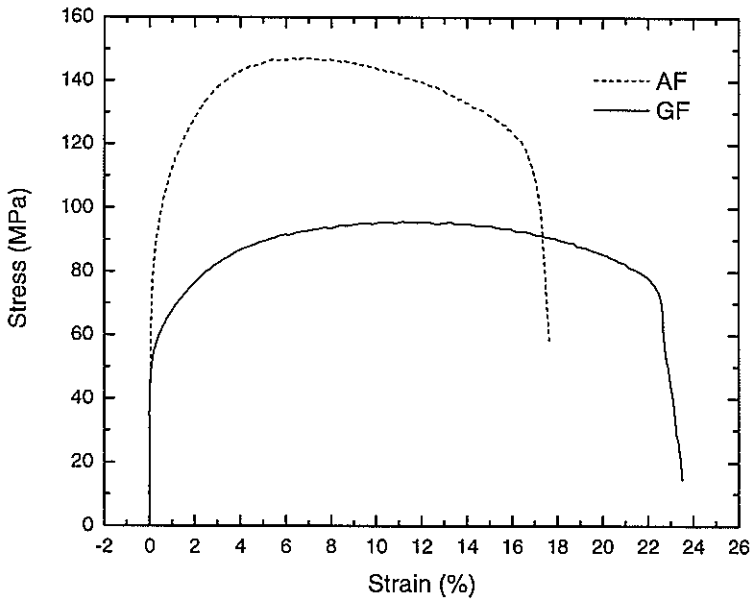

Figure 7. Tensile stress-strain curves of (a) AF sample and (b) GF sample.

Table 6. Tensile properties of AF and GF samples.

Sample	UTS (MPa)	$\sigma_{0.2}$ (MPa)	R.A. (%)	Strain at UTS (%)	Measured elastic modulus (GPa)
AF	147^{+1}_{-1}	88^{+1}_{-1}	44	$6.3^{+0.5}_{-0.5}$	71
GF	95^{+1}_{-1}	53^{+2}_{-2}	50	$11.9^{+1.4}_{-1.4}$	71

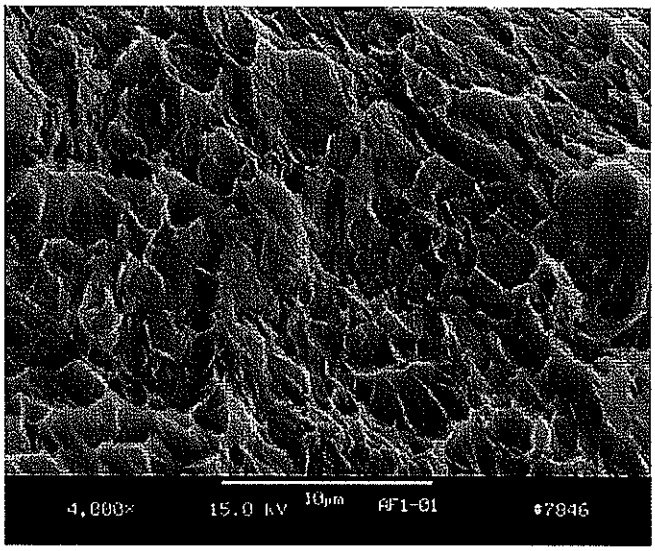

(a)

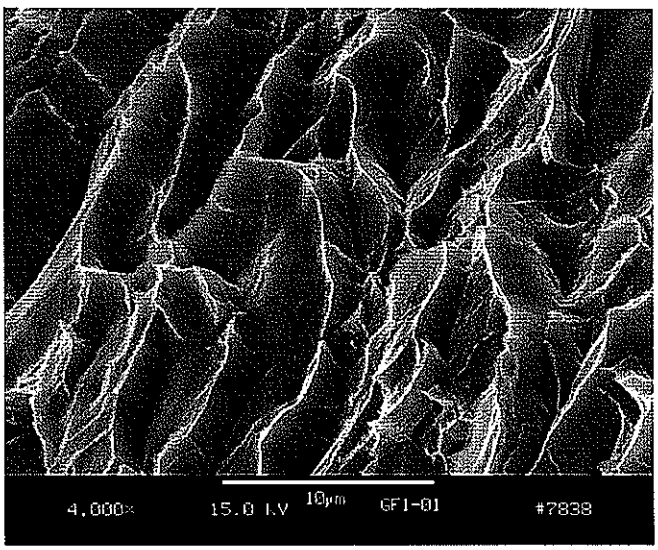

(b)

Figure 8. Fracture surfaces of (a) AF tensile sample, and (b) GF tensile sample.

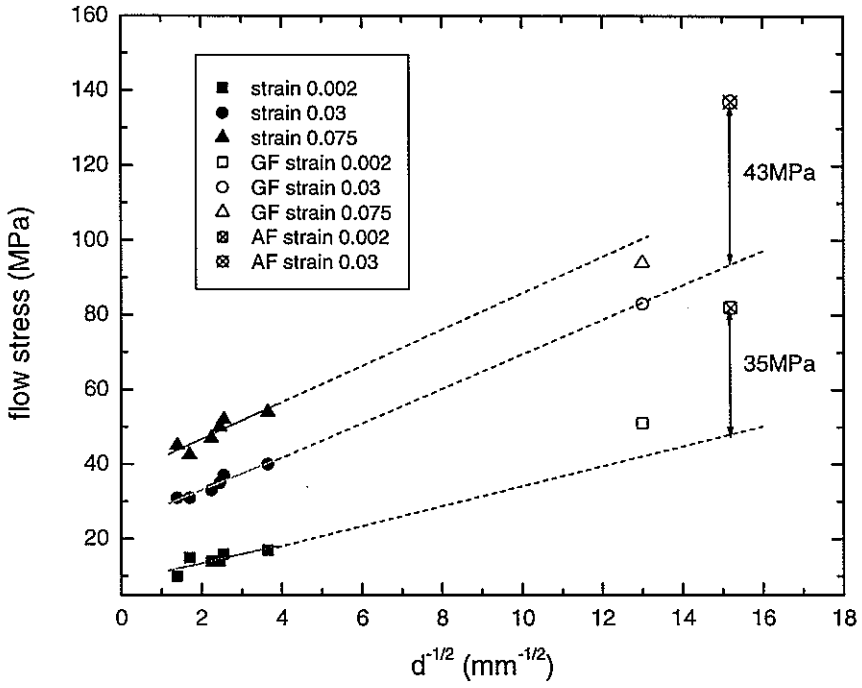

Figure 9. Flow stresses of AF and GF samples at different strain levels compared with high purity Al tensile data in reference [16] and Hall-Petch prediction.

D. Auger measurement on the interface of Al-Cu-Fe quasicrystal reinforcement particles and pure Al matrix

The general appearances of the microstructures of AFF and GFF composites after consolidation are shown in Fig. 10. A fairly uniform distribution of the spherical quasicrystal reinforcement in the composites can be seen from the figures. There are relatively more fine QXL particles in GFF than in AFF, which can be also seen from the micrographs. As Table 7 indicates, the samples are essentially fully dense compared with the theoretical density.

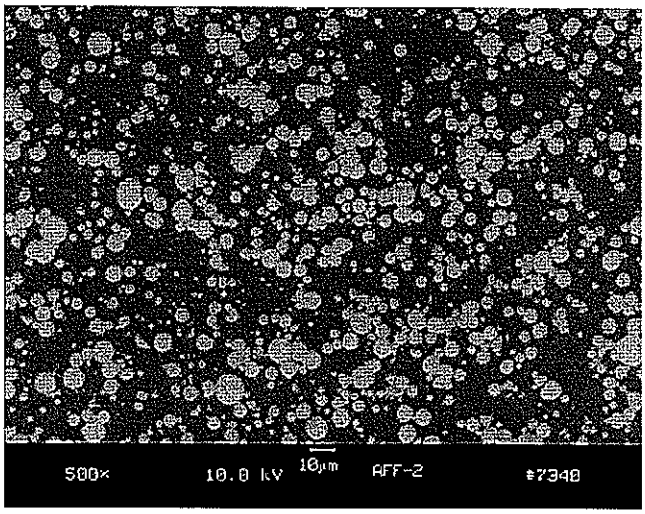

(a)

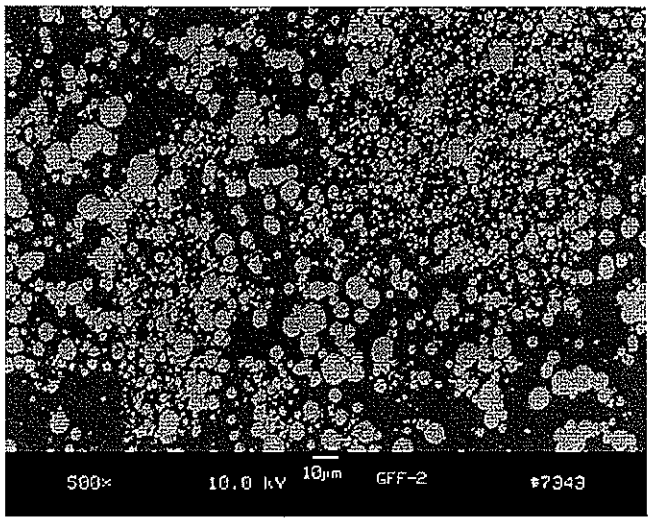

(b)

Figure 10. Microstructures of (a) AFF sample and (b) GFF sample.

Table 7. Summary of density measurements of AFF and GFF composite samples.

Sample	Measured density (g/cm^3)	Theoretical density (g/cm^3)
AFF	3.28	3.3
GFF	3.28	

The fracture surfaces of AFF and GFF tensile samples look very similar, as shown in Fig. 11. Generally, comparative SEM fractography of both mirror halves of the fracture surfaces of the tensile samples shows that all QXL reinforcement particles on the fracture surface were broken and that no particle pull-out appeared. All of the samples displayed a mixed fracture mechanism that combined effects from the matrix and reinforcement. Ductile tearing ridges and micro-dimples appear in the Al matrix area around prior Al particles, most noticeably in the AFF sample. Fracture occurred by brittle cleavage across the quasicrystal particles, which seem to have a very fine microstructure that modulates the cleavage fracture path.

In the high magnification SEM micrographs of Fig. 12, the interface region is shown between a spherical quasicrystal particle and the Al matrix in polished cross-sections of both the AFF and GFF samples that had been lightly etched. Typical Auger results of the Al, Cu, Fe and O levels at the interface regions, shown in Fig. 12, are given in Fig. 13. After several Auger measurements on both kinds of samples, the following phenomenon can be observed: first, the relative concentration of oxygen at the Al/QXL interfaces of the GFF sample is much lower than that of the AFF samples. Second, it was found that after the Fe concentration drops to zero at the interface location, the Cu concentration reaches out from the QXL particle and drops to zero at a detectable displacement away from the interface in both AFF and GFF samples. This measurement indicates that a diffused layer of Cu extends into the Al matrix beyond the interface area which is more significant in the GFF sample than in the AFF sample.

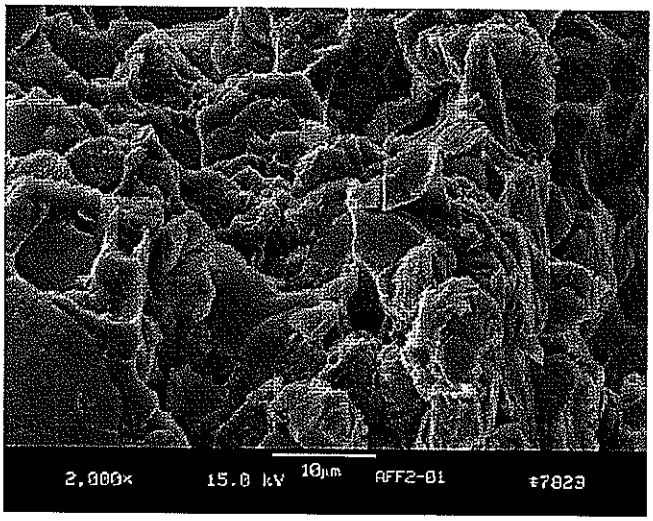

(a)

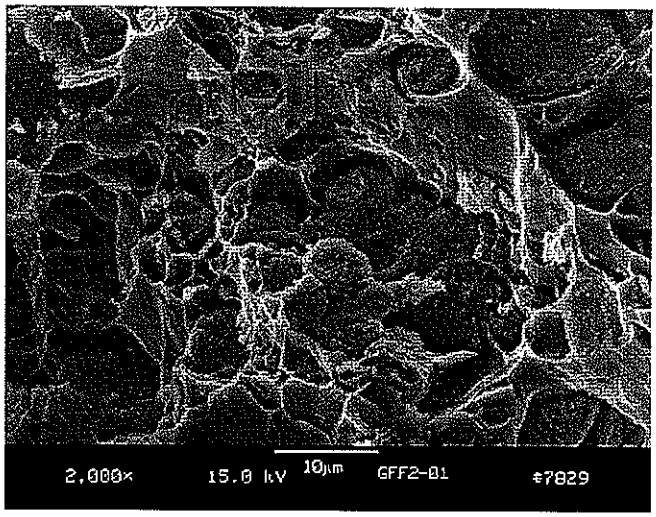

(b)

Figure 11. Fracture surfaces of (a) AFF tensile sample, and (b) GFF tensile sample.

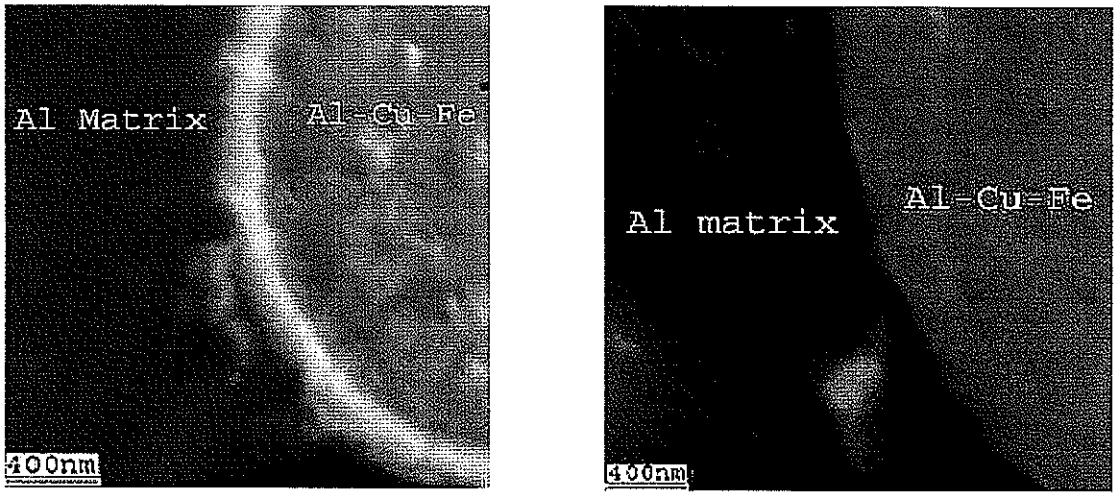

(a) (b)

Figure 12. SEM micrographs of the interface area of Al/QXL in (a) AFF sample (b) GFF sample.

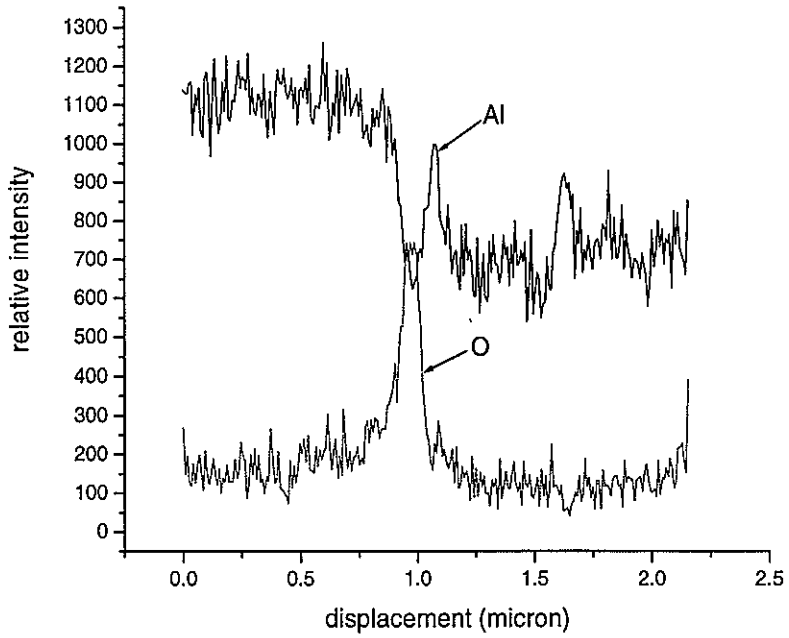

(a)

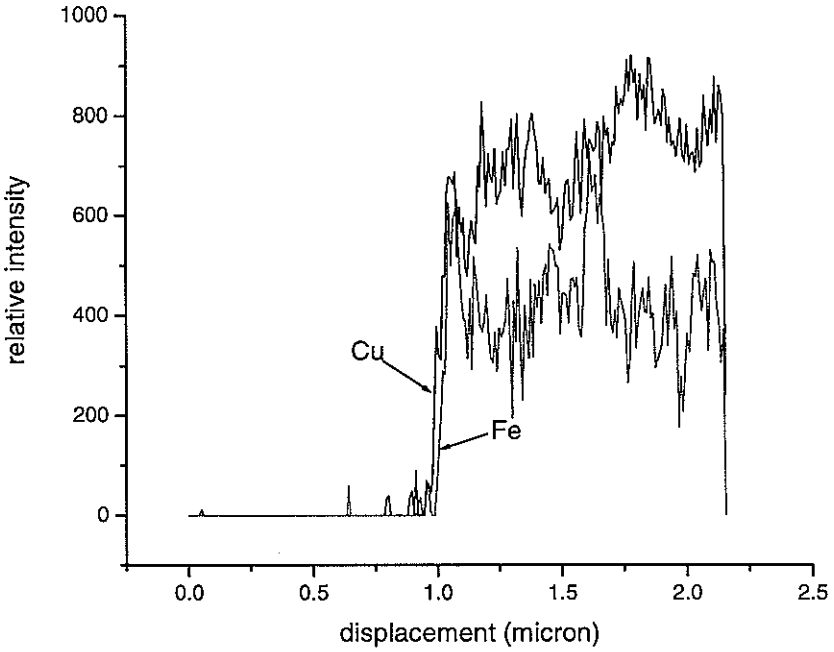
1000
800
600
400
200
0
relative intensity
Cu
Fe
0.0
0.5
1.0
1.5
2.0
2.5
displacement (micron)

(b)

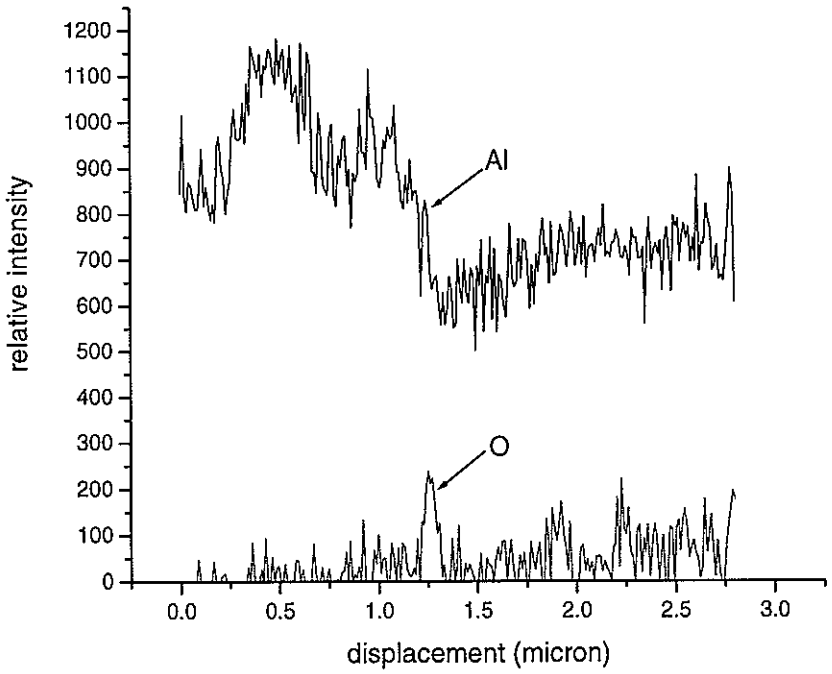
1200
1100
1000
900
800
700
600
500
400
300
200
100
0
relative intensity
Al
O
0.0
0.5
1.0
1.5
2.0
2.5
3.0
displacement (micron)

(c)

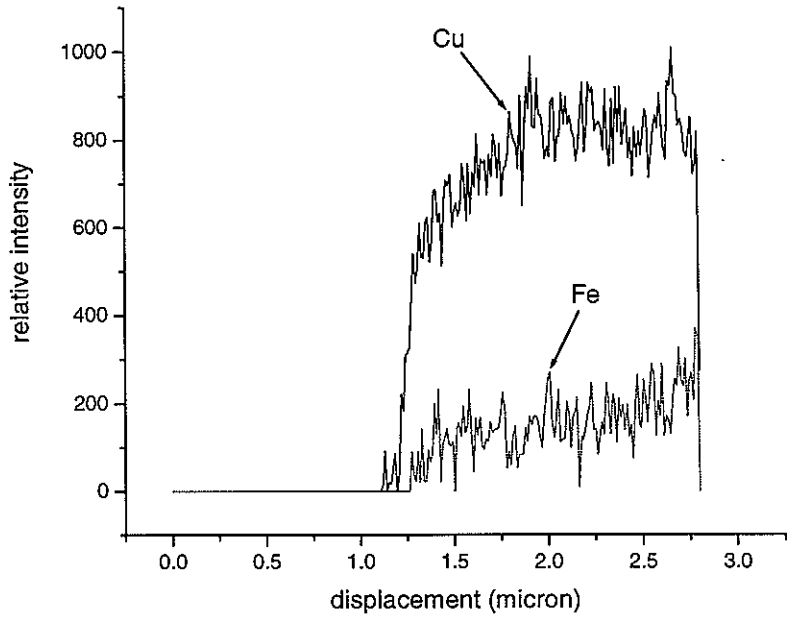

(d)

Figure 13. Auger line scan of Al, Cu, Fe at the interface of Al matrix and on QXL particle

(a) Al and O scan on AFF sample,

(b) Cu and Fe scan on AFF sample,

(c) Al and O scan on GFF sample,

(d) Cu and Fe scan on GFF sample.

4. DISCUSSION

Results of the vacuum sintering experiments indicate that CIGA Al powder needs about 3 times more exposure to 525°C to develop sintering necks with some detectable strength, compared to GARS Al powder. The large difference in the sintering kinetics between these two kinds of Al powders can be directly related to there surface composition, especially oxide thickness. As previously mentioned, extensive studies on the surface chemistry were

performed [9], where the average oxide thickness measurements of GARS Al, 5nm, and CIGA Al powders, 16nm, were obtained from Auger depth profiling measurements and TEM. The bulk oxygen content of the aluminum powders determined by an inert gas fusion (IGF) technique also showed that the GARS Al powder has only 800 ± 50 ppmw oxygen, while the CIGA powder has 2600 ± 80 ppmw oxygen as a contaminant. Quadrapole mass spectrometry (QMS) measurements on the quantity of physisorbed and chemisorbed water on the powder surfaces showed that the GARS Al powders have far less chemisorbed water incorporated into the oxide film than the CIGA Al powders. The QMS measurements also verified that the chemisorbed water cannot be removed by vacuum heating until a temperature of about 550°C is reached. The high temperature stability of the chemisorbed hydrogen implies that it can be detrimental to powder sintering, even if vacuum degassing of Al powder compacts with open porosity is conducted at a lower temperature for extended time periods. As previously mentioned, in-situ characterization of the sintering behavior of die pressed (94% dense) CIGA Al and GARS Al powders has been done by electromagnetic acoustic transducer (EMAT) technology recently by J.C.Foley et al. [14]. The results indicated that the commercial Al powder compact did not sinter, but the GARS Al powder compact showed very significant sintering in a 500°C furnace with a nitrogen purged atmosphere.

Figure 14 provides additional microstructural perspective of sintering development between tap densified loose GARS Al powders after 100 hours of vacuum sintering at 525°C. Well-developed necks apparently have formed extensively between the fine Al particles, as Fig. 14 reveals. According to a description of the geometric changes that occur during solid state sintering of spherical powders by R.M.German, there are roughly three sintering stages, beginning from a point contact condition in tap-densified loose powders [23]. The initial stage of sintering is characterized by the growth of the sinter bond from initial loose powder contacts as shown in fig.15 (b). In the initial stage of sintering, the sintering necks have a

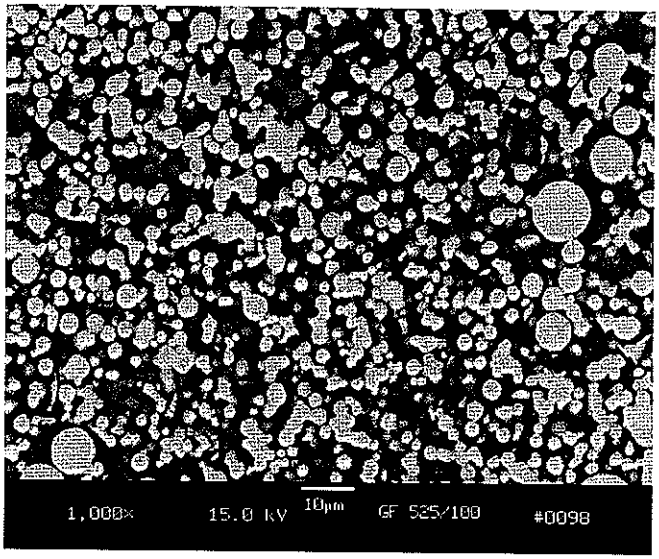

Figure 14. Cross section view of 100 hours vacuum sintering GF sample at 525°C.

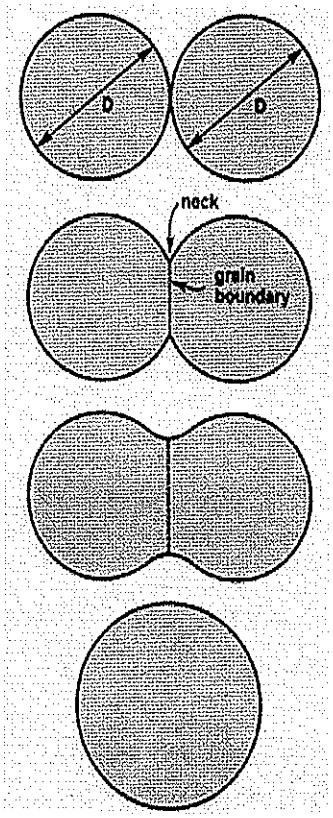

(a) Initial point contact

(b) Early stage neck growth

(c) Late stage neck growth

(d) Terminal condition fully coalesced spheres, where the final dia.= 1.26D.

Figure 15. Two sphere point contact sintering model [18].

small diameter relative to the particle diameter and grow independent of one another. The initial stage ends when the necks begin to impinge at a neck size ratio of approximately 0.3, where the intermediate stage of sintering begins, as shown in fig.15 (c). Although porosity is still very high and some independently growing necks still appear in the GARS Al powder sample shown in Fig. 14, many sintering necks have progressed beyond of initial stage and clearly into the intermediate stage. These experiments suggest that Al powders produced with a thin, high purity surface oxide, e.g., the GARS Al powder of this study, may provide an opportunity for consolidation processing by binder-assisted injection molding and solid state sintering with the proper size distribution and binder selections. The binder selection and development of a debinding cycle that may be used for MIM processing of GARS Al must, of course, be designed to minimize any negative impact on the powder surface chemistry.

It should be noted that some difficulty is involved in quantitative evaluation of loose powder sintering by microstructural analysis of the neck/particle diameter ratio, especially for fine spherical powders that may have as-atomized particle agglomerates. Thus, sintering experiments have been started that rely on measurements of the change in total surface area of the Al powder samples by a BET technique, as a function of vacuum sintering time and temperature, including 525°C. The BET results will give us a more quantitative comparison of the sintering kinetics of both CIGA and GARS powders and a determination of the activation energy for sintering. In order to form the sintering neck between two loosely contacted Al powders, Al must diffuse through the oxide that exists on both powder surfaces. Any differences in sintering kinetics and activation energy between the two kinds of powders can be explained primarily by the differences in their surface oxide thickness. An analysis of the future sintering kinetics results will attempt to model these differences.

The tensile test results and fractography evaluation of the fully densified AF and GF samples

revealed some significant differences in strength and ductility that need to be pursued further by detailed microstructural analysis. While the Hall-Petch relationship fits the apparent grain size of the GF sample, the dislocation barrier spacing of the AF sample is much finer in scale than the apparent grain size. For this reason, TEM analysis has been initiated that will compare the microstructures at high spatial resolution. The TEM analysis will utilize convergent beam electron diffraction and energy dispersive spectroscopy capabilities to determine any differences in precipitate phases or soluble impurity concentrations. An opportunity also exists in the new TEM work to compare the grain size evolution of fully densified samples at various sintering times and temperatures. The potential for simplification of Al P/M part fabrication by direct powder forging of CIP compacts or by die-pressing and solid state sintering of Al and Al alloy powders produced with a thin, high purity surface oxide appears promising. In fact, some recent work [24] with direct powder hot extrusion of Al-Fe-Ce alloy powder made by the GARS method, supports the prospects for significant reduction of the processing steps required for high performance Al alloy bars and mill shapes, compared to that required for such mill shapes made from CIGA or CAA powders.

In a further analysis of interdiffusion in the fully densified GFF and AFF composite samples, Fig. 13 (b) shows that the Cu and Fe compositions in the Al/QXL interface area of the AFF sample drop to zero at nearly the same measurement distance. In contrast, Fig. 13 (d) indicates that the Cu level drops to zero about 0.2 μm beyond the Fe zero point in the GFF sample. From the reference [25], the impurity diffusion coefficient of Cu in fcc-Al at 550°C, D_{Cu}, is $1.4\times10^{-13} m^2/s$, if we assume that there is a "clean" interface between Al matrix and QXL particles without any oxide layer to resist Cu diffusion. After the sample was heated at 550°C for 10 minutes of forging processing, the Cu diffusion distance is predicted to correspond to:

$$x \approx \sqrt{D_{Cu} t} = \sqrt{1.4 \times 10^{-13} m^2 / s \times 600 s} = 9.17 \mu m. \qquad (1)$$

We can also calculate the actual diffusion coefficient of Cu, $D_{Cu}^{'}$ across the Al/QXL interface by using the experimental Cu diffusion distance of 0.2 μm.

$$D_{Cu}^{'} \approx \frac{x^2}{t} = \frac{\left(0.2 \times 10^{-6}\right)^2}{600} = 6.7 \times 10^{-17} m^2 / s. \qquad (2)$$

From comparison of the above calculations, it is shown that the experimental diffusion distance of Cu is much lower than the ideal diffusion distance value and $D_{Cu}^{'} << D_{Cu}$, assuming a readily available source of Cu. However, the reason for the extremely small interdiffusion of Cu and Fe into the fcc-Al may be due, in part, to the effect of the unusually low diffusion coefficients of these and other alloy constituents, e.g., Fe, Co, and Ni, in Al-based QXL phases [26, 27]. While Cu diffusion is not specifically included in the previous results, the diffusion coefficient for Fe in two similar Al-based quasicrystalline phases ranges from 10^{-15} to 10^{-18} at 800°K [26, 27], in good agreement with the experimental estimate of 10^{-17}. While small in extent, a finite amount of Cu appears to have diffused into the Al matrix (most apparent in the GFF sample) and dissolved into solution near the interface, presumably increasing the bond strength between QXL reinforcement particles and the Al matrix. Good bonding can provide a better load transfer from matrix to reinforcement particles and, hence, increase the yield strength and tensile strength, especially for the GFF sample.

The difference between the Cu diffusion distance in GFF and AFF samples can also be explained by the difference of relative concentration of oxygen in the QXL/Al interface of these two kinds of samples which is caused by the different powders used in P/M processing. Fig.12 shows two SEM micrographs of the interface areas in AFF and GFF samples

respectively. In the AFF sample of Fig. 12a, a very obvious oxide and impurity layer can be seen around the Al/QXL interface. The Auger scan across this interface, in Fig. 13a, gives a relatively high oxygen peak at the interface position. In the SEM micrograph of the GFF sample, all the interface areas appear like Fig.12 (b), without apparent charging from a heavy oxide layer, thus it gives a much lower oxygen peak during the Auger scan, in Fig. 13c. For this GFF sample, the powders used are produced by the GARS technique that can result in a relatively "clean" surface on the powders [9, 28, 29]. For the AFF sample, the Al and QXL powders used in the experiment were produced by the CIGA method. Although the atomization spray chamber in the CIGA technique may be partially dried by inert gas purging prior to the start of the process, water has been reported to be chemisorbed into the oxide film, forming aluminum hydroxides, as well as being physisorbed on to the powder surfaces [30]. The excessive oxide coating on commercial purity Al powder may resist the diffusion of the Cu and Fe elements in the interface and, hence, partially degrade the interface bonding between the matrix and the QXL particles. It may also have an effect on the bonding between Al/Al matrix particles, because of the need for interparticle diffusion during the solid state sintering.

Thus, although the AF matrix contributes higher yield strength for the combined strength of the AFF composite material, the relatively weak interface may induce premature composite failure at lower UTS. The UTS and yield strength of AFF sample are 310MPa and 265MPa, respectively. The UTS and yield strength of GFF sample are 304MPa and 227MPa, respectively. The percentage increase of UTS (220%) and yield strength (328%) of the GFF sample are much higher than those of the AFF sample (201% and 111% for UTS and Y.S., respectively) [31]. All of the above experimental results show that GARS powders can promote enhanced solid state sintering and better bonding strength between matrix and reinforcement particles during composite material consolidation, compared to commercial gas atomized powders. This may provide advantages for GARS powders over CIGA

powders in Al matrix MMC consolidation processes because many complex procedures, such as canning, hot degassing and hot extrusion, may be eliminated by using Al powders produced with such a thin, high purity surface oxide.

5. CONCLUSIONS

Solid state vacuum sintering was studied in tap densified powder and in hot quasi-isostatically forged samples composed of commercial inert gas atomized or high purity Al powder, generated by a gas atomization reaction synthesis technique. The GARS process results in spherical Al powder with a far thinner surface oxide. After vacuum sintering at 525°C for up to 100 hours, SEM results show that the GARS Al powder achieved significantly advanced sintering stages, compared to the CIGA Al powder. Tensile results from the forged samples also show that although its UTS is lower, 95MPa vs. 147MPa, the ductility of the GARS pure Al sample is higher than that of the CIGA Al sample. Forging also consolidated a model powder-based composite system composed of an Al matrix reinforced with quasicrystalline Al-Cu-Fe powders, where the same powder synthesis methods were compared. Auger surface analysis detected evidence of increased matrix/reinforcement interfacial bonding in the composite sample made from GARS powder by alloy inter-diffusion layer measurements, consistent with earlier tensile property measurements. The overall results indicate the enhanced ability of GARS-processed Al and Al alloy powders for solid state sintering, which may lead to simplification of current Al powder consolidation processing methods.

ACKNOWLEDGMENTS

The authors greatly appreciate the assistance of Mr. Henry Meeks of Ceracon, Inc. for the HEDBT blending and the quasi-isostatic forging. Also, the assistance of the Materials Preparation Center of the Ames Laboratory is acknowledged for the SEM studies, performed by Mr. Fran Laabs, the automated image analysis, performed by Mr. Hal Sailsbury, the Auger measurements, performed by Mr. Jim Anderegg, and the tensile testing, involving Mr. Arne Swanson. The ultrasonic measurements were performed by Mr. Dan Barnard. The funding of this project from DOE Basic Energy Sciences under contract number W-7405-Eng-82 also is gratefully acknowledged.

REFERENCES

1. J.E.Allison, G.S.Cole, Metal-Matrix Composites in the Automotive Industry: Opportunities and Challenges, JOM, 45 (1) (1993), 19-24.
2. C.K.Narula, J.E.Allison, Advanced Materials for Automobiles, CHEMTECH, 26 (11) (1996), 48.
3. H.C.Neubing, G.Jangg, Sintering of Aluminum Parts: The State-Of-The-Art, Metal Powder Report, 42 (5) (1987) 354-358.
4. W.Kehl, H.F.Fischmeister, Liquid Phase Sintering of Al-Cu Compacts, Powder Metallurgy, 23 (3) (1980) 113-119.
5. N.Chawla, C.Andres, J.W.Jones and J.E. Allison, Effect of SiC Volume Fraction and Particle Size on the Fatigue Resistance of a 2080 Al/SiC_p Composite, Metallurgical and Materials Transactions A, 29A (1998) 2843.

6. N.Chawla, U.Habel, Y.L.Shen, C.Andres, J.W.Jones, J.E.Allison, The Effect of Matrix Microstructure on the Tensile and Fatigue Behavior of SiC Particle Reinforced 2080 Al Matrix Composites, Metallurgical and Materials Transactions A, 31A, (2000), 531.
7. Private communication with Rohith Shivanath of Stackpole Limited, July 2001.
8. I.E.Anderson, J.C.Foley and J.F.Flumerfelt, Simplified Aluminum Powder Metal Processing Routes for Automotive Applications, Proceedings of the First International Conference on Powder Metallurgy Aluminum & Light Alloys for Automotive Applications, MPIF, Princeton, NJ, edited by W.F.Jandeska and R.A.Chernenkoff, 1998, pp. 75.
9. I.E.Anderson and J.C.Foley, Determining the Role of Surfaces and Interfaces in the Powder Metallurgy Processing of Aluminum Alloy Powders, Surface and Interface Analysis, 31 (2001) 599-608.
10. M.P.Thomas, I.G.Palmer, C.Baker, Consolidation and Properties of Thermally Stable Al-Cr-Zr Alloys Produced by Rapid Solidification, in Enhanced Properties in Structural Metals via Rapid Solidification, F.H.Foes, S.J.Savage (eds), ASM: Orlando, Fl, 1986, pp. 337.
11. J.E.Hatch, Aluminum: Properties and Physical Metallurgy, ASM: Metals Park, OH, 1984, pp. 424.
12. M. Jacobson, A.R. Cooper, J. Nagy, Explosivity of Metal Powders, Bureau of Mines, report No. 6516, US Department of the Interior: US Government Publication, Washington, DC, 1964.
13. Unpublished data from John Wright, ALPOCO, Limited, November 2000, and J.W.Wright, Aluminum Powder-Hazardous or Not, in Proceedings of the Second International Conference on Powder Metallurgy of Aluminum & Light Alloys for Automotive Applications, MPIF, Princeton, NJ, edited by R.A.Chernenkoff and W.F.Jandeska, Jr., 2000, pp. 41 -50.

14. J.C.Foley, D.K.Rehbein and D.J.Barnard, Investigation of the Sintering Processing Using Non-contact Electromagnetic Acoustic Transducers, Advances in Powder Metallurgy & Particulate Materials 2001, Proceedings of the 2001 International Conference on Powder Metallurgy and Particulate Materials held on May 13-17, 2001, in New Orleans, Louisiana, sponsored by the MPIF/APMI, pp. 11.26 - 11.40.
15. G.B.Schaeffer, B.J.Hall, Sintering of Aluminum in Argon and Nitrogen, Advances in Powder Metallurgy & Particulate Materials 2002, Proceedings of the 2002 International Conference on Powder Metallurgy and Particulate Materials held on June 16-21, 2002, in Orlando, Florida, sponsored by the MPIF/APMI, pp. 13.139 - 13.149.
16. J.F.Flumerfelt, Aluminum Powder Metallurgy Processing, (Ph.D. Thesis, Iowa State University, 1998).
17. J.E.Shield, A.I.Goldman, I.E.Anderson, T.W.Ellis, R.W.MeCallum, D.J.Sordelet, US Patent No. 5,433,978, July 18, 1995.
18. S.B.Biner, Development of Quasicrystal Reinforced Aluminum Composites for Industrial Applications, Final Report to Center for Advanced Technology Development of Iowa State University, July 1996.
19. J.E.Davidson, Compressibility of Metal Powders, Powder Metallurgy, ninth edition, in: Metals Handbook, American Society for Metals, Vol. 7, p. 287.
20. ASTM E-8 Standard, ASTM 03.01, 1990, pp. 130.
21. C.G.Levi, R.Mehrabian, Microstructures of Rapidly Solidified Aluminum Alloy Submicron Powders, Metallurgical Transactions A, 13 (1982) 13.
22. E.Kovacs-Csetenyi, M.Horvath, N.Q.Chinh, I.Kovacs, Effect of Grain Size on Tensile Stress and Ductility in Al99.99, Phys. stat. sol. (a), 166 (1998) 166.
23. R.M.German, Sintering Theory and Practice, John Wiley & Sons, Inc., 1996, pp. 95.
24. J.C.Foley, D.J.Barnard, Simplified Powder Metallurgy Processing of Al-8Fe-4Ce Alloys, Advances in Powder Metallurgy & Particulate Materials 2002, Proceedings of the 2002

International Conference on Powder Metallurgy and Particulate Materials held on June 16-21, 2002, in Orlando, Florida, sponsored by the MPIF/APMI, pp. 1.103 - 1.114.

25. Shun-ichi Ushino, Shin-itiroh Fujikawa and Ken-ichi Hirano, Impurity diffusion of three radioactive isotopes of Cu in Al, Keikinzoku / Journal of Japan Institute of Light Metals, 41 (7) (1991) 433-439.
26. R.Galle, H.Mehrer, Diffusion in icosahedral Al-Pd-Mn quasicrystals: temperature and pressure dependence, Materials Science and Engineering A, 294-296 (2000) 693-696.
27. Chr.Khoukaz, R.Galle, H.Mehrer, P.C.Canfield, I.R.Fisher, M.Feuerbacher, Diffusion of ^{57}Co in decagonal Al-Ni-Co-quasicrystals, Materials Science and Engineering A, 294-296 (2000) 697-701.
28. J.F.Flumerfelt, I.E.Anderson and J.C.Foley, Consolidation of Pure Aluminum Powders, P/M Aluminum/Mechanical Alloying, Parts 10&11 in Advances in Powder Metallurgy & Particulate Materials, (1997) eds. R.A.McKotch & R.Webb, pp. 11.
29. D.Raybould, Forming of Rapidly Solidified Elevated Temperature Aluminum Alloys Produced by Planar Flow Casting, Dispersion Strengthened Aluminum Alloys, Y.W.Kim and W.M.Griffith, Editors, TMS, Warrendale, PA, 1988, pp.199-215.
30. L.Ackermann, I.Guillemin, R.Lalauze, C.Pijolat, Study of Water Desorption During Degassing of Aluminium Powders, High Strength Powder Metallurgy Aluminum Alloys II, Ed. By G.J.Hildeman and M.J.Koczak, TMS, Warrendale, PA, 1985, pp.175.
31. F.Tang, I.E.Anderson, S.B.Biner, Microstructure and Tensile Properties of Quasicrystal Particle Reinforced Aluminum Matrix Composites, to be published in Materials Science and Engineering A, and presented talk at Special Interest Program of Lightweight & Advanced P/M Materials: Technology for Diversified Applications, 2002 World Congress on Powder Metallurgy & Particulate Materials held on June 16 -21, 2002, in Orlando, Florida, sponsored by the MPIF/APMI.

Microstructures and mechanical properties of pure Al matrix composites reinforced by Al-Cu-Fe alloy particles

A paper published in the Materials Science and Engineering A[1]

F. Tang, I. E. Anderson, S. B. Biner

Ames Laboratory, Iowa State University, Ames, IA 50011

Abstract

A new type of composite material was produced from elemental Al matrix powders and 30 vol.% Al-Cu-Fe quasicrystal particles by a powder metallurgy technique. SEM examination shows that reinforcement particle cracking perpendicular to the loading axis is the dominant failure mechanism for the composites. Because of the fine (dia. < 10 μm) matrix and reinforcement particle sizes that match closely and a homogenous spatial distribution, the UTS and yield strength of this model composite material were improved over the matrix properties by 111% and 220%, respectively, for the commercial purity composite sample. Remarkably, the UTS and yield strength of the composite were improved over the matrix properties by 201% and 328%, respectively, for a high purity version of the composite material. The elastic modulus of the composite, in both versions, is very close to the theoretical upper bound value from the rule of mixtures estimation. This highly effective composite strengthening is also consistent with the good interface bonding between the spherical reinforcement particles and Al matrix that was revealed by fracture surface

[1] Reprinted from Materials Science and Engineering A, vol. 363, no. 1-2, pp.20-29, with permission from Elsevier.

examination. Diffusion layer measurements at the Al/reinforcement interface by an Auger method verified the good bonding condition, as well.

Keywords: Metal matrix composites; Powder metallurgy; Tensile property.

1. INTRODUCTION

The need for advanced engineering materials in the areas of aerospace and automotive industries had led to a rapid development of metal matrix composites (MMC) [1,2]. They can be tailored to have superior properties such as high specific strength and stiffness, while providing weight savings and higher operating temperatures with proper design and fabrication. Composites may also exhibit better thermal and mechanical fatigue and creep resistance than that of monolithic materials. Unfortunately, for current particulate reinforced aluminum (PRA) [3,4], a considerable amount of complexity and cost is added [5] by the need for extensive hot deformation of the blended powder compact to mitigate the deleterious effects of the oxide coating on the prior particle boundaries of the Al alloy powders. The Al oxide coating on most commercially atomized powders is a severe barrier to sintering, especially solid state sintering, and unless thoroughly distributed in the microstructure of an Al MMC, it can significantly reduce ductility and fatigue strength [5]. Further, the SiC particulate normally used in a PRA composite can add a material cost penalty, typically 2 to 4 times the cost of the Al alloy powder, and can present an extreme problem for conventional Al recycling methods. These disadvantages in processing and material cost and the lack of effective recyclability motivate the development of alternatives for both reinforcement materials and Al matrix powder processing techniques [5].

Low composite toughness may be another disadvantage of conventional SiC reinforcement

particles with sharp pointed corners, because it has been shown that the reinforcement particle shape has a great effect on strain field localization in composites under stress [6]. When an additional external stress is applied, the enhanced plastic strain concentration in the matrix around a pointed SiC particle corner could induce fracture at a relatively low level of applied stress, decreasing the ductility of the composite. The study of S.B. Biner shows that the higher the aspect ratio of the reinforcement fiber, the lower the fracture toughness or the area under the stress-strain curve, if there is no interface failure between the fibers and matrix [7]. J.LLorca, et al., also shows that sharp corners of particles act to limit ductility in two ways. Firstly, the strain concentration at the corner promotes early void nucleation and rounding whisker corners would delay void nucleation and, hence, increase ductility. Secondly, the constraint on plastic flow for the whisker-reinforced composites is much lager than the sphere-reinforced composites. The higher the constraint on the plastic flow, the higher the hydrostatic stresses would develop in the Al matrix, which will cause rapid void growth and early failure [8]. A prior study shows that fragmented SiC particles can also cause intolerable tool wear during die pressing and tends to attack the counter materials in wear-prone service, such as in automotive belt pulleys [9]. Thus, in order to reduce the strain concentration around the typical angular reinforcement particles and to improve the ability for wear-resistant applications, spherical Al-Cu-Fe quasicrystal particles were used in the composites of this paper.

Quasicrystalline (QXL) phases were first discovered in aluminum rich transition metal alloys [10]. Since that time, many other alloy systems that form quasicrystalline phases were discovered. It is well known that quasicrystal alloys have very high hardness and high modulus [11, 12]. The original metastable quasicrystals were prepared by very rapid solidification processes, such as melt spinning. Now, experiments show that thermodynamically stable Al-Cu-Fe quasicrystal phase can be produced as spherical powder by gas atomization and can retain its high hardness at elevated temperature [13]. U.Koster

reported a Vickers microhardness of around 1,000 for the stable $Al_{63}Cu_{25}Fe_{12}$ quasicrystal compound in monolithic form [14]. The elastic modulus of this quasicrystal was determined recently to be 182 GPa by an ultrasonic measurement technique [15] on a fully dense sample made by hot (800 °C) isostatic pressing (HIP) of gas atomized powder. For comparison, the elastic modulus of SiC is about 350 - 440 GPa [16]. Thus, direct strengthening considerations dictated that an increased volume fraction of the Al-Cu-Fe QXL phase must be used to approach the yield strength enhancement of SiC reinforced Al composites. It was anticipated that Al-Cu-Fe quasicrystals, produced as spherical fine powders by gas atomization, may act as a very good reinforcement particulate for Al MMC materials [17], if reinforcement particle agglomeration could be avoided.

In order to study the strengthening effect of Al alloy based (Al 2080) composites, Krajewski and Chawla, et al. [18, 4] had to use a series of different thermomechanical treatments in the unreinforced Al alloy and in the composite samples. These distinct treatments were needed to achieve a similar precipitate density and distribution in the microstructure of the unreinforced Al alloy and in the composite matrix in order to compare their mechanical properties in an unbiased manner. In this paper, elemental Al powder was chosen as the matrix material to avoid the complications of matrix heat treatment effects on the strengthening mechanisms because there is no precipitation in the elemental Al matrix. Therefore it is not needed to do special heat treatment on pure Al matrix material and composite materials to achieve same microstructures for considering precipitation effects. The other indirect strengthening mechanisms, such as load transfer mechanism, dislocation density increase caused by mismatch of CTE and elastic modulus of Al matrix and reinforcement particles during thermal processing or deformation, were also studied and the detail are reported in the other paper [19]. Earlier work [20] on monitoring of elemental Al powder sintering had also demonstrated that both types of matrix powders would experience rapid solid state sintering in a die pressed compact at the selected consolidation temperature. In this article we will

report microstructure and mechanical property results of commercial purity and high purity composite samples consolidated from either commercial inert gas atomized (CIGA) powders or gas atomization reaction synthesis (GARS) [21] powders, respectively, using quasi-isostatic hot forging.

2. EXPERIMENTAL PROCEDURE

2.1 Materials

Powders used for the two kinds of composite samples are shown in table 1. For the baseline experiments, commercially inert gas atomized (CIGA) Al and $Al_{63}Cu_{25}Fe_{12}$ quasicrystal powders were obtained. The CIGA Al powder (99.7% purity) had been evaluated thoroughly in earlier work [22, 23] to characterize its surface oxide properties. A patented gas atomization reaction synthesis (GARS) technique was also used to produce 99.99% pure Al and Al-Cu-Fe quasicrystal (QXL) powders [21] in our laboratory.

Table 1. Powders used for AFF and GFF samples and consolidation methods.

Sample name	Powders used	Purity
AFF	CIGA Al powder (<10μm) + 30 vol.% CIGA quasicrystal powder (<10μm)	99.7%
GFF	GARS Al powder (< 10μm) + 30 vol.% GARS quasicrystal powder (<10μm)	99.99%

The Al and Al-Cu-Fe quasicrystal powders were air-classified to less than 10 μm. The

quasicrystal powders from both sources were screened subsequently through a 20 μm screen to eliminate the residual large particles. The size distributions of Al and quasicrystal powders were measured by a laser diffraction method and the results are shown in figure 1 and figure 2, respectively. For both CIGA and GARS quasicrystal powders, 90% of the cumulative volume fraction was less than 10μm and essentially 100% of the quasicrystal powders were less than 15 μm, as shown in figure 2.

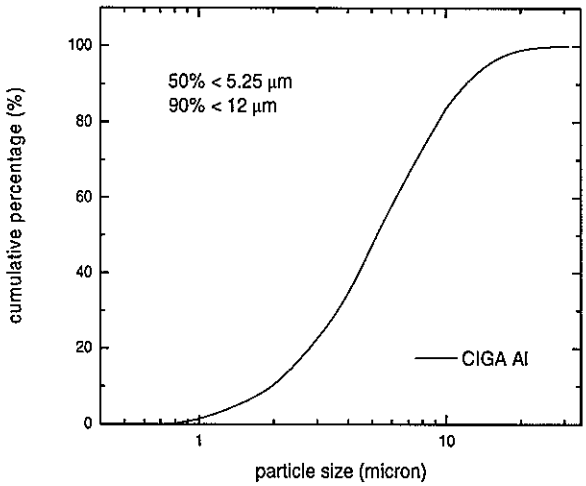

(a)

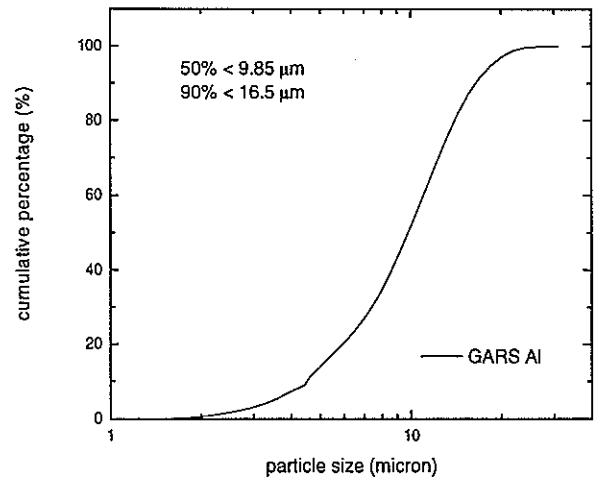

(b)

Figure 1. Size distribution of pure Al powders (a) CIGA Al powder (b) GARS Al powder.

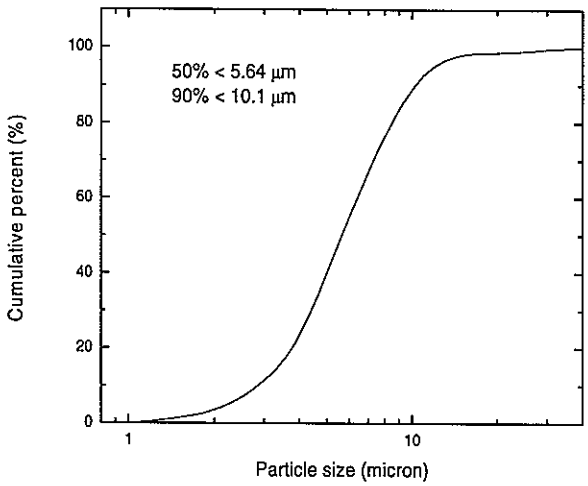

(a)

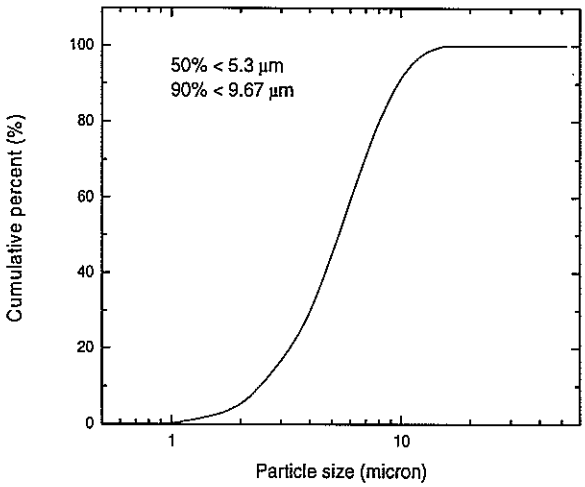

(b)

Figure 2. Size distribution of Al-Cu-Fe quasicrystal powders (a) CIGA QXL powder (b) GARS QXL powder.

2.2 Consolidation processing

The weight of the Al and quasicrystal powders used in consolidation were calculated for making 30 vol.% of loading of quasicrystal reinforcement particles by using the density

values of pure Al and quasicrystal powders. There was very little powder loss during following powder processing and consolidation. First, Al and quasicrystal powders were blended homogeneously by a high energy dynamic blending technology (HEDBT), a proprietary technique practiced by Ceracon, Inc. of Riverbank, CA. The volume fraction of quasicrystal powders in both AFF and GFF samples was 30%. Next, blended powders were cold isostatically pressed (CIP) with a pressure of 200MPa. The "green" samples from CIP were forged at a temperature of 550°C with a quasi-isostatic forging procedure by Ceracon. While die pressed compacts of the GARS Al powder were found to sinter at a significant rate at only 500°C, compacts made from CIGA Al powders needed at least 550°C to approach a reasonable rate for solid state sintering [20]. Thus, the forging temperature was chosen to allow both compacts to experience significant solid state sintering during this solid state consolidation process for the purposes of meaningful comparison of final tensile properties. The dimensions of the resulting bars after forging were about 5.5 cm by 2.5 cm by 1 cm.

Table 2. Quasi-isostatic forging procedure.

Pre-heat Atmosphere	Pre-heating	Forge Temp.	Forge Pressure	Dwell at Pressure
99.999% Argon	550 °C,10 min	550 °C	635 MPa	5 second

2.3 Other tests

The Archimedes technique was used to measure the density of each forged sample. The elastic modulus of forged samples was measured by an ultrasonic method [24]. Cross-sections of the as-received composite samples were mechanically polished for microstructural examination on the surface without any etching. Tensile tests of consolidated composites were performed on an Instron model 1125 tensile test machine under 1.27 mm

per minute monotonic loading. Sample dimensions were in 6.35 mm in diameter and 25.4 mm in uniform gauge length, according to ASTM recommendations [25]. Fractography of the composites and cross-section microstructures near the fracture surface of the tensile samples were examined on an AMRAY 1845 field emission scanning electron microscope.

3. RESULTS

3.1 General microstructures of composites

The general appearance of the microstructures of AFF and GFF composites is shown in figure 3. A fairly uniform distribution of the spherical reinforcements in the composites can be seen from the figures. The spherical shape of the quasicrystal particles is also readily apparent in these SEM micrographs. There are relatively more fine reinforcement particles in GFF than in AFF, which can be also seen from the pictures. Table 3 indicates that the density measurements of the consolidated samples are nearly equal to the theoretical density of the composite. Although the general distribution of the reinforcement particles is generally uniform, there still exists particle clustering in some local areas. This clustering may have produced some deleterious effect in the early stages of fracturing of the material, which will be described, later.

Table 3. Summary of density measurement of composite samples.

Sample	Measured density (g/cm^3)	Theoretical density (g/cm^3)
AFF	3.28	3.3
GFF	3.28	

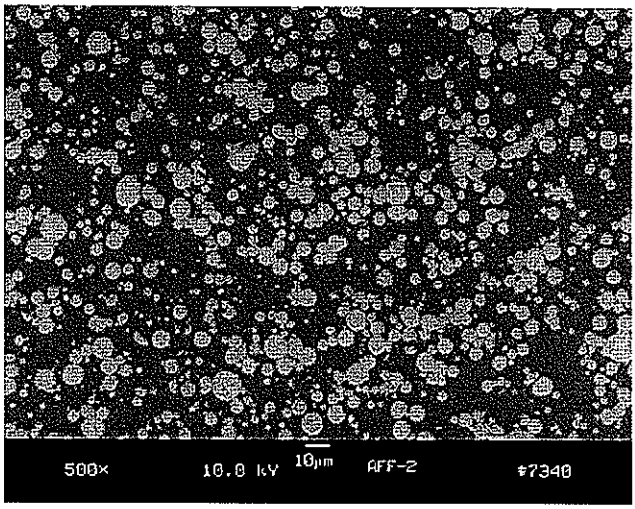

(a)

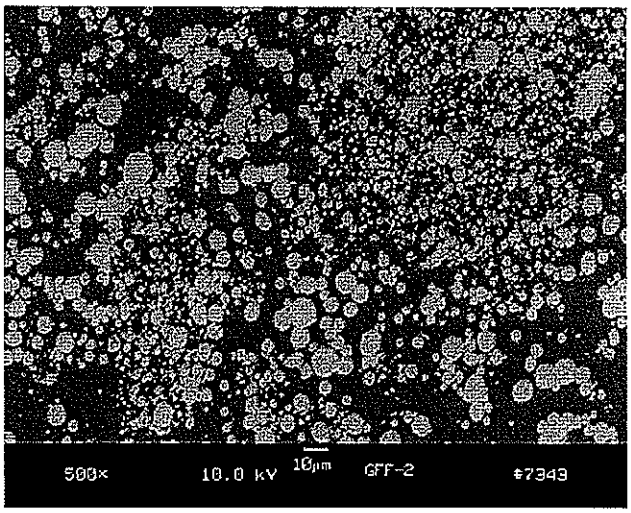

(b)

Figure 3. Microstructures of (a) AFF sample and (b) GFF sample.

3.2 Tensile properties and fracture surface examination

An example of the tensile behavior of the AFF and GFF composite samples is given in figure 4. Measurements of tensile strength and elastic modulus (E) of the samples are shown in

Table 4. The ultimate tensile strength (UTS) shows a large enhancement when compared to the typical ultimate tensile strength, 90 MPa, of ingot processed 1100 Al. A comparison to the UTS of elemental, unreinforced Al samples produced from CIGA Al powder (AF) and GARS Al powder (GF) with very similar grain size will be discussed later. Tensile ductility of the composites is limited to about 1% strain, as shown in figure 4. At the initial stage of the tensile test, i.e. lower than about 0.1% strain, the responses of the AFF and GFF samples are very similar and their stress-strain curves are overlapped. Later in each tensile test, the AFF sample shows a higher work hardening tendency than the GFF sample and the final fracture strain of AFF is lower than that of GFF. Shown in table 4, the elastic modulus values of AFF and GFF samples are 98 GPa and 99 GPa, respectively, which were measured in the linear elastic range of the tensile stress-strain curves in Figure 4. Measured by ultrasonic technique, the elastic modulus of AFF and GFF are 97 GPa and 98 GPa. Above E values measured by two kinds of approach are very consistent. These values are very close to the upper-bound E value of 103 GPa that was calculated by the rule of mixtures based on E values of pure Al and Al-Cu-Fe quasicrystals. The rule of mixtures calculation for estimation of elastic modulus of two-phase composites, which is derived based on principle of minimum potential energy, can be applied to both particulate reinforced composites and fiber reinforced composites [26]. Because the passion ratio of pure Al (υ=0.3) and Al-Cu-Fe alloy phase (υ=0.2) are very close, so the directly using rule of mixtures calculation for upper-bound value has very little error. For particulate reinforced composites, the Halpin-Tsai equations can give a more accurate estimation of actual elastic modulus [27]. The estimation of elastic modulus of AFF and GFF composite materials by Halpin-Tsai equations is 95 GPa, which is close to, but lower than the experimental values.

Figure 5 shows the fractography of failed tensile samples from the AFF and GFF tensile tests. All of the samples displayed a mixed fracture mechanism on the fracture surfaces. In the Al matrix area, figure 5 shows ductile tearing ridges and micro-dimples around prior Al

particles. Fracture occurred by grain boundary separation and brittle cleavage across the reinforcement particles.

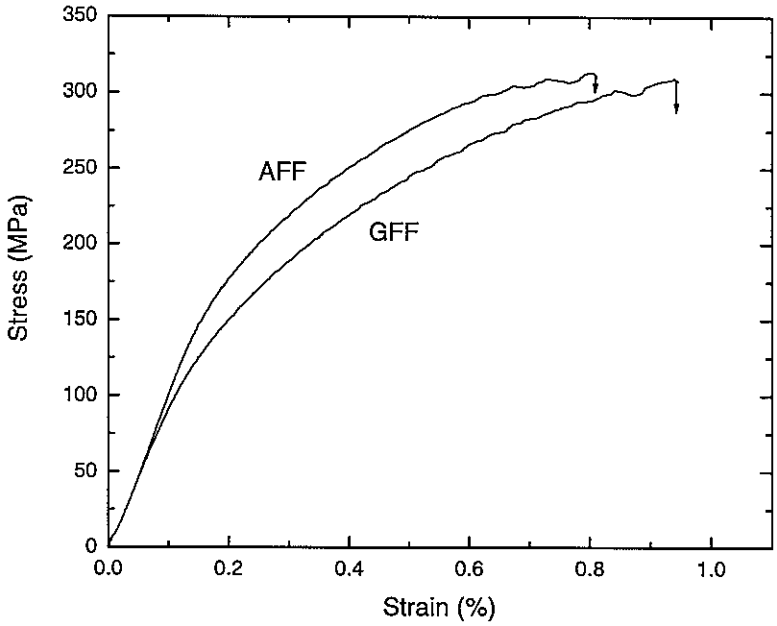

Figure 4. Tensile stress-strain curves of AFF and GFF samples.

Table 4. Tensile strength and elastic modulus of AFF and GFF composite samples.*

Sample	UTS (MPa)	$\sigma_{0.2}$ (MPa)	E_1 (GPa)	E_2 (GPa)
AFF	310	265	98	97
GFF	304	227	99	98

*Note: 1. the UTS and $\sigma_{0.2}$ values are the average values from two tensile samples.

2. E_1 : elastic modulus measured from linear elastic portion of tensile stress-strain curves.

3. E_2 : elastic modulus measured by ultrasonic technique on bulk composite samples.

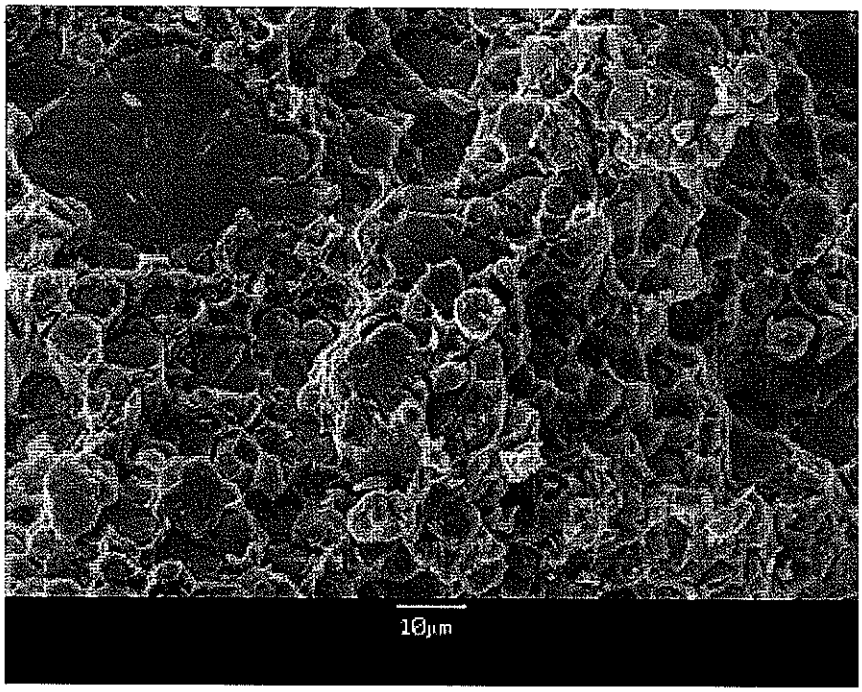

5 (a)

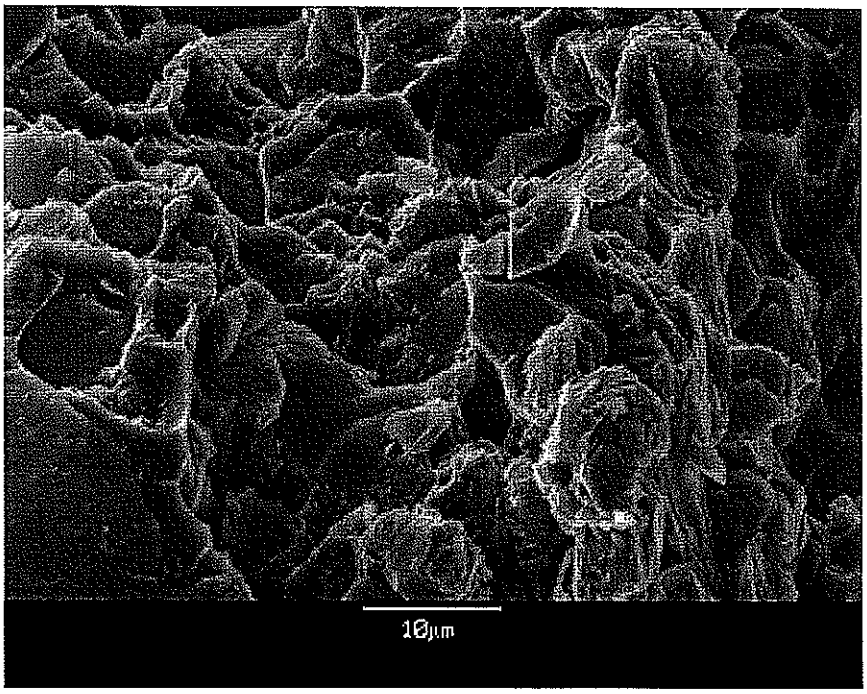

5 (b)

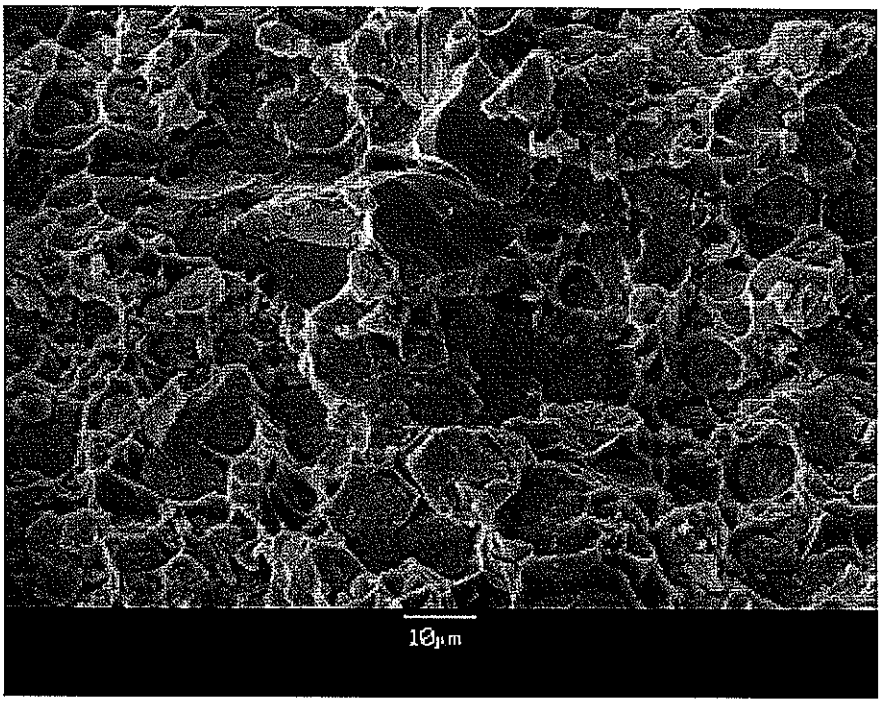

5 (c)

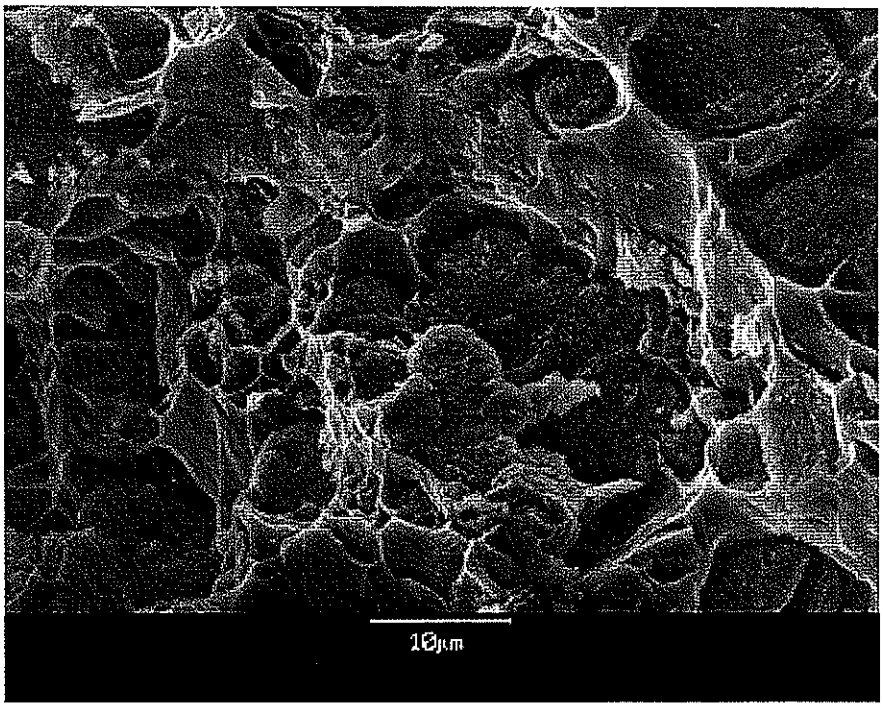

5 (d)

Figure 5. Fracture surfaces of (a) and (b) AFF tensile sample, (c) and (d) GFF tensile sample.

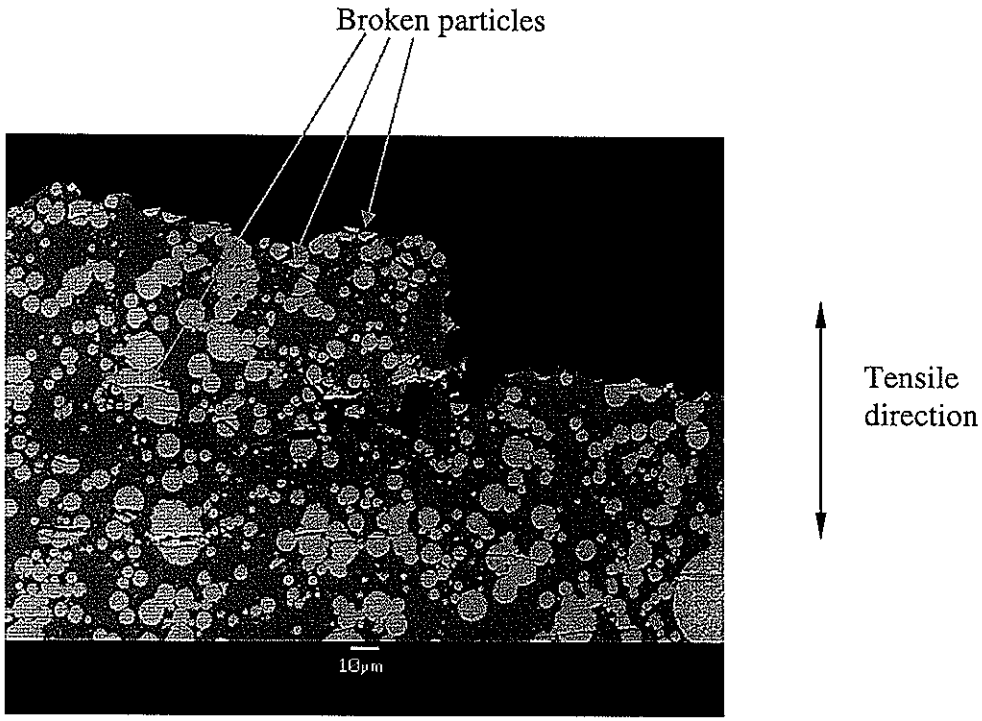

(a)

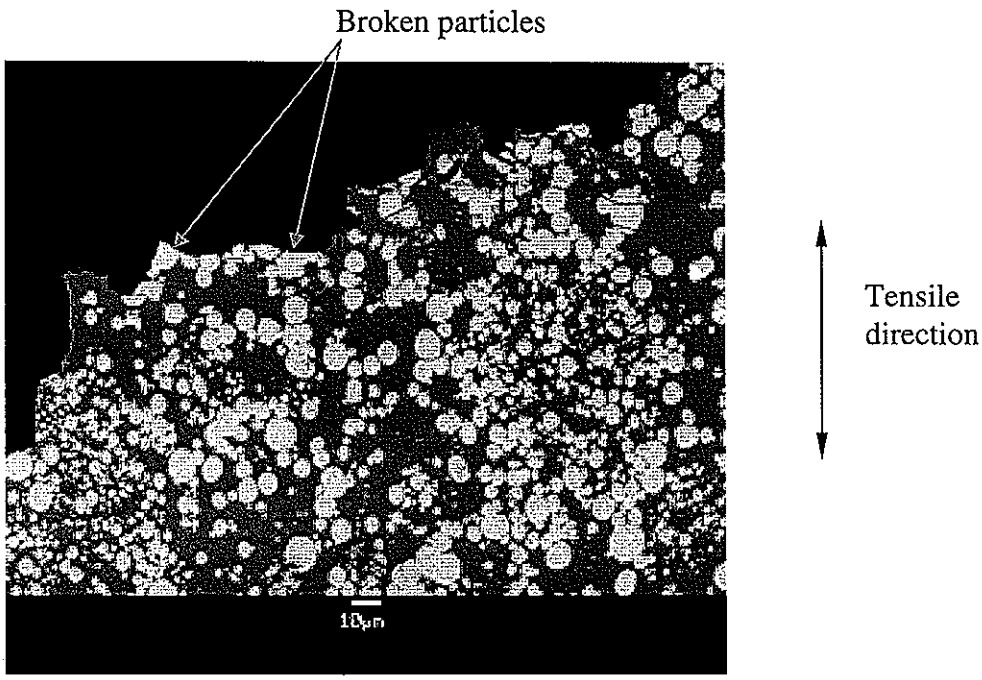

(b)

Figure 6. Cross section of fracture surfaces of (a) AFF tensile sample and (b) GFF tensile sample.

Figure 6 shows the cross-section microstructures near the fracture surfaces of both types of tensile samples. Generally, fractography of both mirror halves of the fracture surfaces of each tensile sample shows that reinforcement particles on the fracture surface were broken and particle pull-out appeared to be absent. As shown in figure 6, in which the fracture surfaces are normal to the tensile direction, most QXL reinforcement particles cracked along the fracture path and QXL/Al interface debonding was rare. Below the fracture interface, there are some reinforcement particles that were broken normal to the tensile direction and the number of the broken particles in the AFF sample is significantly more than that in the GFF sample.

4. DISCUSSION

4.1 Tensile Strength Influences

There is a comparison of tensile properties between elemental Al matrix materials, AF and GF, and AFF and GFF composite materials in table 5. The increase of the ultimate tensile strength (UTS) of the AFF and GFF composite material is 163 MPa (111%) and 209 MPa (220%), respectively, compared with their respective Al matrix properties. The increases of the yield strength (Y.S.) over their corresponding matrix values are 177 MPa for AFF (201%) composite samples and 174 MPa for GFF (328%) composite samples. These Y.S. enhancement values are remarkably high, compared with the yield strength increases reported for similar Al/SiC (< 10 μm) composites. Examples include Y.S. increases of 88 MPa for 1100 Al/20 vol. % SiC [28], about 50 MPa for 6061Al/20 vol. % SiC, and about 100 MPa for 6061Al/30 vol. % SiC [29].

The unusual strength increase of AFF and GFF composites appears to be caused mainly by

several factors: first, uniform distribution of the fine reinforcement particles, second, smaller interparticle spacing in the matrix, and third, good bonding strength between reinforcement particles and matrix. The bonding strength can be inferred from the examination of tensile sample fracture surfaces and the cross-section microstructures of fractured tensile samples. These factors are important because they can delay premature damage, and, thus, increase strength and ductility of the material [30].

Table 5. Comparison of UTS and Y.S. between Al matrix material and composite materials.

		AF	GF	AFF	GFF
Average UTS of tensile samples (MPa)		147^{+1}_{-1}	95^{+0}_{-0}	310^{+4}_{-4}	304^{+6}_{-6}
Average Y.S. of tensile samples (MPa)		88^{+1}_{-1}	53^{+2}_{-2}	265^{+1}_{-2}	227^{+1}_{-1}
Increase of UTS compared with Al matrix	MPa	-	-	163	209
	Percent	-	-	111%	220%
Increase of Y.S. compared with Al matrix	MPa	-	-	177	174
	Percent	-	-	201%	328%

Note: AF – Pure Al sample made from CIGA Al powder (<10μm)

GF – Pure Al sample made from GARS Al powder (< 10μm)

Y.S. – yield strength, defined as the stress at a plastic strain of 0.2%.

All the UTS and Y.S. values comes from the average value of 2 or 3 tensile samples.

In the AFF sample, relatively more broken reinforcement particles can be seen below (but near) the fracture surface, see Fig. 6(a). One possible reason for this observation is that the Al/reinforcement bonding strength in AFF may be not as good as in the GFF sample, since reinforcement particle cracking could be promoted by a locally debonded Al/QXL interface. The Auger measurement results on Al/reinforcement particle interface regions, discussed

later, support this speculation. A related difference in the tensile properties can be seen in Fig. 4, where the plastic strain at UTS of GFF is larger than that of AFF. Because the GARS high purity Al powder has a much lower oxide and impurity content than CIGA Al powder [22, 23], there may be fewer precipitates and oxide residuals within the matrix phase, i.e., GF in Table 5, of GFF to act as secondary strengthening agents. Thus, the stronger matrix phase, i.e., AF in Table 5, of the AFF sample also suggests an alternative explanation for the reinforcement particle cracking below the final fracture surface in Fig. 6(a). Perhaps, the AFF matrix can bear a higher load fraction to the extent that the fracture strength of the QXL particles is exceeded, but only local reinforcement cracking occurs without linking across the matrix.

4.2 Further Comparisons between Matrix and Composite Strength

Table 6 and figure 7 provide a further comparison of tensile properties between CIGA Al (AF) and GARS Al (GF) matrix samples, and AFF and GFF composite samples. It looks reasonable that the Y.S. of AFF is 38 MPa higher than that of GFF because this Y.S. difference is similar to the difference of Y.S. between their pure Al matrix types, AF and GF. However, the QXL powders used in these two kinds of composite samples are also different and the yield strength can be influenced by other factors, such as the interface bonding strength. Therefore, it is hard to say that the Y.S. difference between GFF and AFF composites is caused exclusively by the use of different Al matrix powders. A detailed experimental study and theoretical modeling on the strengthening mechanisms and Y.S. prediction of AFF and GFF composite material made from vacuum hot pressing technique was reported in the other paper [19].

The UTS of GFF is only 6 MPa lower than AFF from table 6, which is much lower than the 52 MPa difference in UTS between AF and GF. This fact is not reasonable at first glance because the stronger matrix in AFF should also make the AFF composite material much stronger. However, it must be considered that different interface conditions exist at prior particle boundaries in AFF and GFF samples. In other words, the relatively weak bonding of some seriously oxidized matrix/reinforcement interfaces in AFF can provide a preferred location for crack initialization and can weaken the load transfer mechanism for composite strengthening. Thus, although the AF matrix provides a higher yield strength, the relatively weak matrix/reinforcement interface may fail the composite at a lower UTS than might be ultimately possible. Maybe due to the same reason, the percentage increase of UTS and yield strength of the GFF sample is also much higher than that of the AFF sample from table 5.

Table 6. Difference of UTS and yield strength between different elemental Al samples and Al/QXL composite samples.

		Difference of UTS (MPa)	Difference of Y.S. (MPa)
Grain size and solid solution strengthening effect	AF – GF	52	35
Powder effect	AFF – GFF	6	38

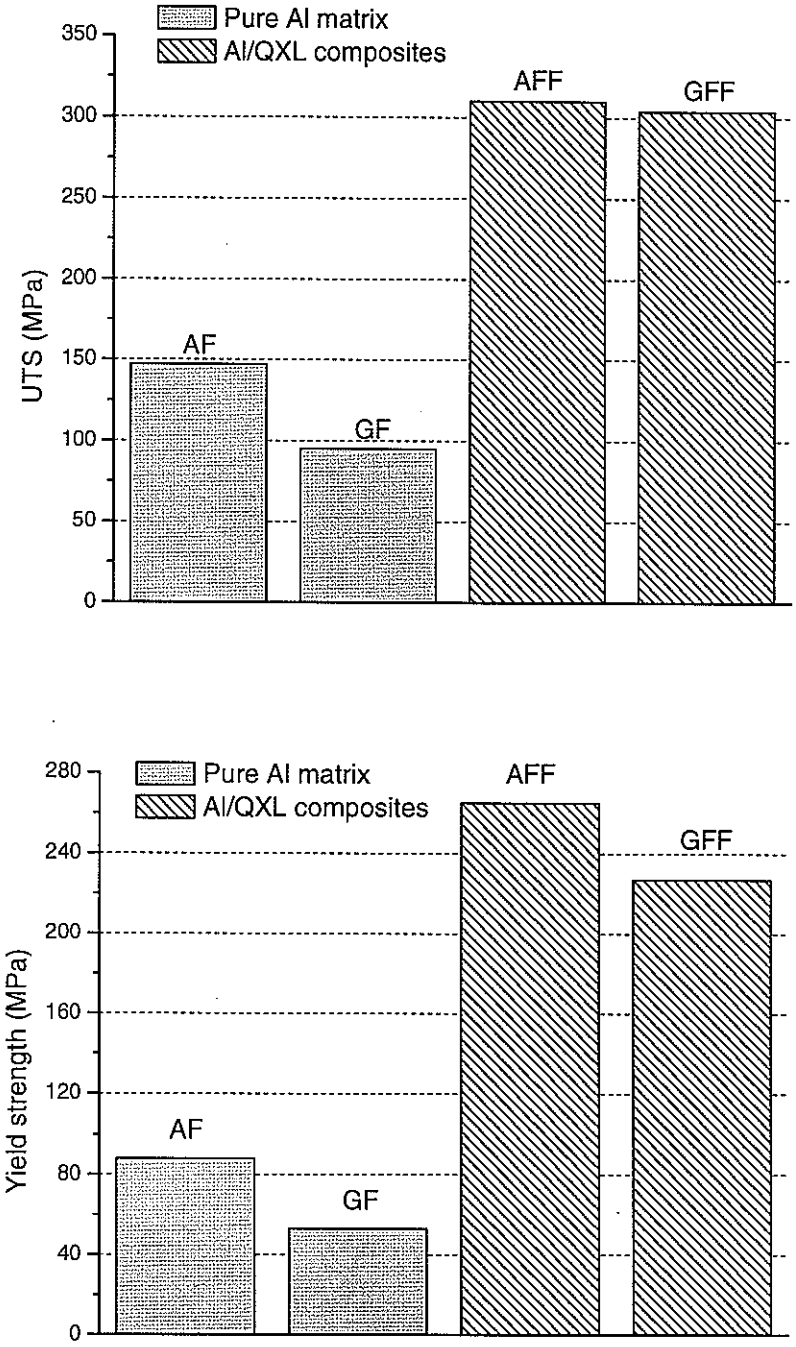

Figure 7. UTS and Yield strength of elemental Al (AF and GF) samples, Al/QXL composite (AFF and GFF) samples.

4.3 General Observations

Thus, it has been proposed [5, 22, 23] that the GARS technique may be very useful for producing Al based MMC materials, such as SiC reinforced Al MMC. During the typical processing of SiC reinforced Al composites, the aluminum oxide surfaces present on CIGA aluminum powder should be broken up in order to increase the ductility of the PRA composites. The break up of the oxide is usually achieved by extensive extrusion processing that produces simple mill shapes, requiring additional processing to fabricate final parts [31]. Ideally, a "clean" aluminum powder may be used to circumvent the requirement for conventional high interparticle shear (extrusion) processing to enable simple net shape consolidation of PRA composites and advanced Al alloys [32]. Detailed powder surface chemistry effects on microstructures and properties of consolidated pure Al and Al MMC materials can be found in reference [33]. A previous study on the interface composition of Al and Al-Cu-Fe QXL reinforcement particles shows that there is only a slight Cu diffusion from reinforcement particles to Al matrix and almost no Fe diffusion [33]. Therefore, there should be no brittle interfacial phases formed in the interface area. For achieving best mechanical properties in the composite material, former studies [9] concluded that it is best to have only slight reaction in the interface, without brittle interfacial phases.

The uniform spatial distribution of the reinforcement particles plays a very important role in the fracture resistance of composites. For example, the micrograph of the composite sample in Fig. 8, made from a CIGA Al and GARS QXL powder mixture in a previous study [17], shows that local clustering regions exist in the samples and that these regions provided a favorable path for cracking. Unfortunately, the local clustering of reinforcement particles is actually caused by the random distribution of particles. In a composite material with a perfectly random distribution of reinforcement particles, promoted by a proper blending method, the local clustering of some adjacent particles will happen naturally. Avoiding and

controlling local clustering is very difficult because it actually requires a non-random distribution and non-impingement of adjacent particles. The higher the volume fraction of reinforcement particles, the more the local clustering or agglomeration of particles occurs. It has been reported that clustered regions induce tri-axial stresses in the matrix [34]. Yielding stress can be achieved earlier in these high stress intensity clustering regions, initiating cracks. Therefore, there is a limitation on the volume fraction of reinforcement in order to achieve good ductility. The particles that are clustered together also may be sintered after the consolidation process, as shown in Figure 8. The whole body of the sintered particle cluster may act as a large particle, whose size and aspect ratio is much larger than the individual particles. The local clustering in the microstructures was not studied in this paper. A quantitative measurement of reinforcement particle distributions is currently in-progress on the composites reinforced with 30 vol. % of particles. The effects of particle distribution and variations in reinforcement loading on the composite strength will be reported in a later paper.

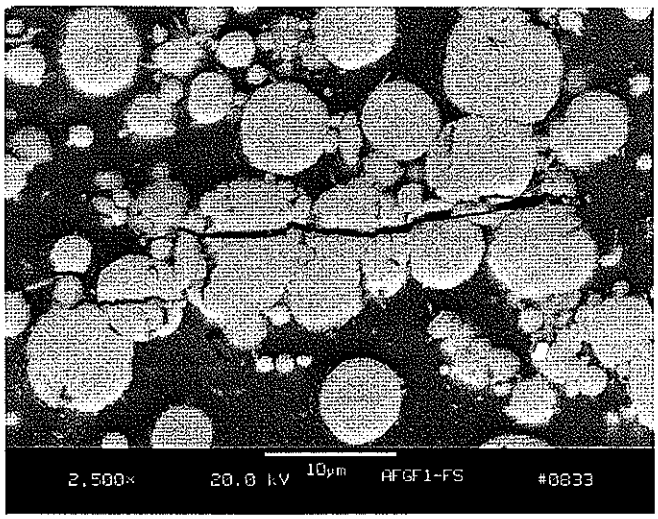

Figure 8. Cross section microstructures of a composite tensile sample similar to AFF showing broken particles in local clustering area [17].

In terms of practical implications, our remarkable strengthening results suggest that with proper care to ensure effective interfacial bonding the list of potential reinforcement phases should be broadened from refractory ceramics to include, e.g., intermetallic compounds that can form a thin solid solution bonding zone with the matrix phase. If isotropic strength at high temperatures is a goal for such composites, these new reinforcement particulates may be produced as spherical powders by atomization, for example. New directions for exploiting the potential benefits from the use of particulate reinforced composites would come naturally if net shape or near-net shape composites became more broadly available. This also may be an opening for re-examination of composite consolidation processing. In Al-based composites, the new process that we utilized for synthesizing Al powders with a thin, oxide film that appears to be penetrated and dispersed by solid state diffusion may allow the use of powder compaction techniques with low interparticle shear characteristics. One of the simplest and most desirable techniques would be ambient temperature die pressing, followed by solid state sintering.

In this paper, the results of a quasi-isostatic hot forging consolidation method, which produces some grain anisotropy [31] and a relatively minor amount of interparticle shear, are reported. In a subsequent paper, we will report the properties of the same composites made by the use of vacuum hot pressing, with a further decreased amount of interparticle shear, a lower strain hardening rate, and almost no grain anisotropy, i.e., one step closer to the goal of consolidation process simplification for net shape Al MMC composite parts. It is hoped that the use of such a model system to represent an ideal particulate-reinforced MMC material can permit pursuit of a fully developed strengthening model that takes into account significant microstructural characteristics of this class of composites. Our paper will also explore the development of such a composite strengthening model in this manner.

5. CONCLUSIONS

1. Spherical Al-Cu-Fe alloy powders can serve as an effective reinforcement particulate for elemental Al-based composites, because of their high hardness, high thermal stability, and a preferred type of matrix/reinforcement interfacial bonding, with reduced strain concentration around the particles.
2. This reinforcement effectiveness is further evidenced by elastic modulus measurements of the composites that fall just below the upper bound predictions of the rule of mixtures for 30 vol.% loading.
3. Ultimate tensile strength and yield strength of both types of composites were increased over the corresponding Al matrix values far beyond typical observations, probably promoted by a fine reinforcement particle size that matched the matrix powders, an improved spatial distribution of the reinforcements, and an improved interface bond strength between matrix and reinforcement particles,
4. Particle cracking of the reinforcement particulate was a dominant failure mechanism for the composites under tensile loading, implying that there is sufficient interfacial bonding between the reinforcement particles and Al matrix to achieve full benefit from the reinforcement.
5. Composite samples made from high purity powders show a higher strengthening effect and ductility than the samples made from commercial purity powders, which may result from improved bonding between the high purity powders.

ACKNOWLEDGMENTS

The authors greatly appreciate the assistance of Mr. Henry Meeks of Ceracon, Inc. for the HEDBT blending and the quasi-static forging. Also, the assistance of the Materials

Preparation Center of the Ames Laboratory is also acknowledged for the SEM studies, performed by Mr. Fran Laabs, and automated image analysis, performed by Mr. Hal Sailsbury. We also appreciate the ultrasonic measurements which were performed by Dan Barnard. Arne Swanson helped with tensile testing. The funding of this project from DOE Basic Energy Sciences under contract number W-7405-Eng-82 also is gratefully acknowledged.

REFERENCES

1. J.E.Allison, G.S.Cole, JOM 45 (1993) 19-24.
2. C.K.Narula, J.E.Allison, CHEMTECH 26 (1996) 48.
3. N.Chawla, C.Andres, J.W.Jones and J.E. Allison, Metallurgical and Materials Transactions A 29 (1998) 2843.
4. N.Chawla, U.Habel, Y.L.Shen, C.Andres, J.W.Jones, J.E.Allison, Metallurgical and Materials Transactions A, 31A (20) (2000) 531-540.
5. I.E.Anderson, J.C.Foley and J.F.Flumerfelt, Proceedings of the first international conference on powder metallurgy aluminum & light alloys for automotive applications, edited by W.F.Jandeska and R.A.Chernenkoff, pp.75.
6. S.Y.Qin, C.R.Chen, G.D.Zhang, W.L.Wang, Z.G.Wang, Materials Science and Engineering A 272 (1999) 363-370.
7. S.B.Biner, Journal of Materials Science, 29 (1994) 2893-2902.
8. J.Llorca, A.Needleman, S.Suresh, Acta metal. mater., 39 (10) (1991) 2317-2335.
9. H.Danninger, G. Jangg, K.Schroder, J.Seyrkammer, H.C.Neubing, Sintered aluminum camshaft belt pulleys, Advances in Powder Metallurgy, vol. 6, 1992, Non-Ferrous Materials, Proceedings of the 1992 Powder Metallurgy World Congress. Part 6 (of 9),

Jun 21-26 1992, San Francisco, CA, USA, Sponsored by: Metal Powder Industries Federation; American Powder Metallurgy Inst, p.1-13.

10. D.Shechtman, I.Blech, D.Gratias, J.W.Cahn, Physical Review Letters 53 (1984) 1951-1953.
11. K.Urban, M.Feuerbacher, M.Wollgarten, MRS Bulletin 20 (1997) 65-68.
12. E.Giacometti, N.Baluc, Scripta Materialia 41 (1999) 989-994.
13. D.J.Sordelet, M.J.Kramer, O.Unal, Journal of Thermal Spray Technology 4 (1995) 235-244.
14. U.Koster, W.Liu, Journal of Non-Crystalline Solids 153&154 (1993) 446-452.
15. D. Barnard, private communication and unpublished data, 2002.
16. M.Bengisu, Engineering Ceramics, Springer-Verlag Inc., 2001, p. 469 - 470.
17. F.Tang, I.E.Anderson, S.B.Biner, J.C.Foley, Advance in Powder Metallurgy & Particulate Materials 2001, ed. by W.B.Eisen and S.Kassam, Proceedings of the 2001 International Conference on Powder Metallurgy & Particulate Materials, May 13-17, New Orleans, LA, Sponsored by APMI/MPIF, Part 9, p. 12 -25.
18. P.E.Krajewski, J.E.Allison, and J.W.Jones, Metall. Mater. Trans. 24 (1993) 2731.
19. F. Tang, I.E.Anderson, Pure Al matrix Composites Produced by Vacuum Hot Pressing: Tensile Properties and Strengthening Mechanisms, to be submitted to Materials Science and Engineering A.
20. J.C.Foley, D.K.Rehbein and D.J.Barnard, Advances in Powder Metallurgy & Particulate Materials 2001, Proceedings of the 2001 International Conference on Powder Metallurgy and Particulate Materials held on May 13-17, 2001, in New Orleans, Louisiana, sponsored by the MPIF/APMI, pp. 11.26 - 11.40.
21. I.E.Anderson, B.K.Lograsso, T.W.Ellis, (Ames Lab, Iowa State University), US Patent No. 5,368,657, Nov. 29, 1994.
22. J.F.Flumerfelt, "Aluminum Powder Metallurgy Processing", (Ph.D. Thesis, Iowa State University, 1998).

23. J.F.Flumerfelt, I.E.Anerson, Advances in Powder Metallurgy and Particulate Materials – 1996, ed. by T.M.Cadle and K.S. (Sim) Narashimhan, Metal Powder Industries Federation, Princeton, NJ, Vol. 1, Part 1, 1996, p. 87-96.
24. J.Krautkramer, H.Krautkramer, Ultrasonic Testing of Materials, Third Edition, Berlin, Heidelberg, New York, 1983, pp. 580-587.
25. ASTM E-8 Standard, ASTM 03.01, p.130, 1990.
26. R.M.Jones, Mechanics of Composite Materials, second edition, Taylor & Francis, Inc., 1999, pp. 140.
27. J.C.Halpin, Primer on composite materials analysis, Technomic Publishing Company, 1992, p.161.
28. R.J.Arsenault, L.Wang, C.R.Feng, Acta Metall. Mater. 39 (1) (1991) 47-57.
29. David L.Mcdanels, Analysis of Stress-Strain, Fracture, and Ductility Behavior of Aluminum Matrix Composites Containing Discontinuous Silicon Carbide Reinforcement, Metallurgical Transactions A, 16 (6) (1985) 1105.
30. W.H.Hunt, T.M.Osman, J.J.Lewandowski, JOM, 44 (1) (1993) 30-35.
31. I.E.Anderson and J.C.Foley, Surface and Interface Analysis 31 (2001) 599-608.
32. F.Tang, I.E.Anderson, S.B.Biner, Solid State Sintering and Consolidation of Al Powders and Al Matrix Composites, Journal of Light Metals, (2-4) (2002) 204 -214.
33. J.C.Foley, W.H.Hunt, D.J.Barnard, F.C.Laabs, Advances in Powder Metallurgy & Particulate Materials, ed. by V.Arnhold, C.L.Chu, W.F.Jandeska, H.I.Sanderow, Proceedings of the 2002 World Congress on Powder Metallurgy & Particulate Materials, June 16-21, Orlando, Florida, Sponsored by APMI/MPIF, p. 1.103-1.114.
34. T.W.Clyne, P.J.Withers, An Introduction to Metal Matrix Composites, Cambridge University Press, 1993, p. 261.

Pure Al matrix Composites Produced by Vacuum Hot Pressing: Tensile Properties and Strengthening Mechanisms

A paper submitted to Materials Science and Engineering A

Fei Tang[1], Thomas Gnaupel-Herold[2], Henry Prask[2], Iver E. Anderson[1]

[1]Ames Laboratory, Iowa State University, Ames, IA 50011

[2]NIST neutron research center, 100 Bureau Drive, Gaithersburg, MD 20899-3460

Abstract

Al matrix composites reinforced by spherical intermetallic particles, were consolidated from gas atomized elemental Al and Al-Cu-Fe alloy fine powders (< 10μm) by a vacuum hot pressing (VHP) technique. The composites were made from two types of powders including commercial inert gas atomized powder (99.7%) and high purity powder (99.99%) produced by a gas atomization reaction synthesis technique. The microstructures and tensile properties of the composites with three different volume fractions of the reinforcement particles (15, 20 and 30 vol.%) were characterized. Yield strength (Y.S.) increase values of the composites, compared with elemental Al matrix Y.S. values, were correlated very well with the predictions of combined strengthening from mechanisms that include load transfer, mismatch of CTE, and geometrically necessary dislocations. For analysis of the load transfer contribution, in-situ neutron diffraction measurements of each type of composite sample were used to measure the actual load bearing stresses of the matrix and reinforcement phases.

Key words: Metal matrix composites; Powder metallurgy; Strengthening mechanisms.

1. Introduction

It is attractive to use particulate reinforced aluminum (PRA) matrix composites in structural applications because of their excellent stiffness-to-weight and strength-to-weight ratios [1, 2]. Such PRA materials also exhibit generally good wear resistance, thermal conductivity, and low thermal expansion, all of which makes them good multifunctional light weight materials [3, 4]. These superior properties suggest many possible uses in weight-sensitive components for aerospace or land transportation. A wide variety of fabrication techniques have been explored for metal matrix composites. These include powder metallurgy, molten metal methods, semi-solid casting, pressure infiltration and spray deposition [1, 4, 5, 6].

The powder metallurgy processing technique is attractive for several reasons [6, 7, 8]. This approach offers microstructural control of the phases that is absent from the liquid phase route. Powder metallurgy processing employs lower temperatures and, therefore, theoretically offers better control of interface reaction kinetics. Because of their basis as a powder, PRA composites often have been deformation processed after powder consolidation to develop the best properties. In this manner, the composites behave like high strength aluminum alloys made by the powder metallurgy technique: i.e. the prior particle oxide skins must be broken up by metal working before the true properties of the matrix metal and, hence, the composite can be achieved. The most common primary breakdown process has been extrusion. Other metal working processes such as rolling, forging, shear spinning and swaging have also been demonstrated. Also, the typical ceramic reinforcements (e.g. SiC) for PRA composites give rise to dulling of many common machine tools, decreasing the machinability of these composites. Thus, it would be quite beneficial if a powder metallurgy process for high strength PRA composites with good ductility could be developed that avoided extensive mechanical deformation and permitted net shape die forming without machining.

Strengthening mechanisms of composites have been studied extensively for many years. The continuum shear lag model was first developed to predict the direct strengthening of continuous fiber reinforced composites originally by Cox [9]. The predominant direct strengthening factor is the volume fraction of reinforcement. Powder processed material tends to give somewhat higher strengths than melt processed composites, probably because of additional strengthening from residual oxide dispersoids from prior particle surface, and the somewhat finer grain size. Unfortunately, for the low aspect ratio whisker or particulate reinforcement particles typically used in current metal matrix composites, the shear lag model underestimates the strength [10, 11]. Nardone and Prewo suggested that better agreement can be obtained if the shear lag model is modified to allow for whisker or fiber end loading effects [12]. The theoretical prediction by means of this direct strengthening model is closer to the experimental results when the reinforcement aspect ratio is small. The difficulty with this continuum approach is that it ignores the secondary strengthening influence of reinforcement particles on the micromechanics of composite deformation, such as the very high matrix work hardening at low strains. The modified shear lag model [12] also ignores modifications in composite microstructures, such as dislocation density increases and residual stresses from processing effects [13].

A model to predict the yield strength of a particle-reinforced metal matrix composites by considering the dislocation density due to mismatch between thermal expansion coefficients (ΔCTE) of particle and matrix was developed by R.J.Arsenault and his colleagues [14, 15]. It was proposed that the high matrix dislocation density caused by ΔCTE should account for the observed secondary strengthening. While this enhanced dislocation density strengthening model is in agreement with the general trends of the strengthening results, it is not sufficient to account for the combined strengthening effect in many composite materials [16, 17]. On the other hand, Orowan strengthening is not a major factor with the 5μm and larger reinforcement particles usually used, but particles of this size can result in quench hardening

and enhanced work hardening because of elastic misfit back stress hardening [14, 18]. Reinforcement particle shape, in terms of aspect ratio, also can influence composite strength, but for the typical SiC particulate aspect ratio range of up to 2:1, it is not expected to be a major factor.

In order to study the secondary strengthening contribution to the total strength of Al alloy based composites, Krajewski and Chawla, et al. [19, 20] had to use a series of complex thermomechanical treatments in both the unreinforced Al alloy and in the composite material. These treatments were needed to ensure that the density and distribution of the dislocations and precipitates were similar in unreinforced Al alloy and in the composites in order to compare the strength. In this paper, elemental Al powder was chosen as the matrix material to avoid the complications of matrix heat treatment effects on the strengthening mechanisms of composite materials and to permit the use of a high temperature consolidation temperature, without promoting partial melting.

In recent research [16], results on elemental Al matrix composites, reinforced by 30 vol.% of spherical Al-Cu-Fe alloy particles and consolidated by quasi-isostatic forging, were introduced. Because of the fine (dia. < 10 μm) matrix and reinforcement particle sizes that match closely and a homogenous spatial distribution, the UTS and yield strength of this model composite material were improved over the matrix properties by 111% and 220%, respectively, for the commercial purity composite sample. Remarkably, the UTS and yield strength of the composite were improved over the matrix properties by 201% and 328%, respectively, for an equivalent composite material produced from metal powders with much thinner oxide surfaces. The elastic modulus values of these composites, in both versions, are very close to the theoretical upper bound value from the rule of mixtures (ROM) for 30 vol.% loading. These results suggested that the selection of potential reinforcement phases for PRA materials should be broadened from refractory ceramics to include, e.g.,

intermetallic compounds that also can form a strong bond with the Al matrix by high temperature solid-state sintering. Also, the results clearly indicated that PRA composites made from powders with a thinner oxide surface can achieve significant improvements in tensile properties over the same composites made from commercial powders with thick oxide and impurity surfaces [21].

In this paper, we will report the tensile properties of similar composites made by vacuum hot pressing (VHP) with a wide range of reinforcement loadings. Compared to quasi-isostatic forging, VHP has a further decreased amount of interparticle shear, strain hardening rate and almost no grain anisotropy compared to the forging method [7]. This VHP approach can be viewed as one step closer to the goal of powder consolidation process simplification for direct net shape forming of PRA composite parts. The tensile property results will be compared to the predictions of the direct and secondary strengthening models for the Y.S. increase of the composite samples.

2. Experimental Procedure

2.1 Materials

Powders used for the two kinds of composite samples are shown in Table 1. For the baseline experiments, commercial inert gas atomized (CIGA) Al and $Al_{63}Cu_{25}Fe_{12}$ quasicrystal powders were obtained. The CIGA Al powder (99.7% purity) had been evaluated thoroughly in earlier work [21-23] to characterize its surface oxide properties. A patented gas atomization reaction synthesis (GARS) technique was also used to produce 99.99% pure Al and Al-Cu-Fe quasicrystal (QXL) powders [24] in our laboratory. The x-ray diffraction results of both CIGA and GARS quasicrystal powders are shown in figure 1. The

results revealed that there are two phases in the as-atomized powder, the major $Al_{63}Cu_{25}Fe_{12}$ quasicrystal (icosahedral) phase and some β-Al(Cu, Fe) cubic phase.

Table 1. Powders used for AFF and GFF samples.

Samples	Powders used	Purity
AFF-15	CIGA Al powder (<10μm) + 15, 20, or 30 vol. % CIGA Al-Cu-Fe quasicrystal powder (<10μm)	99.7%
AFF-20		
AFF-30		
GFF-15	GARS Al powder (< 10μm) + 15, 20, or 30 vol. % GARS Al-Cu-Fe quasicrystal powder (<10μm)	99.99%
GFF-20		
GFF-30		

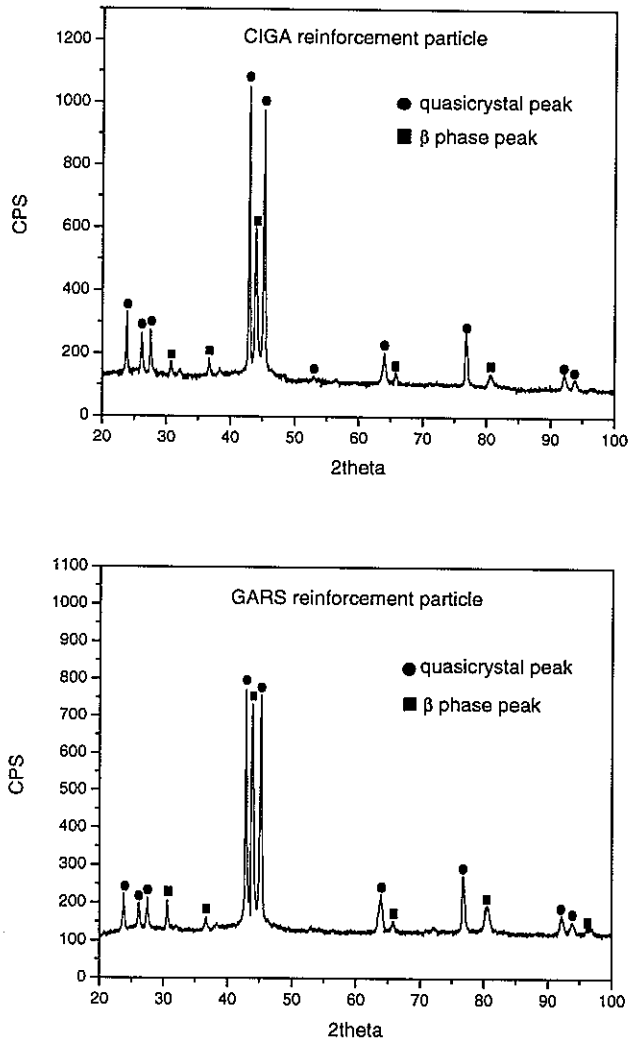

Figure 1. X-ray diffraction of CIGA and GARS Al-Cu-Fe alloy reinforcement powders.

The Al and Al-Cu-Fe quasicrystal powders were air classified to less than 10 μm. The quasicrystal powders from both sources were screened subsequently through a 20 μm screen to eliminate the residual large particles. The size distributions of Al and quasicrystal powders were reported elsewhere [25].

2.2 Consolidation processing

First, powders were blended homogeneously. Then, blended powders were compacted by cold isostatic pressing (CIP) with a pressure of 280MPa, intending to produce a green density of about 90%. The green samples from CIP were machined to match the hot press die dimensions and vacuum (10^{-5} torr) hot pressed (VHP) at 550°C for 6 hours, using a pressure of 175 MPa for 5 hours (after the first hour at 550°C). Because the first GFF-20 sample, initially VHP at 175 MPa, was not fully dense, a second GFF-20 composite sample was consolidated at 245 MPa by the VHP process to get full density and was used for the subsequent analysis. Table 2 summarized some VHP processing parameters.

Table 2. Vacuum hot pressing parameters.

Temperature (°C)	Soak at Temp. (hour)	Pressure (MPa)	Dwell at Pressure (hour)
550	6	175 or 245	5

2.3 Other tests

X-ray diffraction characterization of composite samples was performed using a Philips PW1830 generator with Cu K_α radiation. The Archimedes technique was used to measure the density of each composite sample. Microhardness of bulk Al-Cu-Fe quasicrystal materials was measured with a Vickers indenter at a load of 500g. The elastic modulus of composites samples was measured by an ultrasonic method [26]. Tensile tests of consolidated composites were performed on an Instron model 1125 tensile test machine under 1.27 mm

per minute monotonic loading. Tensile sample dimensions were 6.35 mm in diameter and 25.4 mm in uniform gauge length, according to ASTM recommendations [27]. Microstructures of the composites and fractography of the tensile samples were examined on an AMRAY 1845 field emission scanning electron microscope. The coefficient of thermal expansion (CTE) of the Al_7Cu_2Fe (ω) phase was measured by a Perkin-Elmer TMA7 thermal-mechanical analyzer (TMA). Neutron diffraction (in-situ) measurement procedures for determining load bearing stresses during tensile tests were reported in detail, elsewhere [28].

3. Results and Discussion

3.1 General Microstructures

As shown in figure 2 and figure 3, the reinforcement particles are spherical in shape and distributed quite uniformly in all samples. Some local clustering still can be found [29] in all the samples, especially in 30 vol. % loading samples. The density measurements of the composite samples are shown in table 3, which shows that all of the samples are essentially fully dense.

3.2 X-Ray Diffraction of Composites

X-ray diffraction results on all the composite samples are shown in figure 4 and 5. The elemental Al matrix phase peaks are apparent, but the quasicrystal and β phase peaks, which are seen in figure 1, were not observed in the resulting patterns. Instead, there are diffraction peaks of an ω phase (Al_7Cu_2Fe), which is a crystalline phase with the density of 4.18 g/cm^3 [10]. As often reported in previous research, the Al-Cu-Fe quasicrystal phase is stable when annealing at about 700 $^{\circ}$C [30-32]. However, Koster et al. reported that Al-Cu-Fe quasicrystal

phase, with a density of 4.7 g/cm^3 [10], may react with Al phase to form ω phase during heat-treatment [33]. Because the VHP process lasts 5 hours at 550˚C, it is reasonable to expect that Al atoms may diffuse into the Al-Cu-Fe quasicrystal particles and may react to form the ω phase.

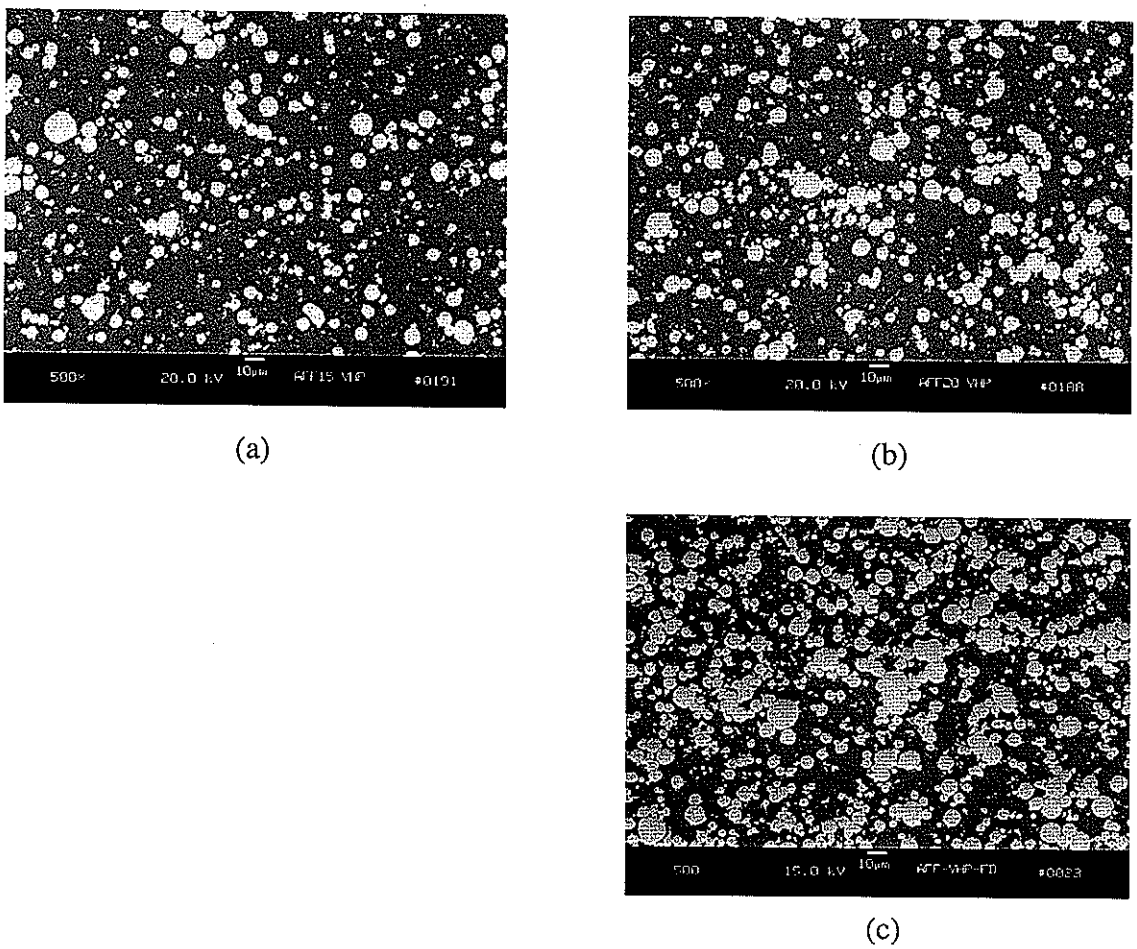

(a) (b)

(c)

Figure 2. Back-scattering electron SEM micrographs of microstructures of AFF composite samples (a) AFF-15, (b) AFF-20, (c) AFF-30.

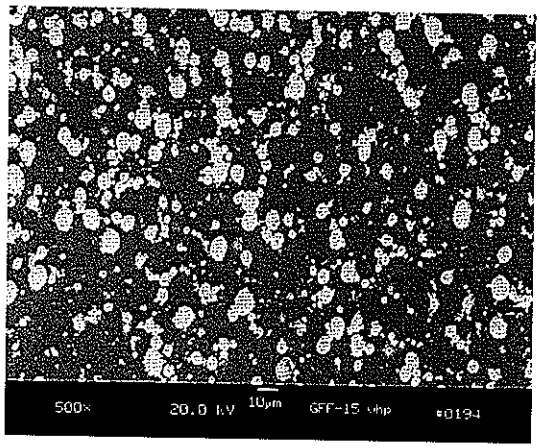

(a)

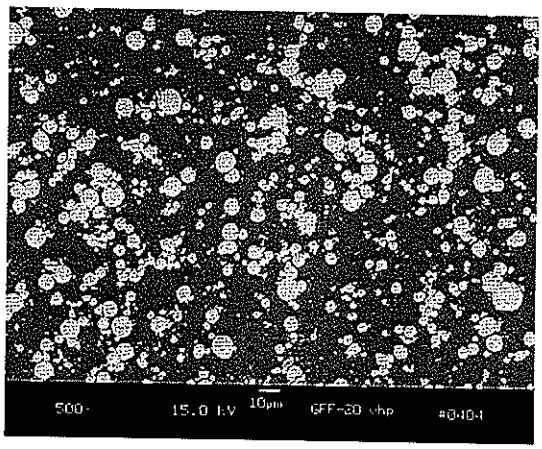

(b)

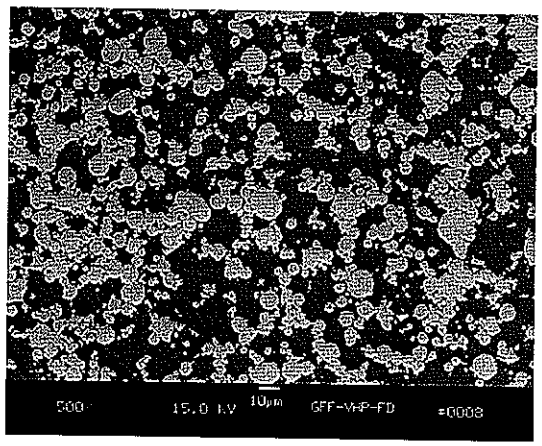

(c)

Figure 3. Back-scattering electron SEM micrographs of microstructures of GFF composite samples (a) GFF-15, (b) GFF-20, (c) GFF-30.

Table 3. Density of all the composite samples.

Samples	AFF-15	GFF-15	AFF-20	GFF-20	AFF-30	GFF-30
Density (g/cm^3)	3.0	3.0	3.09	3.09	3.28	3.28
Theoretical density (g/cm^3)	3.0		3.1		3.3	

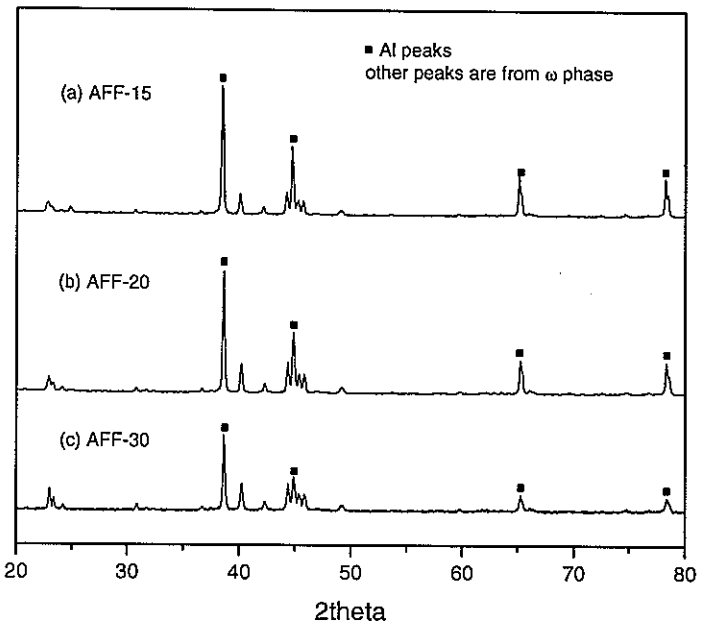

Figure 4. X-ray diffraction measurement of AFF composite samples (a) AFF-15, (b) AFF-20, (c) AFF-30.

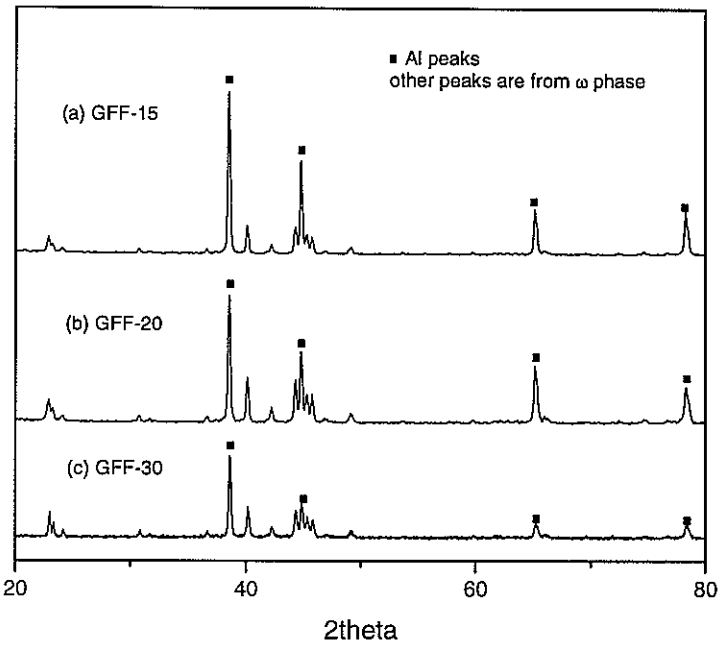

Figure 5. X-ray diffraction measurement of GFF composite samples (a) GFF-15, (b) GFF-20, (c) GFF-30.

3.3 Elastic Modulus and Static Mechanical Properties

The elastic modulus (E) of the ω and quasicrystal phases were measured by an ultrasonic method. The E values were 168 GPa for the ω phase and 182 GPa for the quasicrystal phase. This result shows that the modulus of the ω phase is only slightly lower than the initial quasicrystal phase. The microhardness values of these two phases are also very similar, shown in table 4. The quasicrystal and ω phase materials used for the modulus measurements were fully dense samples made by hot isostatic pressing (HIP) of gas atomized powder of the stoichiometric alloys at 800˚C and 700˚C, respectively. The CTE of ω phase, as measured by TMA, is $15.45\times10^{-6}K^{-1}$, which is slightly larger than the CTE of the quasicrystal phase, $12.6\times10^{-6}K^{-1}$ [34]. The similarity of the properties between these two phases may suggest that although there may be no quasicrystal remaining in the reinforcement particles, the resulting ω phase can still act as an effective reinforcement for promoting the modulus and strength of the composites.

Table 4. Properties of $Al_{63}Cu_{25}Fe_{12}$ quasicrystal phase and Al_7Cu_2Fe (ω) phase.

	Elastic modulus (GPa)	Microhardness (H_v)	CTE ($\times10^{-6}K^{-1}$)
$Al_{63}Cu_{25}Fe_{12}$	182	922 ± 25	12.6 [34]
Al_7Cu_2Fe	168	935 ± 80 [33]	15.45

The elastic modulus measurements for the composite materials range from 80-100 GPa, as reinforcement loading is increased from 15 to 30 vol.%. As we can see in figure 6, most of the modulus values of the composites are close to or at the upper-bound model values. This observation indicates the effectiveness of the reinforcement in this composite material and is consistent with good bonding between Al and reinforcement particle phases. The modulus of ω phase was used for all of the model calculations of the composite modulus.

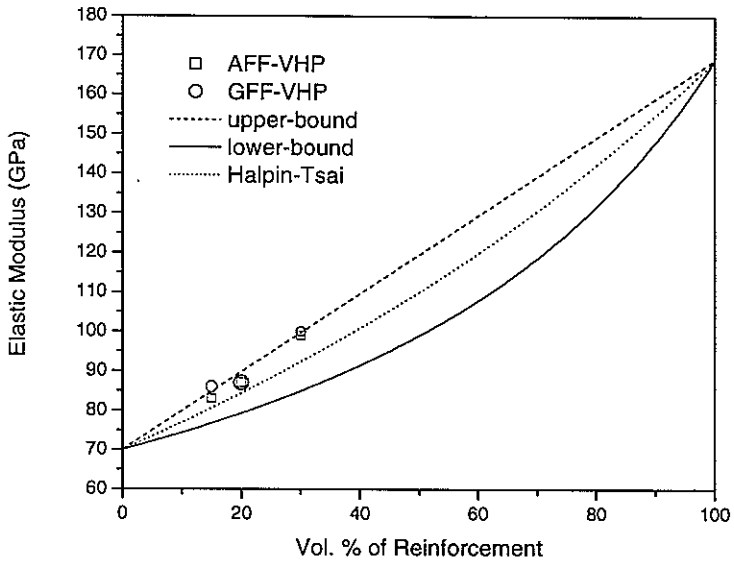

Figure 6. Elastic modulus of AFF and GFF composite materials compared with three modulus prediction models including iso-strain (upper-bound) model [35], iso-stress (lower-bound) model [35] and Halpin-Tsai equations [36].

3.4 Tensile Properties

The tensile property values including elastic modulus, ultimate tensile strength (UTS) and yield strength (Y.S.) of all the AFF and GFF composite samples are shown in table 5. The Y.S. and UTS of GFF-VHP samples are much above the corresponding values of the corresponding elemental Al matrix sample, whose Y.S. is 53 MPa and UTS is 95 MPa [25]. The same is true for the AFF-VHP samples. The Y.S. and UTS of the corresponding elemental Al matrix of AFF samples are 88 MPa and 145 MPa, respectively [25].

Table 5. Tensile properties of GFF and AFF composite samples.

	GFF-VHP			AFF-VHP		
Samples	GFF-15	GFF-20	GFF-30	AFF-15	AFF-20	AFF-30
E (GPa)	86	87	100	83	87	99
UTS (MPa)	154	222	238	176	178	233
$\sigma_{0.2}$ (MPa)	109	135	191	135	154	199

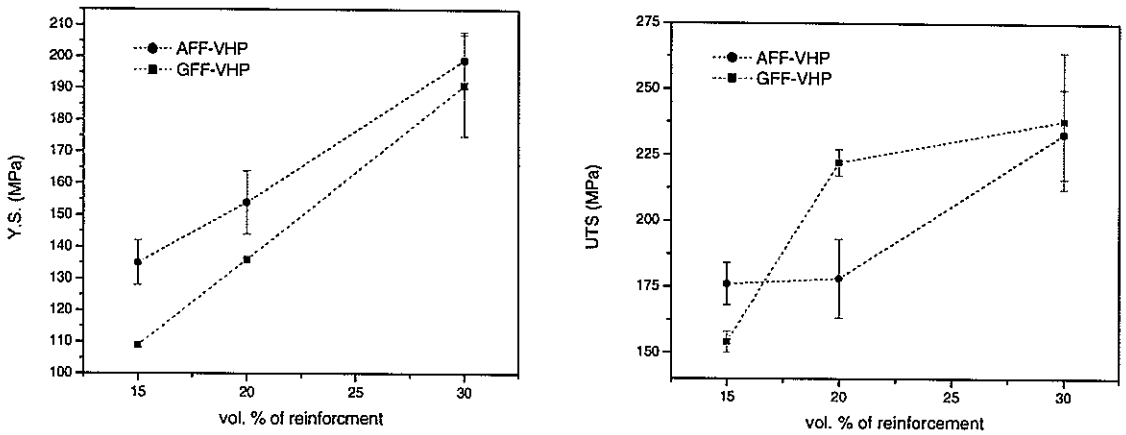

(a) (b)

Figure 7. Yielding strength (Y.S.) and ultimate tensile strength (UTS) of (a) AFF and (b) GFF composite samples. (Some data scattering bars are very small and contained in the symbol of data points.)

Figure 7 gives a more clear comparison of Y.S. and UTS between AFF and GFF samples. Figure 7(a) shows that for both AFF and GFF samples, Y.S. has a quite linear relationship with the reinforcement volume fraction. The Y.S. of AFF samples with different volume fractions of reinforcement are consistently higher than GFF samples. This is reasonable because the commercial purity AFF samples contain more oxide or dissolved impurities that would promote higher strength. From Figure 7(b), we can see that the UTS of AFF is obviously higher than GFF at 15 vol.% reinforcement loading, but at the 20 and 30 vol.% loading AFF samples show lower or about the same UTS values as GFF samples. After tensile samples pass the yielding point, there will be more and more micromechanical damage accumulated inside the material along with the tensile strain increase. When the damage accumulates to some critical level, the tensile strain reaches the UTS point and the tensile sample fails. If the damage accumulation rate is faster, then UTS will be reached earlier and its value will be lower. From this analysis, we can see that although GFF samples have a lower Y.S. level than AFF samples, they may have better bonding strength between consolidated particles and better micromechanical ductility. This improved interparticle

bonding can be attributed to the high purity of GFF samples and, more importantly, to the very thin initial oxide layer on the GARS-processed powder surfaces. The above results are another example that is consistent with our previous studies of elemental Al, which showed that the powder surface chemistry has a very significant effect on the powder sintering kinetics and final materials properties [21].

3.5 Fracture Mode

Figure 8 and figure 9 show the fracture surfaces of AFF and GFF samples. AFF-15, GFF-15, AFF-20 and GFF-20 samples all show a mixture of fracture modes. In the Al matrix area, there are small dimples and tearing ridges, which suggest a very ductile fracture in the matrix area. There are many reinforcement particles cracking on the fracture surface, but there are also some small spherical particles apparently on the surface, which suggests some interface debonding between matrix and finer reinforcement particles. There are also a few particles debonding on the AFF-30 samples, but no particle pull-out appears on the GFF-30 sample fracture surfaces, which may show that the GARS powders can be more easily sintered than CIGA powders because of a much thinner oxide layer on the GARS powder surfaces, compared to the CIGA powder. Much more detailed experiments and analysis on the sintering behavior of these two kinds of powders can be found in many previous reports [16, 21, 22, 25]. Generally the AFF-30 and GFF-30 fracture surfaces look simpler than the others, with more uniform ductile fracture in the pure Al matrix. Maybe such a high loading of hard particles can promote increased green density of powder mixtures and local plastic shearing deformation during CIP and hot pressing, which will surely enhance the sintering and bond strength between particles. Especially in those relatively low volume fraction (15 and 20 vol.%) samples, the pressure applied during the VHP process may need to be increased to further enhance the local yielding of the matrix particles and, hence, the sintering of each composite sample.

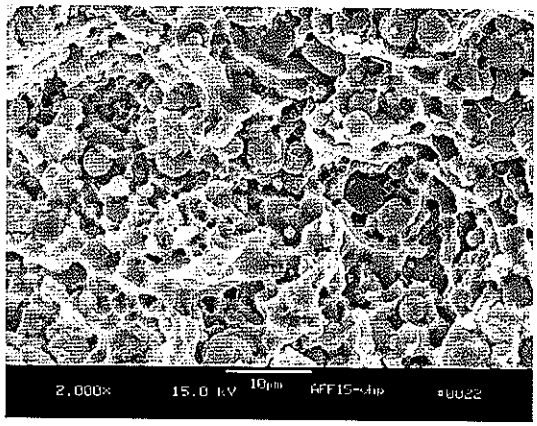

(a)

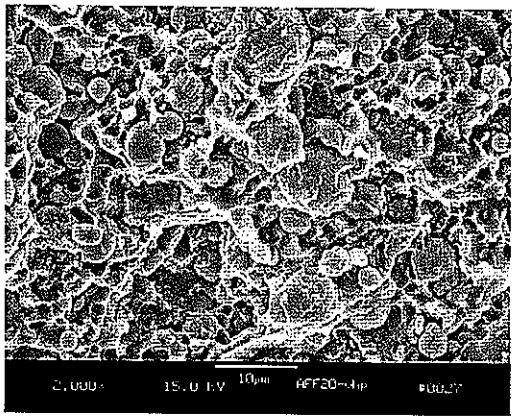

(b)

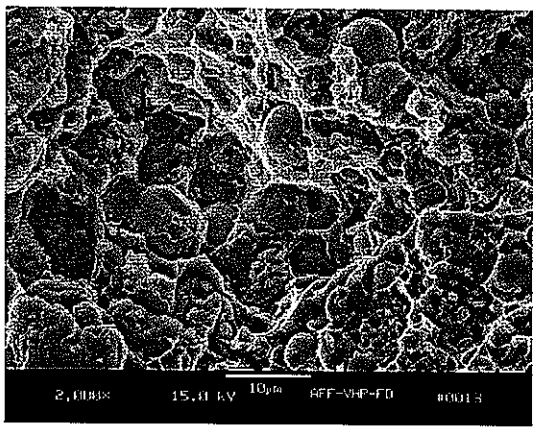

(c)

Figure 8. Secondary electron SEM micrographs of Fracture surfaces (a) AFF-15, (b) AFF-20, and (c) AFF-30 VHP composite samples.

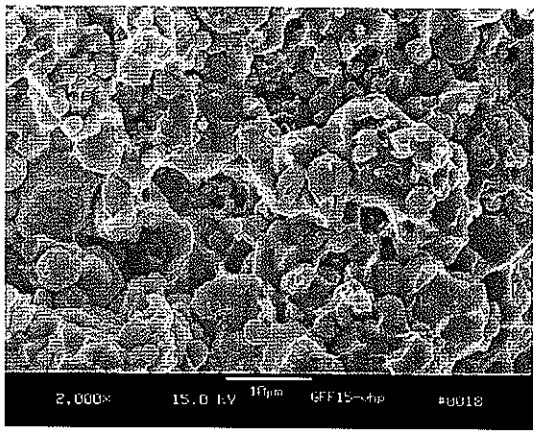

(a)

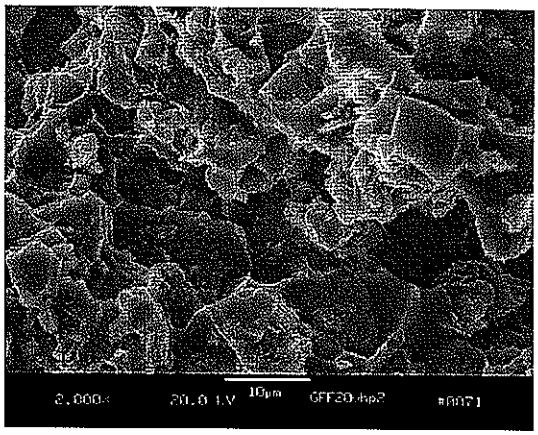

(b)

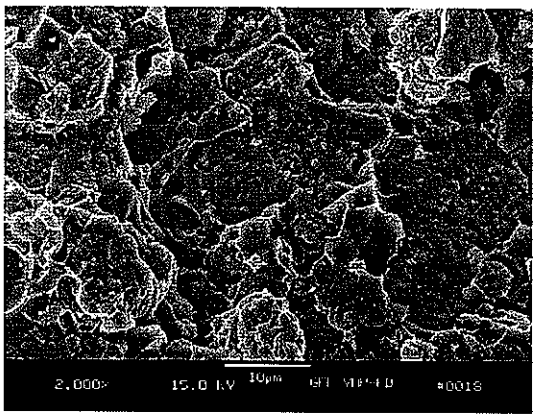

(c)

Figure 9. Secondary electron SEM micrographs of Fracture surfaces (a) GFF-15, (b) GFF-20, and (c) GFF-30 VHP composite samples.

4. Hybrid Model for Y.S. Prediction

During the past two decades a large number of investigations have been carried out to reveal the strengthening mechanisms of metal matrix composites, and both continuum and micromechanical models have been developed. As a result of these investigations the major mechanisms which may contribute to the direct and secondary strengthening of a composite have been deduced:

(a) Direct strengthening from load transfer from the matrix to the reinforcement via shear stresses at the interface between the components (shear-lag theory) [12],
(b) Secondary strengthening form increased density of dislocations generated during cooling from an elevated processing temperature because of the differential thermal contraction between matrix and reinforcement [14, 37],
(c) Secondary strengthening from artificially reduced interparticle spacing from extremely fine precipitates due to the creation of Orowan loops (Orowan strengthening) [25], and
(d) Geometrically-necessary dislocation (secondary) strengthening, which is also common in those precipitation strengthened materials [38] and occurs during initial plastic deformation in a micromechanical manner.

All the above strengthening mechanisms, from a theoretical point of view, seem suitable for particulate-reinforced Al matrix composites. For studying the above mechanisms, the elemental Al matrix composites consolidated by a VHP process in this report can be a very suitable material because of their simplified microstructures, without matrix phase precipitates. As a solid state sintering process, the VHP process can use relatively low applied pressure during consolidation and inter-particle shearing stresses are located mostly in a thin layer of material close to the die wall. The dwell time at high temperature of VHP is much longer and the sample cooling rate after full consolidation is much slower than high strain-rate consolidation methods, e.g., a quasi-isostatic forging process [16]. Thus, residual dislocation density in the sample matrix and dislocation strengthening produced by VHP should be significant reduced. Because the Al matrix used in the composites was produced from commercial purity (99.7%) and high purity (99.99%) elemental powder, there should not be much possible precipitation strengthening effect, but some minor solid solution strengthening is possible, especially in the commercial purity PRA composites. Most dislocations in the as-received VHP composites should be produced by the CTE difference (ΔCTE) between the matrix and reinforcement phases after each consolidated composite

sample is cooled down from the high processing temperature. Increased dislocation density may also result from tensile property differences between phases during plastic deformation (geometrically necessary dislocations). Therefore, a combined strengthening model that includes the effects of several mechanisms will be tested on these VHP composite samples in the following sections.

4.1 Load Transfer Mechanism

The continuum shear lag model was developed originally to predict the strength of continuous fiber reinforced composites by Cox [9]. The model centers on the transfer of tensile stress from matrix to a fiber by means of interfacial shear stresses. For the aspect ratio of SiC whiskers (10:1) and SiC flake fragments (2:1) typically used in particle reinforced metal matrix composites, the continuum shear lag model underestimates the strength [10, 11]. Nardone and Prewo proposed a modified shear lag theory and suggested that better agreement is obtained if the equation is modified to allow for whisker or fiber end loading effects, giving the following equation for strength prediction [12].

$$\sigma_{cy} = \sigma_{my}\left[\frac{1}{2}V_R(s+2)+V_m\right] \qquad (1)$$

where s is the aspect ratio of the reinforcement, and σ_{cy} and σ_{my} represent the yield strength of composite and matrix material, respectively. V_R and V_m represent the volume fraction of reinforcement and matrix, respectively. They also showed that the Orowan strengthening mechanism was insufficient to account for the increase in yield strength of the particulate reinforced Al alloy matrix composites [12]. The difficulty with this continuum approach to load sharing prediction is that it ignores the influence of reinforcement particles on the matrix microstructure, such as increased dislocation density caused by CTE difference, modulus and strain incompatibility between matrix and reinforcement phases, and processing procedures.

By carefully matching the matrix precipitate microstructures, Chawla et al. [39] showed that there is a good correlation between the experimental data of SiC-reinforced T8-tempered Al alloy (Al2080) matrix composites and T6-tempered matrix samples of Al2080 using the above modified shear lag model. However, other studies reported by Arsenault et al. [10] showed that the shear lag model can only give a very small predicted amount of Y.S. increase, compared with experimental results. For example, if we apply equation (2) for the composites with a 30 vol.% of reinforcement reported in this paper, the Y.S. increase prediction would be only 15% above the Y.S. of the elemental Al matrix. In other words, a numerical Y.S. increase of only about 8 MPa and 13 MPa for GFF and AFF samples, respectively, are predicted instead of the much higher values given in Table 5.

Actually, the load transfer capability or partitioning between phases in composite materials can be directly measured in-situ by the X-ray or neutron diffraction methods [40, 41]. From these measurements, the specific load partitioning between each phase in a composite can be found. Therefore, we can clearly know how much load is transferred to reinforcement phases and calculate load transfer strengthening from these actual measurement values, instead of using the shear-lag model.

For making an accurate assessment of the load transfer strengthening contribution, the actual load bearing stresses in Al matrix and reinforcement particles were measured in-situ while applying external tensile stress by a neutron diffraction method at the NIST Neutron Research Center. The detailed neutron diffraction measurement procedure is reported in another paper [28]. The applied tensile stress level during the load partitioning measurement of all the composites samples was well within the elastic region of the material. The neutron diffraction measurement results of phase bearing stresses in all composite samples are shown in figure 10. The load bearing ratios of Al matrix and reinforcement phases in table 6 were

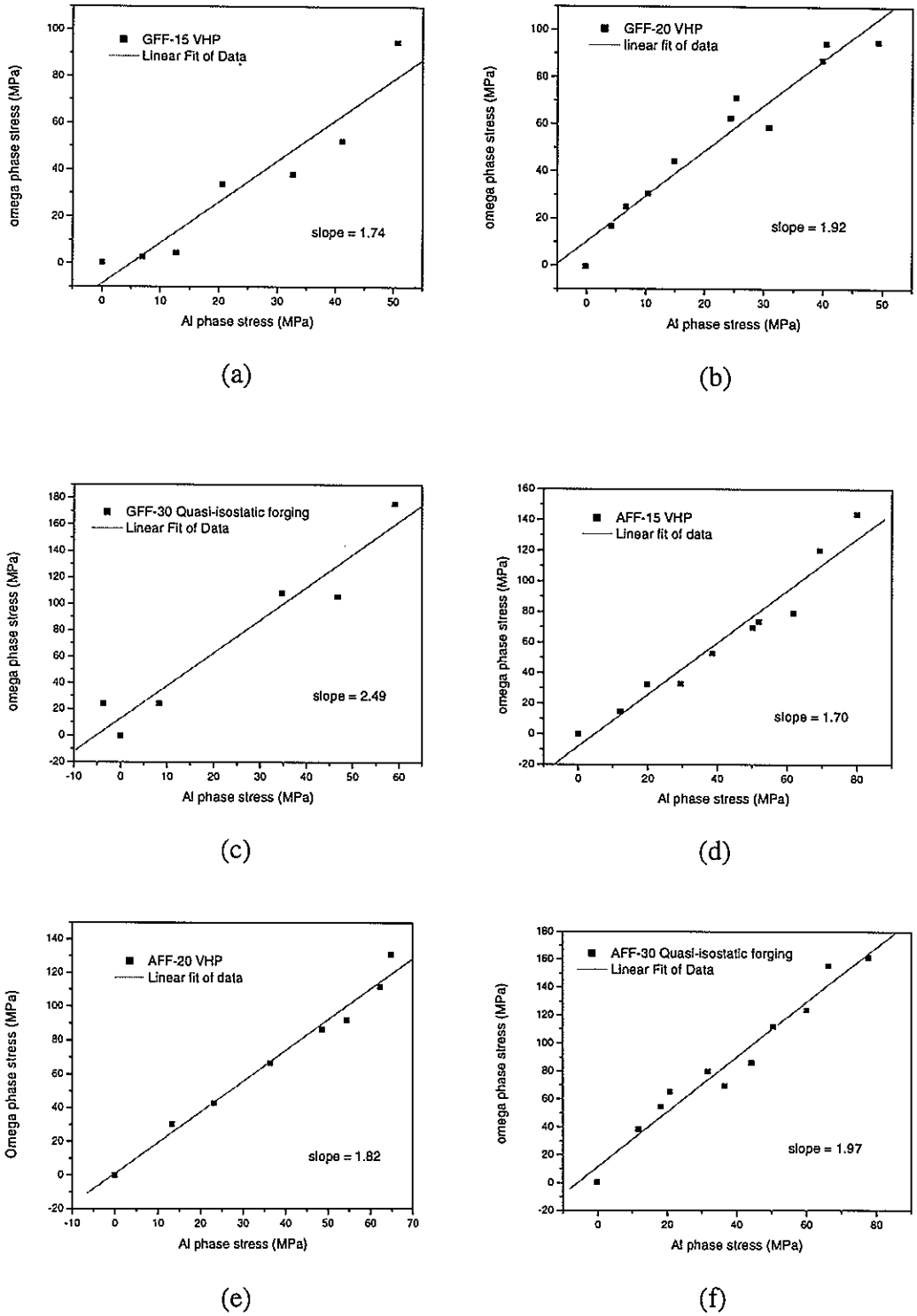

Figure 10. Neutron diffraction measurement of load partitioning between Al matrix and reinforcement particles [32] (a) GFF-15, (b) GFF-20, (c) GFF-30, (d) AFF-15, (e) AFF-20, and (f) AFF-30.

obtained by linearly fitting the curves in figure 10. These load bearing ratios measured in the elastic range were used in the subsequent load transfer strengthening analysis, although the operative load bearing ratios may have some minor decrease due to the hardening of the Al matrix during the plastic yielding portion of tensile deformation. Later, we will show that actually the load transfer strengthening contribution in Table 7 is only composed of a small portion of the total strengthening. Therefore, the above approximation will not cause any significant difference in predicting total strengthening of the composites.

Table 6. Load bearing ratio of reinforcement phase and Al matrix in the composites [32].

	GFF-15	GFF-20	GFF-30	AFF-15	AFF-20	AFF-30
Processing	VHP	VHP	Quasi-isostatic forging	VHP	VHP	Quasi-isostatic forging
σ_C^R / σ_C^M	1.74	1.92	2.49	1.70	1.82	1.97

Now with these measurement results of load partitioning and load bearing ratios, we can calculate directly how much direct load transfer strengthening these composite materials demonstrate. Note that the load transfer calculations assume that the load bearing ratios of the 30 vol.% loaded and quasi-isostatically forged samples are equal to that of the VHP samples at the same loading. In other words, the processing method should not affect the load transfer effect as long as the matrix and the reinforcement particles are bonded well and each sample is fully dense.

According to references [42, 43], the average phase stresses in an Al matrix and in the reinforcement particles can be measured by neutron diffraction and have the following relationship with the external applied stress:

$$\sigma^A = V_R \sigma_c^R + (1 - V_R)\sigma_C^M \qquad (2)$$

where σ^A is the external applied stress on the PRA composites, V_R is the volume fraction of reinforcement, and σ_C^R and σ_C^M are the average bearing stresses of the reinforcement particles and the matrix, respectively,

Therefore the yield strength increase in the PRA composites that results from the load transfer effect ($\Delta\sigma_y^{LT}$) can be calculated as follows:

$$\Delta\sigma_y^{LT} = \sigma^A - \sigma^M \qquad (3)$$

where σ^M is the yield stress of the unreinforced matrix material. Therefore

$$\Delta\sigma_y^{LT} = V_R\sigma_C^R + (1-V_R)\sigma_C^M - \sigma^M \qquad (4)$$

where $\Delta\sigma_y^{LT}$ is the Y.S. increase from the load transfer mechanism. Assuming that the Al matrix bearing stress σ_C^M is approximately equal to the yield strength of the pure Al matrix material σ^M when the composite is yielding, the load transfer strengthening can be calculated by following equation (5):

$$\Delta\sigma_y^{LT} = \left(\frac{\sigma_C^R}{\sigma_C^M} - 1\right)V_R\sigma^M \qquad (5)$$

where the results are summarized in Table 7. As shown in Table 7, the load transfer strengthening of the composites samples only contributed a small part of the observed strengthening, which is also consistent with the results of Al/SiC composites [10].

4.2 Thermal Expansion Mismatch Model

In addition to the direct strengthening from the load transfer effect, an important indirect strengthening contribution to be considered should be the plastic deformation effect caused by ΔCTE between the Al matrix and the reinforcement particles. Arsenault and collaborators [14, 15] showed that an increased dislocation density of the matrix does result from a difference in the coefficient of thermal expansion (CTE) of an Al matrix and SiC reinforcement particles and that the increased matrix dislocation density does promote a large portion of the observed increase in Al/SiC composite yield strength. In other words, because the coefficient of thermal expansion of a typical aluminum alloy is about ten times that of SiC, there can be relatively high residual stress around each SiC particle at ambient temperature after thermal processing of such composites [14]. The equation proposed for prediction of yield strength increase by ΔCTE is, as follows [15],

$$\Delta\sigma_y^{CTE} = \alpha\mu b\left[\frac{V_R}{1-V_R}\frac{B\varepsilon}{b}\right]^{1/2}\left[\frac{1}{t}\right]^{1/2} \qquad (6)$$

where α is a constant that is equal to 1.25, μ is the shear modulus of the pure Al matrix, 26.4GPa, b is the Burgers vector, about 2.86×10^{-10} m, V_R is the volume fraction of reinforcement, B is 12 for spherical particle reinforcement, ε is the misfit strain due to the ΔCTE, and t is the average diameter of the reinforcement (about 5.5 μm) [25].

For analysis of the PRA composites of this study, the CTE of each reinforcement particle in the composite, ω phase, is $15.45\times10^{-6}K^{-1}$ and the CTE of pure Al is $23.6\times10^{-6}K^{-1}$. The processing temperature is 550°C and, assuming room temperature is 20°C, the temperature difference is 530°C, i.e. 530 K. Then, misfit strain ε can be calculated by equation (7) and is equal to 6.54×10^{-6},

$$\varepsilon = (\Delta CTE)(\Delta T) \qquad (7)$$

A summary of the results calculated with equation 7 are found in Table 7. Inspection of the results in Table 7 showed that ΔCTE strengthening represents a relatively large portion of the total observed strength increase, which is consistent with the results from Arsenault [10, 14, 15].

4.3 Geometrically Necessary Dislocation Strengthening Model

When an external tensile load is applied to a composite material and it arrives at the matrix yielding point, there will be geometrically necessary dislocations (GND) generated in the Al/reinforcement interface area because of the yield strength and elastic modulus differences between Al and reinforcement particles, as shown in Figure 11. Otherwise, extensive interface debonding between Al and particles would take place in the composites. At the 0.2% strain of the composite material samples, AFF and GFF, the Al matrix already had some plastic deformation, as we can see in the stress-strain curves in figure 12. In order to compensate for the strain incompatibility between matrix and particles, extensive GND dislocations must be generated in the matrix.

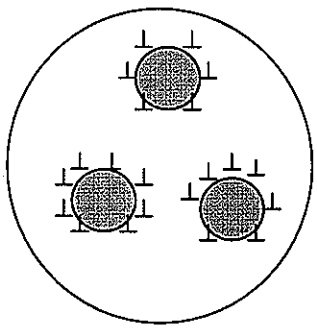

Figure 11. Schematic GND dislocations around reinforcement particles

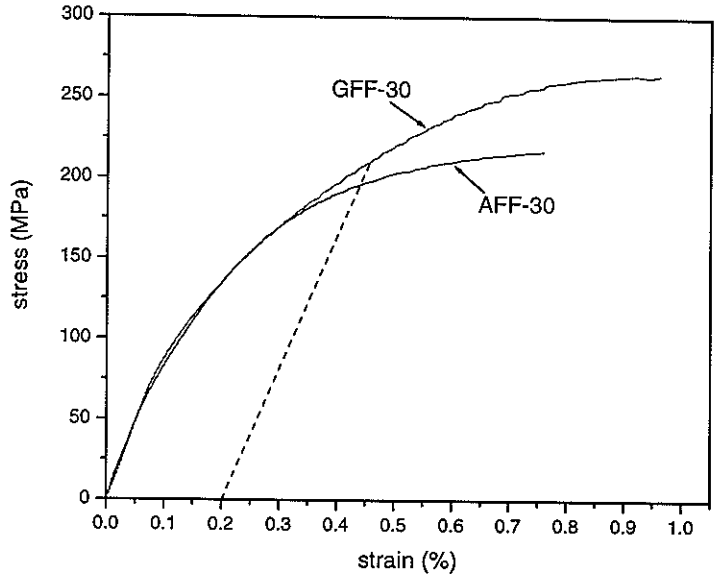

Figure 12. Stress and strain curves of AFF-30 and GFF-30 samples.

A GND density increase around each interface region also will cause a secondary (indirect) strengthening effect for the composite material. This GND effect can be also seen in some precipitation strengthening materials, where it acts to increase the population and spatial density of dislocation barriers far beyond the initial precipitate distribution. The yield strength increase caused by GND strengthening ($\Delta\sigma_y^{GND}$) can be calculated by the following equation [38].

$$\Delta\sigma_y^{GND} = \alpha\mu b\sqrt{\frac{8V_R\varepsilon_y}{bD}} \qquad (8)$$

where α is a constant that is equal to 1.25, μ is the shear modulus of the pure Al matrix, 26.4GPa, b is the Burgers vector, about 2.86×10^{-10} m, V_R is the volume fraction of reinforcement, D is the diameter of the prismatic dislocation loop around the reinforcement particles, and ε_y is the yielding strain. By using an approximate D value of 5.5 μm, which is the average diameter of reinforcement particles [25] and ε_y value of 0.2%, the yield strength

increase from the GND effect for each sample was calculated. Again, the calculated results are found in Table 7. The contributions from the GND strengthening mechanism increases with increased of the reinforcement particle volume fraction. The previous study of Sekine [44] also showed that the GND mechanism is a significant contribution to composite strengthening, which is consistent with our analysis results.

Table 7. Y.S. increase values calculated from different mechanisms and experimental values (MPa).

	$\Delta\sigma_y^{LT}$	$\Delta\sigma_y^{CTE}$	$\Delta\sigma_y^{GND}$	Combined Prediction	Experimental results
AFF-15	9	28	15	52	50
GFF-15	6			49	56
AFF-20	14	34	18	66	69
GFF20	10			62	80
AFF-30	25	45	44	114	114
GFF-30	24			113	138

4.4 Combined Effect of Strengthening Mechanisms

In the calculation results from each of the three well-accepted direct and indirect strengthening contributions shown in Table 7, one can observe an under-prediction of the observed values for the Y.S. increases in our composite samples, if applied individually. Consistent with the micromechanical aspects of current composite strengthening theory, the yield strength increase may be better predicted from a combination of both an elastic effect, i.e., load transfer, and plastic-type effects, i.e., ΔCTE and GND effects. The plastic-type effects can be added to account for the highly local yielding phenomen that occurs between reinforcement particles and the matrix phase, prior to reaching the 0.2% yield strength, a macroscopic yielding point. Thus, the combined effect can be calculated for the two kinds of Al/QXL composites by eqn. (9),

$$\Delta\sigma_y = \Delta\sigma_y^{LT} + \Delta\sigma_y^{CTE} + \Delta\sigma_y^{GND} \qquad (9)$$

Table 7 shows the calculation results for each composite sample, using equation 9. Comparing the experimental Y.S. increase values with predicted values from the combined calculation, very good agreement with the relationship given in equation 9 was found for all the composite samples. The Y.S. increase values in Table 7 were calculated based on the 0.2% Y.S. values of elemental CIGA Al and GARS Al matrix materials [25], which are 85 MPa and 53 MPa, respectively. Figure 13 shows a graphical view of the agreement between the experimental and predicted values for AFF and GFF VHP samples, as a function of reinforcement content.

For the AFF samples, the predicted values agree with the experimental values so well that the predicted trend almost overlaps with the experimental one. For GFF samples, the general trend of the prediction and the actual Y.S. increase values also agree quite well, except that the predicted values are all lower than the experimental values. All of the GFF composite materials show higher experimental Y.S. increase values than theoretical predictions. This observation suggests that the use of high purity powders may allow operation of some additional, but unknown, strengthening effect that remains to be explored.

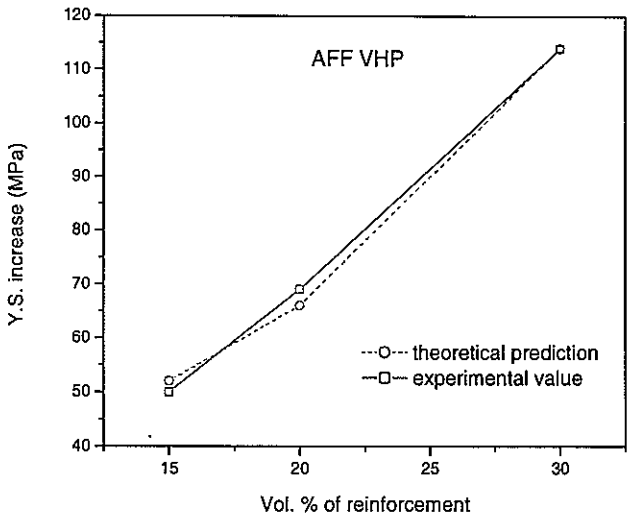

(a)

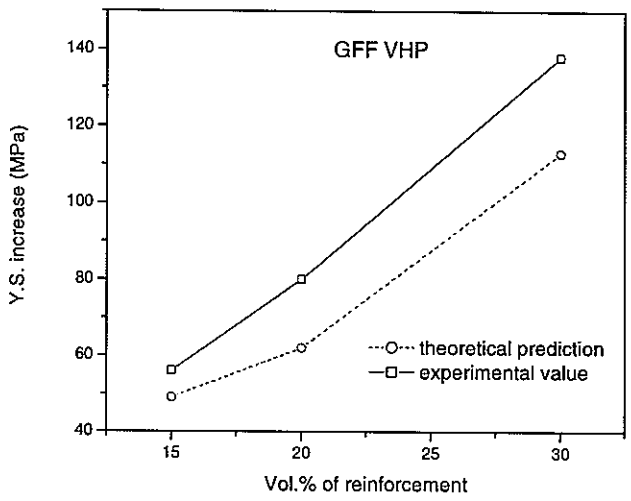

(b)

Figure 13. Comparison of experimental and predicted Y.S. increase values (a) AFF sample, (b) GFF sample.

5. Summary

Microstructures and tensile properties of elemental Al matrix composite reinforced by Al-Cu-Fe alloy particles were characterized. It was found that the quasicrystalline phase in the Al-Cu-Fe reinforcement particles transformed to a crystalline ω phase, which has similar elastic modulus, CTE, and hardness properties. With a relatively low strain hardening rate and interparticle shearing during the consolidation processing procedure, the composites produced by VHP have lower strength than that produced by a quasi-isostatic forging process. However, the VHP composites still show good elastic modulus, close to the theoretical upper-bound. Finally, by using the measured load bearing capabilities of both phases in the composites and by combining three major strengthening mechanisms, the Y.S. increase of both AFF and GFF composite samples can be predicted quite accurately. This suggests that for elemental Al matrix composite samples without precipitation strengthening and severe

strain hardening during consolidation, the load sharing, ΔCTE, and GND strengthening mechanisms can be combined to predict accurately the yield strength of the composites.

Acknowledgements

The authors greatly appreciate the assistance of the Materials Preparation Center of the Ames Laboratory for the CIP and VHP consolidation processing, performed by Mr. Paul Wheelock, and the SEM studies performed by Mr. Fran Laabs. The ultrasonic measurements were performed by Dan Barnard. Arne Swanson helped with tensile testing. Dr. Dan Sordelet provided HIP consolidated bulk Al-Cu-Fe quasicrystal and Al_7Cu_2Fe (ω phase) alloy samples for CTE and microhardness measurements. The discussions with Dr. S.B.Biner are also greatly appreciated. The funding of this project from DOE Basic Energy Sciences under contract number W-7405-Eng-82 is gratefully acknowledged.

References

1. J.E.Allison, G.S.Cole, JOM, 45 (1) (1993) 19-24.
2. B.Maruyama, W.H.Hunt, JOM, 51 (11) (1999) 59.
3. Varuzan M. Kevorkijan, JOM, 51 (11) (1999) 54-58.
4. C.K.Narula, J.E.Allison, CHEMTECH, 26 (11) (1996) 48.
5. A.M.Patton, J. Inst. Met., 100 (7) (1972) 197-201.
6. D.J.Lloyd, International Materials Reviews, 39 (1) (1994) 1-23.
7. R.M.German, Sintering theory and practice, John Wiley & Sons publishing, Inc., New York, NY, 1996, pp.326-360.
8. S.B.Biner, Development of Quasicrystal Reinforced Aluminum Composites for Industrial applications, Final Report to Center for Advanced Technology Development of Iowa State University, July 1996.
9. H.L.Cox, Brit. J. Appl. Phys., 3 (1952) 73-79.

10. R.J.Arsenault, L.Wang, C.R.Feng, Acta Metall. Mater., 39 (1991) 47-57.
11. David L.McDanels, Metallurgical Transactions A, 16 (1985) 1105.
12. V.C. Nardone and K.M. Prewo., Scripta Metallurgica, 1986, vol. 20, pp. 43.
13. M.Gupta, M.K.Surappa, Key Engineering Materials, 104-107 (1995) 259-274.
14. R.J. Arsenault and N. Shi., Materials Science and Engineering A, 81 (1986) 175-187.
15. R.J.Arsenault, Proceedings of the 9th Risø International Symposium on Metallurgy and Materials Science, Sep 5-9 1988, Roskilde, Denmark, Sponsored by Riso Natl Lab, Roskilde, Den, p. 279-284.
16. F.Tang, I.E.Anderson, S.B.Biner, Microstructure and Tensile Properties of Quasicrystal Particle Reinforced Aluminum Matrix Composites, Materials Science and Engineering A, in press.
17. E.Fras, S.Wierzbiński, A.Janas, H.F.Lopez, Metall. and Mater. Trans. A, 33A (2002) 3831-3838.
18. M.Taya, K.E.Lulay, D.J.Lloyd, Acta Metall. Mater., 39 (1991) 73-87.
19. N.Chawla, U.Habel, Y.L.Shen, C.Andres, J.W.Jones, J.E.Allison, Metallurgical and Materials Transactions A, 31A (2000) 531-540.
20. P.E.Krajewski, J.E.Allison, and J.W.Jones, Metall. Mater. Trans., 1993, vol. 24, pp. 2731.
21. I.E.Anderson and J.C.Foley, Surface and Interface Analysis, 31 (2001) 599-608.
22. J.F.Flumerfelt, I.E.Anderson and J.C.Foley, Consolidation of Pure Aluminum Powders, P/M Aluminum/Mechanical Alloying, Parts 10&11 in Advances in Powder Metallurgy & Particulate Materials, 1997, eds. R.A.McKotch & R.Webb, pp. 11.
23. J.F.Flumerfelt, Aluminum Powder Metallurgy Processing, Ph.D. Thesis, Iowa State University, 1998.
24. J.E.Shield, A.I.Goldman, I.E.Anderson, T.W.Ellis, R.W.McCallum, D.J.Sordelet, US Patent No. 5,433,978, July 18, 1995.
25. F.Tang, I.E.Anderson, S.B.Biner, Journal of Light Metals, 2 (4) (2002) 201-214.

26. J.Krautkramer, H.Krautkramer, Ultrasonic Testing of Materials, Third Edition, Berlin, Heidelberg, New York, 1983, pp. 580-587.

27. ASTM E-8 Standard, ASTM 03.01, p.130, 1990.

28. Fei Tang, Thomas Gnaupel-Herold, Henry Prask, Junfeng Mei, Iver E. Anderson, Residual stresses and stress partitioning measurements by neutron diffraction in Al/AlCuFe composites, submitted to Materials Science and Engineering A.

29. F. Tang, J.Spowart, H.Meeks, T.Gnaupel-Herold, H.J.Prask, I. E. Anderson, Consolidation Effects on Tensile Properties of a Pure Al Matrix Composites, to be submitted to Metall. Trans. A.

30. F.Faudot, A.Quivy, Y.Calvayrac, D.Gratias, M.Harmelin, Materials Science and Engineering A, 133A (1991) 383-387.

31. D.Gratias, Y.Calvayrac, Journal of Non-Crystalline Solids, 153&154 (1993) 482-488.

32. F.W.Gayle, A.J.Shapiro, Metallurgical Transactions A, 23A (1992) 2409-2417.

33. U.Koster, W.Liu, Journal of Non-Crystalline Solids, 153&154 (1993) 446-452.

34. A.M.Korsunsky, A.I.Salimon, Scripta Materialia, 44 (2001) 217-222.

35. R.M.Jones, Mechanics of Composite Materials, Taylor & Francis, 1999, pp. 143.

36. John C. Halpin, Primer on composite materials analysis, Technomic Publishing Company, 1992, pp.161.

37. F.Bonollo, R.Guerriero, E.Sentimenti, I.Tangerini, W.L.Yang, Mater. Sci. and Engi. A, 144 (1991) 303-309.

38. M.A.Meyers and K.K.Chawla, Mechanical Metallurgy, Prentice-Hall Inc., 1984, pp. 423.

39. N.Chawla, Advances in Powder Metallurgy & Particulate Materials, ed. by V.Arnhold, C.L.Chu, W.F.Jandeska, H.I.Sanderow, Proceedings of the 2002 World Congress on Powder Metallurgy & Particulate Materials, June 16-21, Orlando, Florida, APMI/MPIF, p. 5.82-5.94.

40. A.J.Allen, M.A.M.Bourke, S.Dawes, M.T. Hutchings, P.J.Withers, Acta Metall. Mater., 40 (1992) 2361-2373.

41. H.Li, J.B. Li, Z.Q.Kang, Z.G.Wang, Journal of Materials Science Letters, 15 (1996) 616-619.

42. P.J.Withers, Proceddings of the NATO Advanced Research Workshop on Measurement of Residual and Applied Stress Using Neutron Diffraction, edited by M.T.Hutchings, A.D.Krawitz, Oxford, United Kingdom, March 18-21, 1991, Kluwer Academic Publishers, 1992, p. 421-437.

43. K.V.Acker, J.Root, P.V.Houtte, E.Aernoudt, Acta mater., 44 (10) (1996) 4039-4049.

44. H. Sekine, R. Chen, Composites, 26 (1995) 183-188.

Consolidation effects on tensile properties of an elemental Al matrix composites

A paper submitted to Metallurgical and Materials Transactions A

F. Tang[1], H. Meeks[2], J.E.Spowart[3], [4]T. Gnaeupel-Herold, [4]H.Prask, I. E. Anderson[1]

[1] 223 Metals Development, Ames Laboratory, Iowa State University, Ames, IA 50011

[2] Ceracon, Inc., 5150 Fairoaks Blvd. #101-330, Carmichael, CA 95628

[3] UES Incorporated, AFRL/MLLM Bldg 655, 2230 Tenth St. Suite 1, Wright-Patterson AFB, OH 45433

[4] NIST Center for Neutron Research, 100 Bureau Dr. Stop 8562, Gaithersburg, MD 20899-8562

Abstract

In a simplified composite design, an unalloyed Al matrix was reinforced by spherical Al-Cu-Fe alloy particles (30 vol.%), using either commercial purity (99.7%) or high purity (99.99%) fine powders (dia.<10μm). This composite material was consolidated by either vacuum hot pressing (VHP) or quasi-isostatic forging. The spatial distribution of reinforcement particles in both VHP and forged samples was shown to be almost the same by quantitative characterization with a multi-scale area fraction analysis technique. The tensile properties of all composite samples were tested and the forged materials showed significantly higher strength, while the elastic modulus values of all composite materials were close to the upper bound of theoretical predictions. Neutron diffraction measurements showed that there were high compressive residual stresses in the Al matrix of the forged samples and relatively low Al matrix residual stresses (predominantly compressive) in the VHP samples. By tensile tests and neutron diffraction measurements of the forged samples after annealing, it was shown

that the high compressive residual stresses in the Al matrix were relieved and that tensile strength was also reduced to almost the same level as that of the VHP samples. Therefore, it was deduced that increased compressive residual stresses and enhanced dislocation densities in the forged composites raised the tensile strength to higher values than those of the VHP composites.

Keywords: Metal matrix composites; Powder metallurgy; Residual stress; Strengthening mechanism.

1. INTRODUCTION

Metal matrix composites (MMC) have emerged as an advanced engineering material in the areas of aerospace and automotive industries [1, 2]. They can be tailored to have superior properties such as high specific strength and stiffness, while providing weight savings and higher operating temperatures with proper design and fabrication over monolithic materials. Composites may also exhibit better thermal and mechanical fatigue and creep resistance than those of monolithic materials. However, the Al oxide coating on most commercially atomized powders is a severe barrier to sintering, especially solid state sintering, and unless thoroughly distributed in the microstructure of an Al MMC by extensive hot deformation processing, e.g., forging or extrusion, it can significantly reduce ductility and fatigue strength [3]. These disadvantages in processing and material cost and the lack of effective recyclability of ceramic reinforcement particles, such as SiC, motivate the development of alternatives for both reinforcement materials and Al matrix powder processing techniques [3].

In our former studies [4, 5], we reported the tensile properties of a new type of particulate reinforced Al matrix (PRA) composite material reinforced by spherical Al-Cu-Fe alloy

powders. The new PRA materials with 30 vol.% reinforcement particles were produced by a quasi-isostatic forging process and exhibited excellent elastic modulus (approximately 100 GPa) and tensile yield strength, about 3 times higher than the specific matrix materials [4, 5]. A prior study also showed that fragmented SiC reinforcement particles in conventional PRA composites can cause intolerable tool wear during die pressing and tend to attack the counter materials in wear-prone service, such as in automotive belt pulleys [6]. Thus, in order to reduce the stress concentration around the typical angular reinforcement particles [7, 8] and to improve the ability for wear-resistant applications, spherical Al-Cu-Fe quasicrystal particles can be an excellent alternative reinforcement for Al matrix composites.

In order to increase the strength and stiffness of the composite material, the reinforcement particle loading should be as high as possible. But previous studies showed that local reinforcement particle clustering may become a serious problem when the reinforcement loading is very high, e.g., at 30 vol.%. Some ceramic reinforcement particles that may become clustered, such as SiC, usually can not be sintered and bonded together at the consolidation temperature used for PRA materials. Weak bonding between these ceramic particles may play a major role in micro-crack initiation and growth, which can deteriorate the tensile properties of the PRA materials. Therefore, a high volume fraction of SiC, such as 30 vol.%, usually is not used in most of current structural composites and extensive hot deformation of the composites is also needed to break the reinforcement particle agglomerations. In this report, 30 vol.% of the Al-Cu-Fe quasicrystal phase alloy particles was used in producing composites because it is possible that these alloy particles can be sintered and well-bonded with each other during composite consolidation and that a very homogeneous particle distribution can be obtained by existing powder blending techniques. In order to measure the reinforcement particle spatial distributions, a quantitative image analysis method, which is called multi-scale analysis of particle area fraction (MSAAF) [9],

will be used to quantitatively analyze and compare the particle spatial distributions in the composites of this study.

Many aspects of the microstructures of PRA materials, such as particle size, shape, aspect ratio and precipitation in an Al alloy matrix, etc., can significantly affect the final tensile properties [7 -13]. Previous investigations of Al/SiC composites have also shown that a tensile type thermal residual stress in the Al alloy matrix can have a reverse contribution to the composite yield strength under uniaxial tensile loading conditions [14-15]. The compressive yield strength was shown to be higher than the tensile yield strength in Al/SiC composites [14-15]. The residual stresses in the Al matrix made by different processing methods were also measured by neutron diffraction in our previous study [16, 17] and its effects on tensile properties are examined in this paper. In some previous studies of the strengthening effect of Al alloy-based (Al 2080) composites, Krajewski and Chawla, et al. [18, 19] used a series of different thermomechanical treatments in the unreinforced Al alloy and in the composite samples. These distinct treatments were needed to achieve a similar precipitate density and distribution in the microstructure of the unreinforced Al alloy and in the composite matrix in order to compare their mechanical properties in an unbiased manner. In this study, a simplified elemental Al matrix composite system reinforced by spherically shaped AlCuFe alloy particles was used to clarify the consolidation effects on the composite tensile properties. By using an elemental Al matrix, the strengthening mechanisms from the reinforcement particles are truly isolated from matrix phase precipitation and aging effects.

Earlier work [20] on the monitoring of elemental Al powder sintering had also demonstrated that both high purity (99.99%) and commercial purity (99.7%) of matrix powders would experience rapid solid state sintering in a die pressed compact at the selected consolidation temperature. In this article we will report microstructure and mechanical property results of commercial purity and high purity composite samples consolidated from either commercial

inert gas atomized (CIGA) powders or gas atomization reaction synthesis (GARS) [21] powders, respectively, using vacuum hot pressing or quasi-isostatic forging. The resulting microstructures and tensile properties of materials made by both of techniques will be compared. The effects of the spatial distribution of reinforcement particles and residual stresses in both kinds of samples will also be analyzed.

2. EXPERIMENTAL PROCEDURE

2.1 Materials

Powders used for the two kinds of composite samples are shown in table 1. For the baseline experiments, commercially inert gas atomized (CIGA) Al and $Al_{63}Cu_{25}Fe_{12}$ quasicrystal powders were utilized. The CIGA Al powder (99.7% purity) had been evaluated thoroughly in earlier work [22-24] to characterize its surface oxide properties. A patented gas atomization reaction synthesis (GARS) technique [21] was used to produce 99.99% pure Al and Al-Cu-Fe quasicrystal (QXL) powders in our laboratory.

Table 1. Powders used for AFF and GFF samples and consolidation methods.

Sample name	Powders used	Purity
AFF Forged / VHP	CIGA Al powder (<10μm) + 30 vol.% CIGA quasicrystal powder (<10μm)	99.7%
GFF Forged / VHP	GARS Al powder (< 10μm) + 30 vol.% GARS quasicrystal powder (<10μm)	99.99%

The Al and Al-Cu-Fe quasicrystal powders were air classified to less than 10 μm. The quasicrystal powders from both sources were screened subsequently through a 20 μm screen

to eliminate the residual large particles. The size distributions of Al and quasicrystal powders were measured by a laser diffraction method and the results were reported previously [4].

2.2 Consolidation processing

For making composite samples, first, Al and quasicrystal powders were blended homogeneously. The volume fraction of quasicrystal powders in both AFF and GFF samples was 30%. Next, blended powders were cold isostatically pressed (CIP) at 200MPa for the quasi-isostatic forged samples and, slightly higher, 280 MPa for the VHP samples. The "green" samples from CIP were forged with a quasi-isostatic forging procedure by Ceracon, Inc. (Carmichael, CA) at a temperature of 550°C. Consolidation by vacuum hot pressing (VHP) was performed in our laboratories at 550°C. While die pressed compacts of the GARS Al powder were found to sinter at a significant rate at only 500°C, compacts made from CIGA Al powders needed at least 550°C to approach a reasonable rate for solid state sintering [20]. Thus, the forging or hot pressing temperature was chosen to allow both AFF and GFF compacts to experience significant solid state sintering during these solid state consolidation processes in order to make meaningful comparisons of final tensile properties. The parameters used in the consolidation procedures are shown in table 2 and table 3. The dimensions of the resulting bars after forging were approximately 5.5 cm by 2.5 cm by 1 cm and, after VHP, the bars were cylindrical in shape with a diameter of 19 mm and height of about 65 mm.

Table 2. Quasi-isostatic forging procedure.

Pre-heat Atmosphere	Pre-heating	Forge Temp.	Forge Pressure	Dwell at Pressure
99.999% Argon	550°C,10 min	550°C	635 MPa	5 second

Table 3. Vacuum hot pressing parameters.

Temperature	Soak at Temp.	Pressure	Dwell at Pressure
550°C	6 hours	175 MPa	5 hours

2.3 Other tests[1]

The Archimedes technique was used to measure the density of each forged or VHP sample. The elastic modulus of composites samples was measured by an ultrasonic method [25]. Tensile tests of consolidated composites were performed on an Instron model 1125 tensile test machine under 1.27 mm per minute monotonic loading. Sample dimensions were 6.35 mm in diameter and 25.4 mm in uniform gauge length, according to ASTM recommendations [26]. Fractography of the composite tensile samples were examined on an AMRAY 1845 field emission scanning electron microscope. The reinforcement particles spatial distributions were measured by a multi-scale analysis of area fraction (MSAAF) technique which was described in detail elsewhere [15]. Some of the composite tensile samples made by forging were annealed at 550°C for 5 hours in a vacuum furnace in a 10^{-7} torr level vacuum atmosphere before their tensile properties were measured by tensile tests described above. Neutron diffraction measurements were used to measure the residual stresses in the as-received and annealed forged composite samples, in the form of cubic coupons with dimensions of 3x3x3 mm^3. For calculation of residual stress, atomized elemental Al powders were used as stress-free standard materials. The details of the experimental procedure for the neutron diffraction measurement of residual stresses in composites have been described previously [16].

[1] Certain commerical equipment, instruments, or materials are identified in this report to specify adequately the procedures used. In no case does such identification imply recommendation or endorsement by the National Institute of Standards and Technology, nor does it imply that the materials or equipment identified are necessarily the best available for the purpose.

3. RESULTS

3.1 General microstructures of composites

The general appearance of the microstructures of AFF and GFF composites is shown in figure 1. The density of all the composites is 3.28 g/cm^3, which is very close to the theoretical density of 3.3 g/cm^3. The spherical shape of the reinforcement particles is also readily apparent in these SEM micrographs. Although the distribution of the reinforcement particles is generally uniform, there still exists particle clustering in some local areas. This clustering may have produced some deleterious effects in the early stages of fracturing of the material. In order to account for the effect of particle distribution on the tensile properties of the composite samples, the particle spatial distributions in all the composites were characterized by the MSAAF technique [15], which will be described later. The high magnification SEM pictures of those particle clustering areas are shown in figure 2. It is apparent that the particles that touch each other in the clusters are actually sintered and sintering necks between the particles can also be seen in the pictures. This capability of sintering between reinforcement Al alloy particles may be a significant advantage over common ceramic reinforcement particles, such as SiC or Al_2O_3, et al., because the un-sintered low bonding strength interface between reinforcement particles in such ceramic cluster areas can become a crack initiation site very easily during service. X-ray diffraction studies were done on these composite materials and the results were reported in another paper [17]. The X-ray diffraction analysis results showed that the Al-Cu-Fe quasicrystal phase in the reinforcement particles was transformed into an Al_7Cu_2Fe (ω) phase by the reaction between Al matrix and particles during the P/M consolidation process [17].

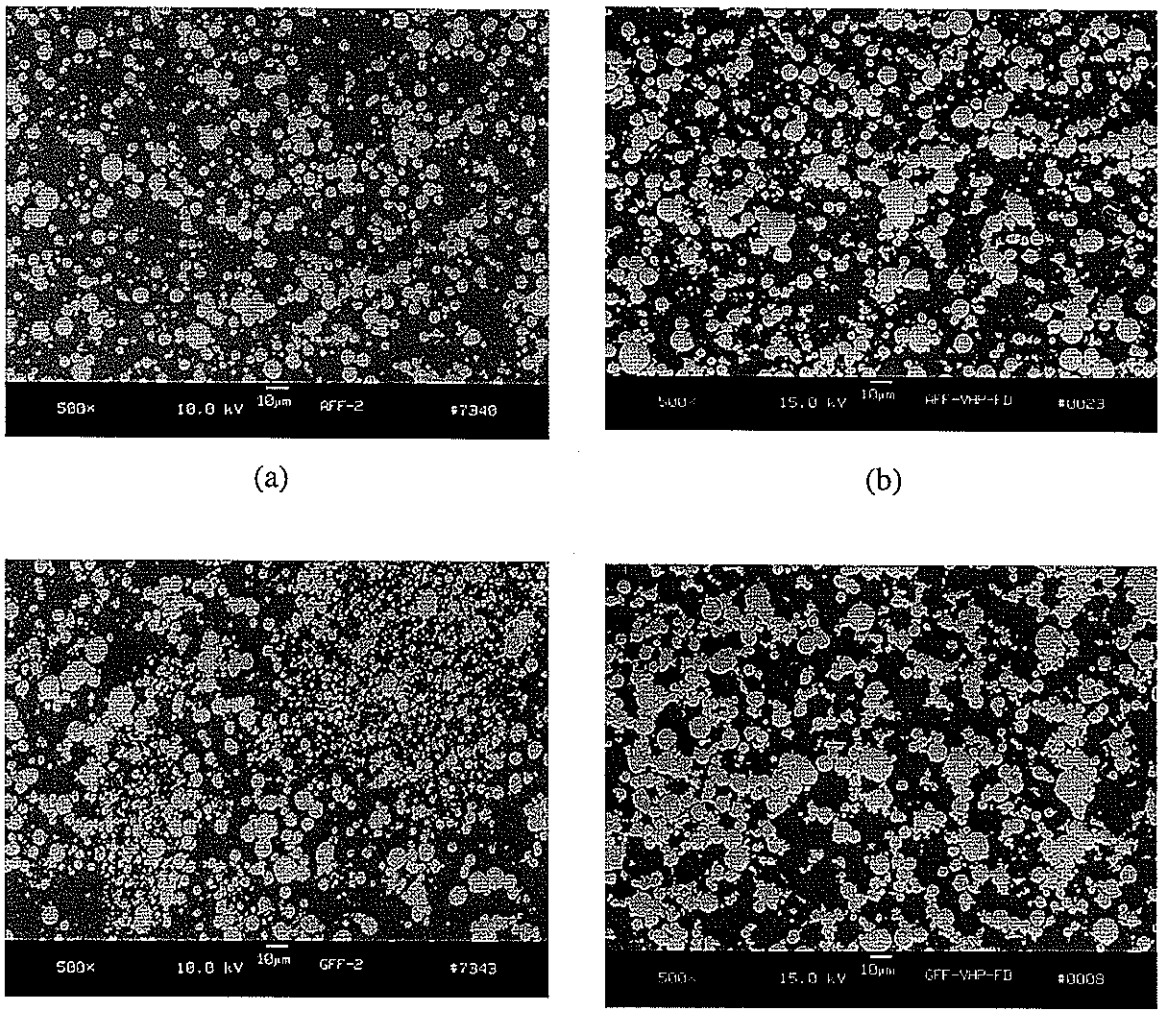

Figure 1. Microstructures of composite samples (a) AFF forged sample, (b) AFF VHP sample, (c) GFF forged sample and (d) GFF VHP sample.

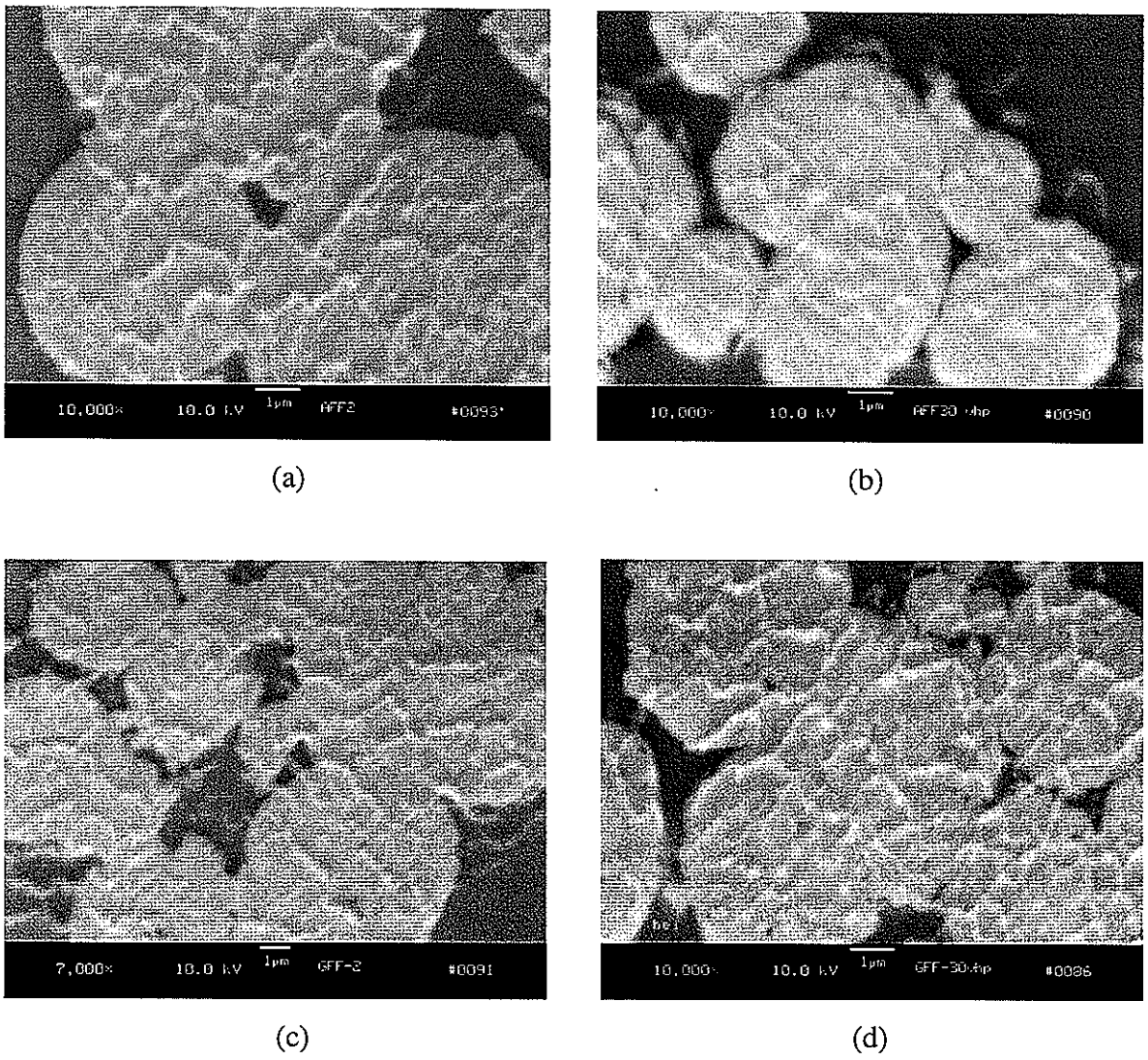

Figure 2. High magnification SEM micrographs of reinforcement particle clusters in the composite samples (a) AFF forged sample, (b) AFF VHP sample, (c) GFF forged sample and (d) GFF VHP sample.

3.2 Tensile properties and fracture surfaces examination

The tensile strength and elastic modulus (E) of the AFF and GFF composite samples are given in table 4. The ultimate tensile strength (UTS) shows a large enhancement when compared to the typical ultimate tensile strength, 90 MPa, of ingot processed 1100 Al. Tensile ductility of the composites is limited to about 1% strain for all the composites samples. Shown in table 4, the elastic modulus values of composites samples range from 97 to 100 GPa. These values are very close to the theoretical upper-bound elastic modulus value of 99 GPa that was calculated by the rule of mixtures based on E values of pure Al and ω phase Al-Cu-Fe alloy with an elastic modulus value of 168 GPa [17].

Table 4. Tensile strength and elastic modulus of pure Al matrix materials (CIGA Al and GARS Al), AFF and GFF composite samples.*

Sample		UTS (MPa)	$\sigma_{0.2}$ (MPa)	Measured elastic modulus (GPa)
CIGA Al (forged)		147	88	71
GARS Al (forged)		95	53	71
AFF	forged	310^{+4}_{-4}	265^{+1}_{-2}	97
	VHP	233^{+17}_{-17}	199^{+9}_{-9}	99
GFF	forged	304^{+6}_{-6}	227^{+1}_{-1}	98
	VHP	238^{+26}_{-26}	191^{+16}_{-16}	100

*Note: the UTS and $\sigma_{0.2}$ values are the average values from 2 - 4 tensile samples.

Figure 3 shows the fractography of failed tensile samples from the AFF and GFF tensile tests. All of the samples displayed a mixed fracture mechanism on the fracture surfaces. In

the Al matrix area, figure 3 shows ductile tearing ridges and micro-dimples around prior Al particles. Fracture occurred by grain boundary separation and brittle cleavage across the reinforcement particles.

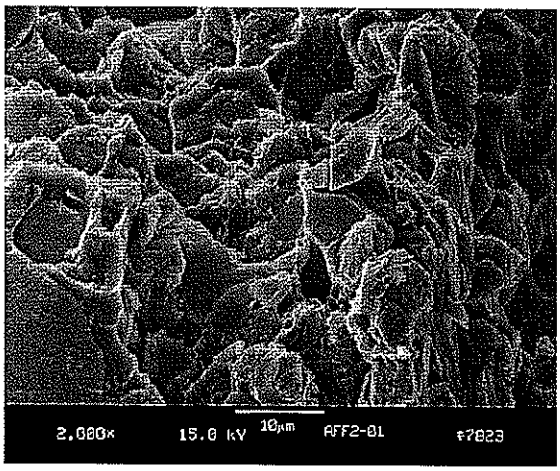

(a)

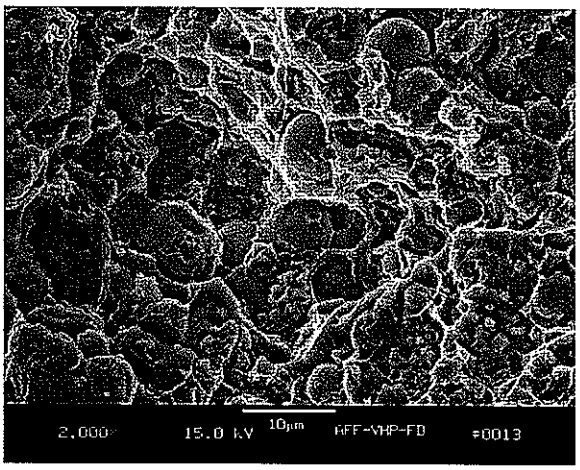

(b)

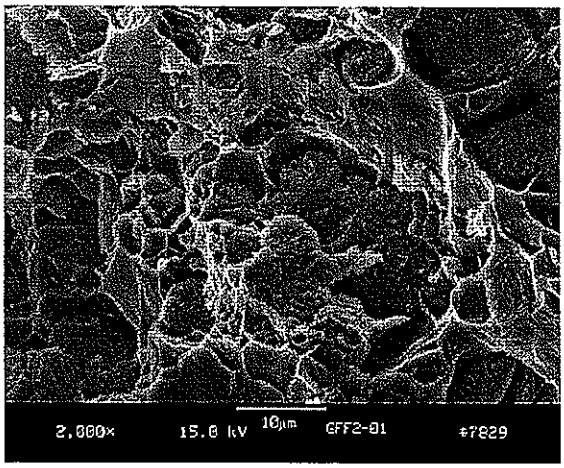

(c)

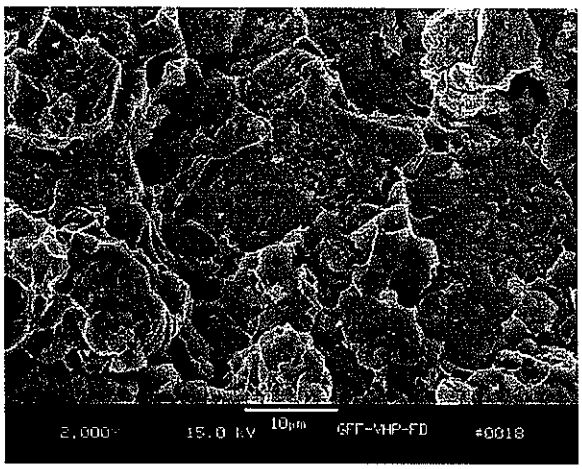

(d)

Figure 3. Fracture surfaces of (a) AFF forged sample, (b) AFF VHP sample, (c) GFF forged sample, (d) GFF VHP sample.

3.3 Particle distribution characterization by MSAAF technique

MSAAF studies were performed at the Air Force Research Lab (AFRL) to analyze the particle spatial distribution of both forged and VHP composite samples. The detailed theory and analysis procedures of the MSAAF technique were reported in a previous paper [15]. The basic principle of MSAAF technique is to characterize the spatial heterogeneity in composite microstructures by obtaining statistical information about the variability of reinforcement particle area fractions over various length scales by quantitative image analysis methods. The smaller the length scale, the larger the variability will be. By taking large field of view pictures of microstructures of composites at the mm length scale, and, then, doing image analysis to characterize the particle area fraction at different length scales from this technique, the particle spatial distribution from very small scale (several microns) to relatively large scale (mm) can be quantitatively characterized. The high-resolution and (reverse) contrast enhanced, large field of view pictures of AFF and GFF forged and VHP samples are shown in figure 4. The actual length scale of these compressed high resolution micrographs is 1.2×1.2 mm and they were taken with a specialized SEM at the US Air Force Research Laboratory (AFRL). From the pictures, it is obvious that there is no serious large agglomeration area in all the composite samples. There are some clustering areas of very fine particles in the GFF forged samples, but from figure 4(d), it can be seen that most of the fine particles in these regions do not touch each other and are separated by Al matrix. Because these large field of view SEM pictures contained many thousands of reinforcement particles, the statistics of the MSAAF analysis of reinforcement particle spatial distribution should be reliable and accurate [15].

In Figure 4(a) and 4(b), it can be seen that there are some large (apparently singular) reinforcement particles (dark contrast) in AFF forged and VHP samples. In GFF type composites, there are almost no large reinforcement particles, as shown in Figure 4(c) and

4(d). It is possible that the large particles may reduce incrementally the tensile strength and ductility of these AFF type composites.

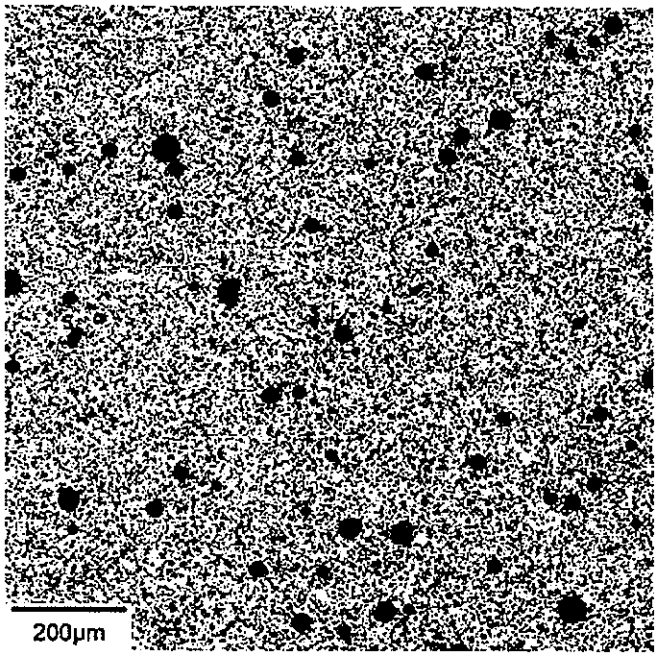

4(a) AFF VHP

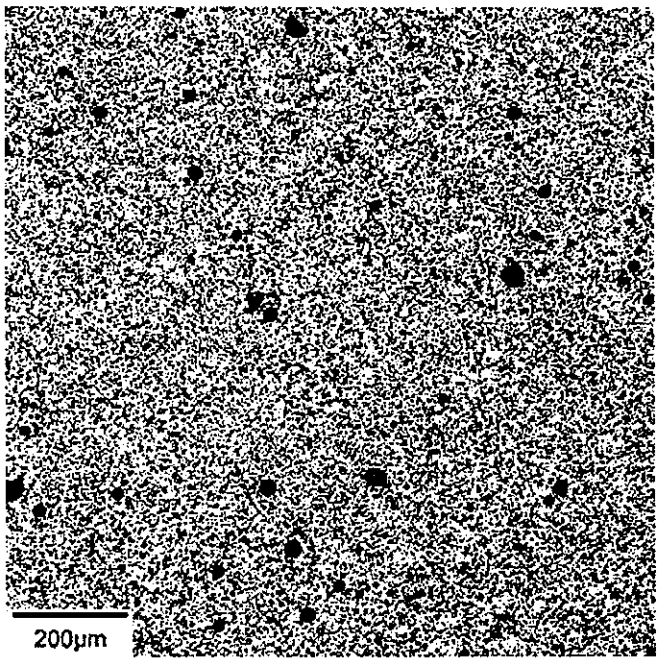

4(b) AFF Forging

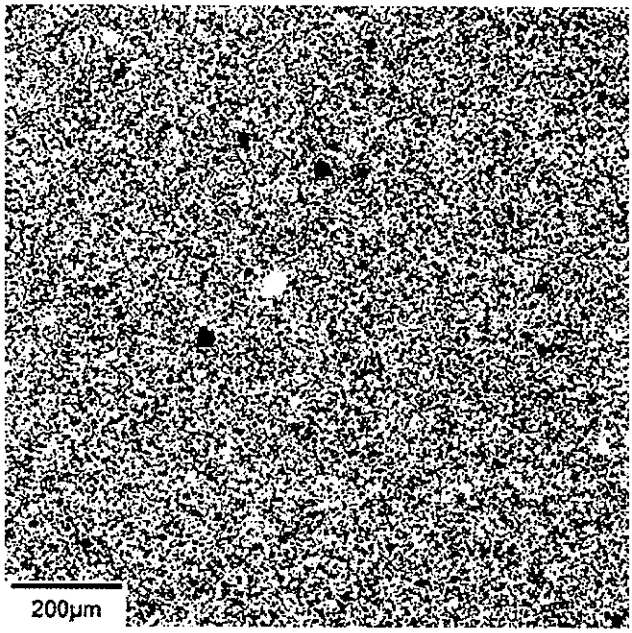

4(c) GFF VHP

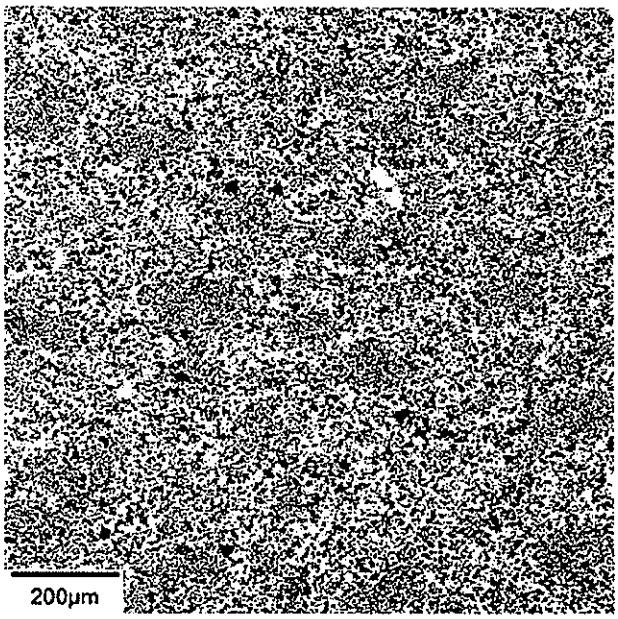

4(d) GFF Forging

Figure 4. Large field of view SEM pictures of composite samples, (a) AFF VHP, (b) AFF Forging, (c) GFF VHP and (d) GFF Forging.

The MSAAF analysis results of these composite samples are shown in table 5 and figure 5 for assessing the particle spatial heterogeneity. In figure 5, the vertical scale is related to variability of particle area fraction and the horizontal scale is the length scale used to measure the particle area fractions. At a specified length scale in the MSAAF plot, a smaller variability of the particle area fraction implies a more homogeneous particle distribution. A new term is also defined, the homogeneous length scale L_H, which is equal to the length scale where MSAAF plot curves intercept the horizontal axis. At the length scale above L_H, the variability of particle area fraction measured will be smaller than the specified value, which is 0.01 in the figure 5. The smaller the L_H, the more homogeneous the particle distribution is. The slope of the right tail of the MSAAF curves can also be used to assess the particle distribution heterogeneity. The closer this slope is to -1.0, the more homogeneous is the particle distribution. A slope of -1 means a perfect random arrangement of reinforcement particles.

In figure 5 showing the MSAAF results, the curves are derived from the curve-fitting of the ten analysis points [15]. The results show that, generally, the four kinds of composites have very similar homogeneity of particle spatial distributions and that only relatively small differences can be observed from MSAAF analysis plots. In terms of the homogeneous length scale and the slope, the VHP samples have relatively better homogeneity because they have lower L_H values and their slopes are closer to -1 than the forged samples.

Another observation from the MSAAF plots is how homogeneous each material is at small length scales. Between about 1 and 20 microns, the forged composite material appears to be slightly more homogeneous than the VHP material because the curves of both forged samples lie below the curves of both VHP samples in Figure 5. This could be due to the forging process being better at breaking-up agglomerations of reinforcement particles because of greater pressures and more inter-particle shear involved, relative to VHP. More

heterogeneity in the forged materials microstructures is indicated by the MSAAF plots in the length scales larger than approximately 20μm, since the forged material curves lie above the VHP curves at larger size scales.

Table 5. Reinforcement particles distribution characterization results in all composite samples.

material	slope	L_H (0.01) (μm)
AFF-forging	-0.85	1560 ± 50
AFF-VHP	-0.94	1170 ± 40
GFF-forging	-0.84	1720 ± 60
GFF-VHP	-1.02	825 ± 25

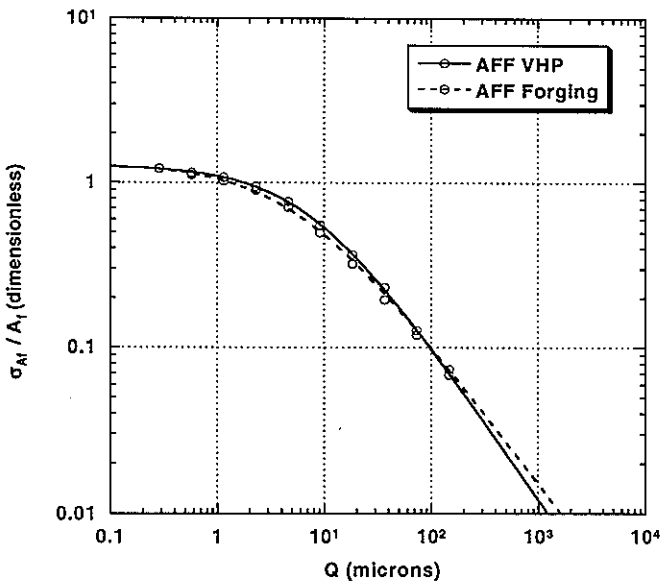

(a)

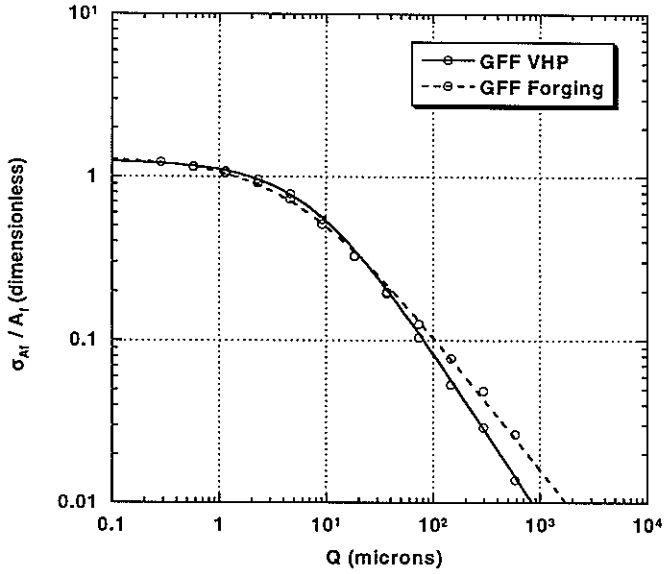

(b)

Figure 5. Reinforcement particle distribution characterization by MSAAF technique (a) AFF samples and (b) GFF samples.

4. DISCUSSION

4.1 Tensile Strength Comparison

As shown in Table 6, compared with the tensile properties of elemental Al matrix materials, including CIGA Al and GARS Al, which are shown in Table 4 [20], the increases of Y.S. and UTS of all the AFF and GFF composite materials are very significant. These Y.S. enhancement values are remarkably high, compared with the yield strength increases reported for similar Al/SiC (< 10 μm) composites. Examples include Y.S. increases of 88 MPa for 1100/SiC/20_p [27], about 50 MPa for 6061/SiC/20_p, and about 100 MPa for

6061/SiC/30_p [12]. These unusual tensile property increases of the composite materials were discussed in a previous report [4].

The results also showed that the strength enhancement values of VHP composite samples are apparently lower than those of the forged composite samples. Because the initial powder materials used for AFF and GFF samples produced by forging and VHP methods are actually the same and the particle spatial distribution in forged and VHP composites are also shown (see Fig. 5) to be almost identical, there must be some other factors related to these two processing methods that significantly affected the final tensile properties. Therefore, the residual stresses of these composite samples that resulted from phase transformation of quasicrystal to ω phase and from the elevated temperature processing procedures were measured by neutron diffraction. The detailed neutron diffraction measurements and results were reported elsewhere [16]. The effect of residual stresses on the tensile properties of the composites is discussed in the following section.

Table 6. Comparison of UTS and Y.S. between composite materials.

Strength increase compared with Al matrix		AFF forged	AFF VHP	GFF forged	GFF VHP
ΔUTS	MPa	+163	+86	+209	+143
	Percent	111%	59%	220%	151%
ΔY.S.	MPa	+177	+111	+174	+138
	Percent	201%	126%	328%	260%

Note: Y.S. – yield strength, defined as the stress at a plastic strain of 0.2%.

4.2 Effect of Compressive Residual Stresses in Al Matrix

In Figure 6 the residual stresses in the Al matrix of composite materials produced by VHP and forging methods are presented [16]. The residual stresses in Figure 6 were calculated from (111) lattice plane data, using as-atomized elemental Al powder as a stress-free d_0 standard. It is apparent that the forged composite materials have consistently higher compressive stresses in the Al matrix than the VHP samples. The coefficient of thermal expansion (CTE) of the ω phase ($15.5\times10^{-6}K^{-1}$ [16]) is lower than that of the Al phase ($23.6\times10^{-6}K^{-1}$), which is expected to produce a significant contribution to a tensile type residual stress in the Al matrix, similar to the residual stresses in most Al/SiC composites. However, the residual stress results for the Al matrix of the Al/AlCuFe composite materials are quite large and of a compressive type. The only exception is the AFF VHP sample where the Al matrix residual stress is a small tensile stress.

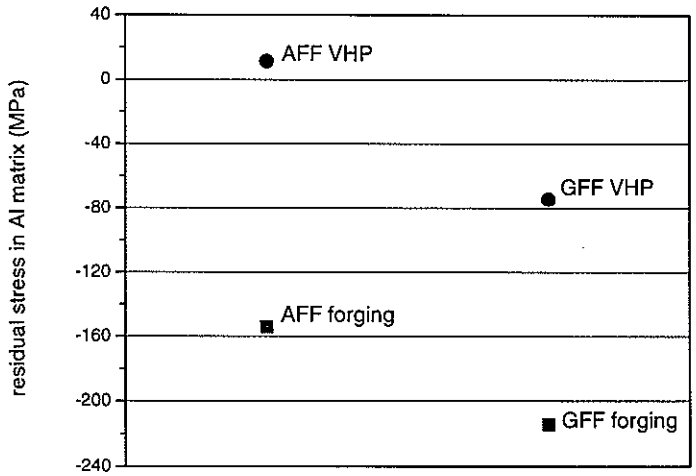

Figure 6. Residual stresses in Al matrix of AFF and GFF forged and VHP composite samples determined by neutron diffraction [16].

To explain this unusual behavior, it can be noted that during consolidation processing, by either forging or VHP, almost all of the Al-Cu-Fe quasicrystal phase particles (density ρ = 4.7g/cm^3) were reacted with the Al matrix and transformed to a lower density ω phase (ρ = 4.18g/cm^3). Therefore, the significant volume expansion (about 12%) of the reinforcement particles becomes a major effect for producing compressive residual stresses in the Al matrix. As a low strain rate and relatively long time (5 hours) processing method with very slow (furnace) cooling, vacuum hot pressing is similar to a high temperature annealing treatment for these composite materials. Thus, it would be expected that the residual stresses in VHP samples are much lower than those inside the quasi-isostatic forged materials that experience a high strain rate and short dwell time (10 minutes) with a rapid (approximately 10^3 °C/min) cooling rate.

Figure 7 further compares the Y.S. and UTS of all the composite samples. Showing the same trend as the residual stresses in Al matrix shown in Figure 6, the Y.S. and UTS of both AFF and GFF forged samples are significantly higher than those of the VHP samples. Furthermore, the numerical stress differences of the Y.S. and UTS between forged and VHP samples look similar to the residual stress differences. In other words, it appears that an extra increment of UTS, for example, is added to the forged samples by the need to first relieve compressive residual stress in the matrix before the tensile stress of the test can be borne. To study the residual stress effect on the tensile strength, the AFF and GFF forged tensile bars were annealed at 550°C for 5 hours and furnace cooled, which is the same temperature and time the VHP samples experienced. The residual stresses and tensile strength of these annealed samples were then measured by neutron diffraction and tensile tests. Unfortunately, during the tensile test of the AFF forged and annealed sample, the tensile bar was broken at the threaded grip region, so that only the tensile test of the GFF forged and annealed sample was successfully performed, as shown in Figure 8. However, the residual stresses in the Al matrix after annealing of both AFF and GFF samples were measured and are compared to the

previous results in Figure 9. It is possible that the AFF forged and annealed sample experienced premature failure due to embrittlement from thermally induced porosity [28] and this possibility is under investigation.

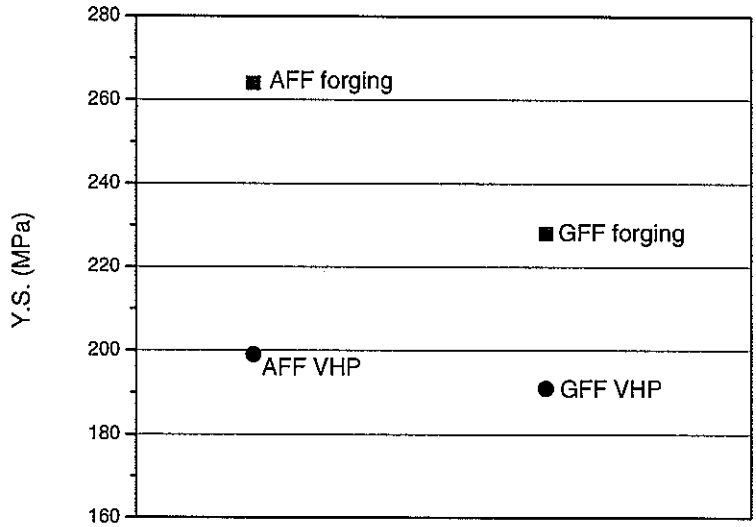

(a)

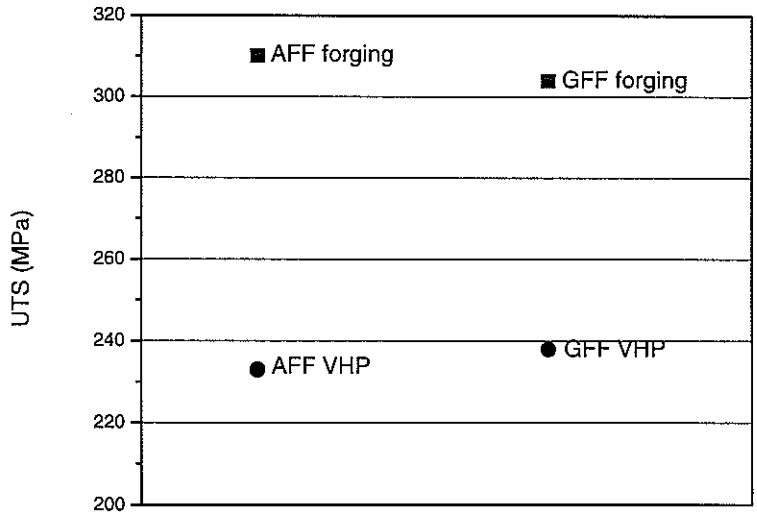

(b)

Figure 7. Y.S. and UTS comparison of the AFF and GFF composite materials produced by quasi-isostatic forging and VHP, (a) Y.S., (b) UTS.

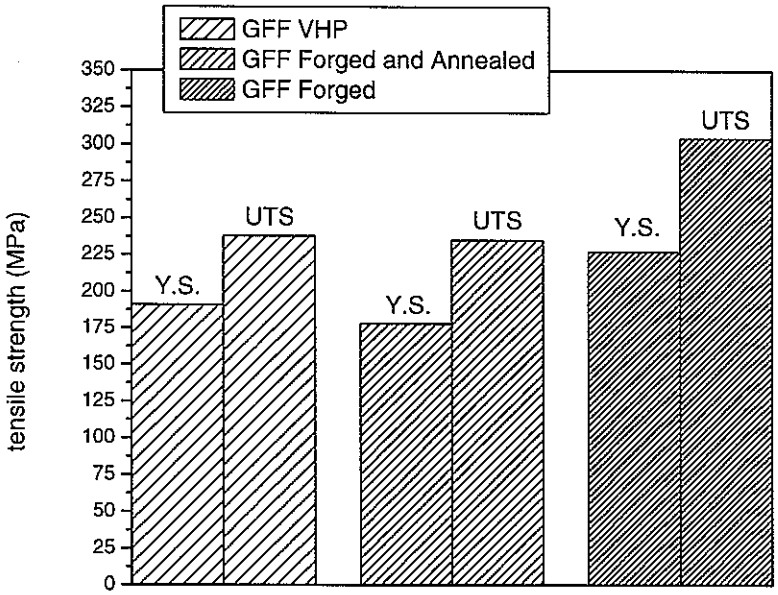

Figure 8. Comparison of Y.S. and UTS of forged and annealed GFF composite samples.

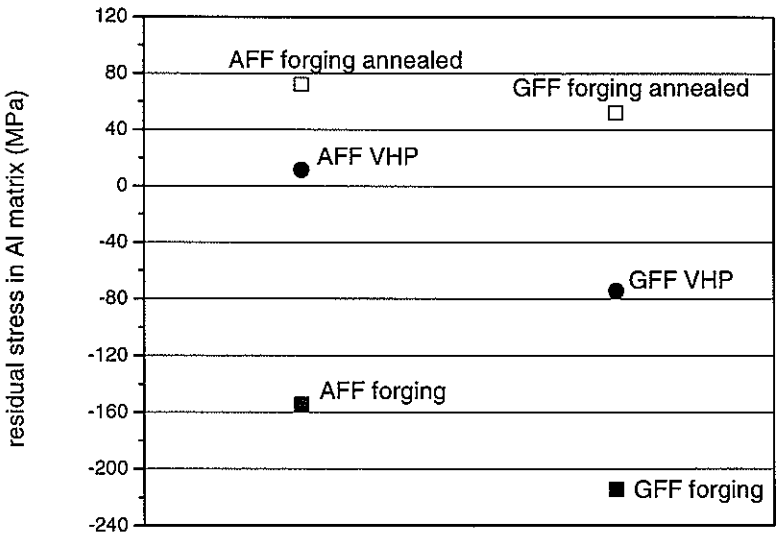

Figure 9. Comparison of Al matrix residual stress in the annealed forged and VHP composite samples [16].

Apparently from figure 9, after a long annealing time the relatively large compressive stresses in the Al matrix of the forged samples were relieved. The final balance of effects resulted in residual tensile type stresses, which can be explained by the CTE mismatch of the Al matrix and the reinforcement phase. Additional elevation of the residual tensile stress in the matrix, above the VHP levels, may be explained by other changes in the dislocation densities or composite microstructures that can occur during annealing.

Figure 10 shows a fracture surface of the forged and annealed tensile sample, which still exhibits ductile tearing of the Al matrix and broken reinforcement particles, similar to the fracture surfaces of the un-annealed tensile samples, shown in Figure 3. The differences of both Y.S. and UTS of GFF VHP and GFF forged and annealed samples are very small, as shown in Figure 8. The Y.S. difference is about 13 MPa and the UTS difference is only 3 MPa. Two observations can be made. First, we can see that the annealing of the forged sample does result in a significant decrease of the tensile properties; the Y.S. and UTS of the

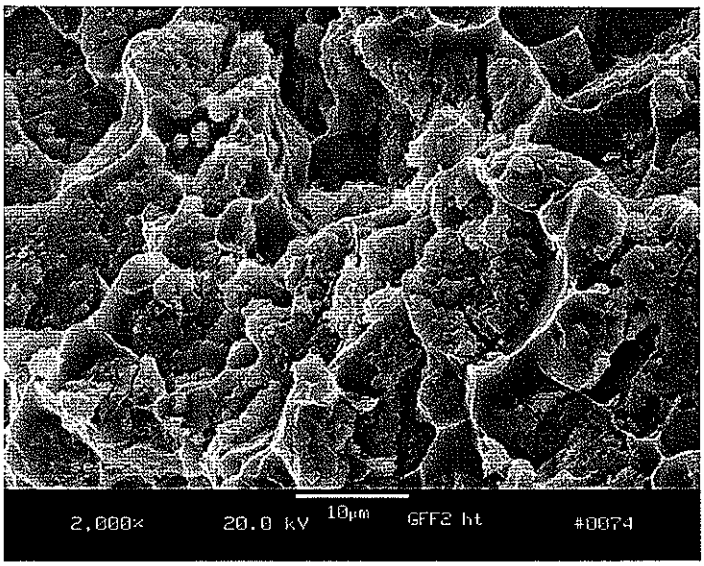

Figure 10. SEM fractography of the forged and annealed GFF composite tensile sample.

annealed GFF sample were reduced by 49 MPa and 69 MPa, respectively. Second, the tensile strength of the GFF forged sample after annealing is almost the same as that of the GFF VHP composite samples, even though a slight residual tensile stress has been observed in the annealed sample.

From current residual stress measurement results, it may not be possible to derive a quantitative relationship between the residual stress values and the tensile strengths. Similar to the effect of tensile residual stress in Al/SiC composites, it can only be qualitatively inferred that a high compressive residual stress in the Al matrix may promote the tensile strength of the forged AFF and GFF composites. Of course, the residual stress itself may not be the only factor affecting the tensile strength of the composites. It is also possible that the minor inter-particle shear characteristics [29] or a sub-grain dislocation array structure may have played a role in enhancing the tensile properties of the composite materials made by the quasi-isostatic forging process. Some inter-particle shear was indicated by earlier microstructural analysis which showed that the quasi-isostatic forging process results in grain anisotropy of about 1:1.68 [20], compared to essentially an ideal equi-axed grain matrix for the VHP process [29]. Although we have no direct evidence of this, we also know that the quasi-isostatic forging process, which is a high strain rate, high consolidation pressure (635MPa), and rapid cooling process, should produce and retain a higher dislocation density in the matrix than the VHP process, which involves a low strain rate, relatively low pressure (175MPa), and slow cooling.

5. CONCLUSIONS

1. Elemental Al-based composites reinforced with 30 vol.% of spherical Al-Cu-Fe alloy powders were produced by quasi-isostatic forging and by VHP processing methods.

Elastic modulus measurement results for both kinds of composites are almost the same and the modulus values are very close to the upper bound predictions of the rule of mixtures. UTS and Y.S. of both types of composites were increased over the corresponding Al matrix values significantly and forged samples showed significantly higher tensile strength than VHP samples. Composite samples made from GARS powders, the GFF samples, exhibited a higher strengthening effect and ductility than the samples made from commercial Al powders, which may result from improved inter-particle bonding due to the reduced oxide surface films of the GARS powders. Particle cracking of the reinforcement particulate was a dominant failure mechanism for the composites of both types under tensile loading, implying that there is sufficient interfacial bonding between the reinforcement particles and Al matrix to achieve full benefit from the reinforcement. We also observed that Al-Cu-Fe reinforcement particles can be sintered together to form strong agglomerates.

2. As shown by quantitative analysis of the reinforcement particle spatial distribution in all composite material samples for a wide range of length scales, the high level of reinforcement particle dispersion was almost the same in the forged and VHP samples. Therefore, the significant tensile strength differences between forged and VHP composite samples may not result from any minor particle spatial distribution differences.

3. Compressive residual stresses formed in the Al/Al-Cu-Fe alloy composite materials during consolidation appear to be very beneficial to the tensile properties. The high strain rate and short processing time of quasi-isostatic forging probably were responsible for higher compressive residual stresses in the Al matrix and, presumably, a higher dislocation density than VHP processed materials. After annealing for about the same time as the duration of the VHP process, the tensile strength of a forged composite sample was reduced to the same strength level as that of the VHP composite samples.

Relief of the compressive residual stresses was verified after annealing by neutron diffraction.

ACKNOWLEDGMENTS

The assistance of the Materials Preparation Center of the Ames Laboratory is acknowledged for consolidation of the VHP composites, performed by Mr. Paul Wheelock, and for the SEM studies, performed by Mr. Fran Laabs. We also appreciate the ultrasonic measurements which were performed by Dan Barnard. Arne Swanson helped with tensile testing. The funding of this project from DOE Basic Energy Sciences under contract number W-7405-Eng-82 also is gratefully acknowledged.

REFERENCES

1. J.E. Allison, G.S. Cole: JOM, 1993, vol. 45, pp. 19-24.
2. C.K. Narula, J.E. Allison, CHEMTECH, 1996, vol. 26, pp. 48.
3. I.E. Anderson, J.C. Foley and J.F. Flumerfelt: Proceedings of the first international conference on powder metallurgy aluminum & light alloys for automotive applications, edited by W.F.Jandeska and R.A. Chernenkoff, pp.75.
4. F. Tang, I.E. Anderson, S.B. Biner: Microstructures and mechanical properties of pure Al matrix composites reinforced by Al-Cu-Fe alloy particles, Materials Science and Engineering A, in press.
5. F. Tang, I.E. Anderson, S.B. Biner, J.C. Foley: Tensile properties of pure Al based Al-Cu-Fe quasicrystal reinforced model MMC, Advance in Powder Metallurgy & Particulate Materials 2001, Part 9, p.12 -25.

6. H. Danninger, G. Jangg, K. Schroder, J. Seyrkammer, H.C. Neubing: Advances in Powder Metallurgy, vol. 6, 1992, Non-Ferrous Materials, Proceedings of the 1992 Powder Metallurgy World Congress. Part 6 (of 9), Jun 21-26 1992, San Francisco, CA, USA, Sponsored by: Metal Powder Industries Federation; American Powder Metallurgy Inst, p.1-13.
7. S.B. Biner: Journal of Materials Science, 1994, vol. 29, pp. 2893-2902.
8. J. Llorca, A. Needleman, S. Suresh: Acta metal. mater., 1991, vol. 39, no. 10, pp. 2317-2335.
9. J.E. Spowart, B. Maruyama, D.B. Miracle: Materials Science and Engineering A, 2001, vol. A307, pp. 51-66.
10. P.M. Singh, J.J. Lewandowski: Metallurgical Transactions A, 1993, vol. 24, no. 11, pp. 2531-2543.
11. S.Y. Qin, C.R. Chen, G.D. Zhang, W.L. Wang, Z.G. Wang: Materials Science and Engineering A, 1999, vol. 272, pp. 363-370.
12. L.C. Davis, C. Andres, J.E. Allison: Materials Science and Engineering A, 1998, vol. 249, pp. 40-45.
13. D.L. Mcdanels: Metallurgical Transactions A, 1985, vol. 16A, pp.1105-1115.
14. N. Shi, B. Wilner, R.J. Arsenault: Acta Metall. Mater., 1992, vol. 40, pp. 2841-2854.
15. R.J. Arsenault, M. Taya: Acta Metall. Mater., 1987, vol. 35, pp. 651-659.
16. F. Tang, T. Gnaupel-Herold, H.J. Prask, J.F. Mei, I.E. Anderson: Neutron diffraction measurement on Residual Stresses and Stress Partitioning in Al/AlCuFe Composites, submitted to Materials Science and Engineering A.
17. F. Tang, I.E. Anderson, T. Gnaupel-Herold, H. Prask: Pure Al matrix Composites Produced by Vacuum Hot Pressing: Tensile Properties and Strengthening Mechanisms, to be submitted to Materials Science and Engineering A.
18. P.E. Krajewski, J.E. Allison, J.W. Jones: Metall. Mater. Trans., 1993, vol. 24, pp. 2731.

19. N. Chawla, U. Habel, Y.L. Shen, C. Andres, J.W. Jones, J.E. Allison: Metallurgical and Materials Transactions A, 2000, vol. 31A, pp. 531-540.

20. F. Tang, I.E. Anderson, S.B. Biner: Journal of Light Metals, 2002, vol. 2, no. 4, pp. 201-214.

21. I.E. Anderson, B.K. Lograsso, T.W. Ellis: (Ames Lab, Iowa State University), US Patent No. 5,368,657, Nov. 29, 1994.

22. I.E. Anderson and J.C. Foley: Surface and Interface Analysis, 2001, vol. 31, pp. 599-608.

23. J.F. Flumerfelt: Aluminum Powder Metallurgy Processing, (Ph.D. Thesis, Iowa State University, 1998).

24. J.F. Flumerfelt, I.E. Anerson: Advances in Powder Metallurgy and Particulate Materials – 1996, ed. by T.M. Cadle and K.S. (Sim) Narashimhan, Metal Powder Industries Federation, Princeton, NJ, Vol. 1, Part 1, 1996, p. 87-96.

25. J. Krautkramer, H. Krautkramer: Ultrasonic Testing of Materials, Third Edition, Berlin, Heidelberg, New York, 1983, pp. 580-587.

26. ASTM E-8 Standard, ASTM 03.01, p.130, 1990.

27. R.J. Arsenault, L. Wang, C.R. Feng: Acta Metall. Mater., 1991, vol. 39, no. 1, pp. 47-57.

28. D. Eylon, S.W. Schwenker, F.H. Froes: Metallurgical Transactions A, 1985, vol. 16A, no. 8, pp. 1526-1531.

29. R.M. German, Sintering Theory and Practice, John Wiley & Sons, Inc., 1996, pp. 343-350.

Residual stresses and stress partitioning measurements by neutron diffraction in Al/Al-Cu-Fe composites

A paper submitted to Materials Science and Engineering A

F. Tang[1], T. Gnäupel-Herold[2], H.Prask[2], I. E. Anderson[1]

[1]Ames Laboratory, Iowa State University, Ames, IA 50011

[2] NIST Center for Neutron Research, 100 Bureau Dr. Stop 8562, Gaithersburg, MD 20899

Abstract

An unalloyed Al matrix was reinforced by spherical Al-Cu-Fe alloy particles, using either commercial purity (99.7%) or high purity (99.99%) powders (dia.<10μm) and consolidated by either vacuum hot pressing or quasi-isostatic forging. Unusually pronounced strengthening in this simple metal matrix composite system prompted the in-situ study of residual stress effects in these samples to understand its possible role in the behavior. Residual stresses were measured in composites reinforced by 15, 20, and 30 vol.% reinforcement particles. Contrary to typical Al/SiC composites, the Al matrix exhibits compressive residual stresses. This unusual stress state may be promoted by a combination of effects including volume expansion of reinforcement particles caused by a phase transformation and the stiffness mismatch between the matrix and reinforcement phases. Matrix/reinforcement load transfer was also studied by neutron diffraction, using an in-situ tensile frame. It was found that the load bearing stress ratio of reinforcement and matrix phases increases linearly with the reinforcement volume fraction. The composites produced from metal powders with a thinner oxide surface layer showed higher load transfer efficiency

than the composites made from commercially atomized metal powders, as expected from the higher observed strength in the higher purity ocmposites.

Keywords: Neutron diffraction, Metal matrix composites, Residual stresses, Load partitioning.

1. Introduction

Internal residual stresses are produced in most materials after various kinds of thermal mechanical processing. This is especially true for metal matrix composites (MMC), in which thermal residual stresses can result from mismatch of the coefficients of thermal expansion (CTE) between matrix and reinforcement phases. Thermal residual stress caused by CTE mismatch between phases is a type of micro-stress that exists at the grain size scale in composite materials [1-3]. In Al/SiC composites, usually there is a tensile type thermal residual stress in the Al matrix and a compressive stress in the SiC [3] because the CTE of SiC is much lower than that of Al. The properties of MMC materials, such as yielding strength, creep and fatigue behaviors are significantly affected by these thermal residual stresses. Therefore, the ability to tailor or characterize the internal stresses is very important for fully utilizing the advantages of MMC materials. Neutron diffraction has proven to be very effective and accurate for non-destructively measuring the internal residual stresses [4-6]. It has several major advantages compared with conventional hole-drilling or x-ray diffraction methods, such as relatively large penetration depth and simultaneous measurement of the strains of multiple phases.

With proper apparatus design, the stress and strain states of different phases in an MMC can be measured in-situ by neutron diffraction during various kinds of mechanical tests [7-8].

Such in-situ tensile tests have been used to determine the actual load bearing capacities of the matrix and reinforcement phases [4, 5, 7, 8]. The results showed qualitatively that the reinforcement phases have higher internal stresses than the Al matrix. Further analysis of the load sharing distribution between matrix and reinforcement phases in the current MMC samples may help to demonstrate quantitatively how the external load is partitioned between Al matrix and Al-Cu-Fe reinforcement particles. The results may also advance the state of understanding the load transfer strengthening mechanisms of composite materials, in general.

In our recent research [9, 10], results on elemental Al matrix composites, reinforced by 30 vol.% of spherical Al-Cu-Fe alloy particles and consolidated by quasi-isostatic forging, were introduced. The UTS and yield strength of this model composite material were improved over the matrix properties by 111% and 220%, respectively, for the commercial purity composite sample. Remarkably, the UTS and yield strength of the composite were improved over the matrix properties by 201% and 328%, respectively, for an equivalent composite material produced from metal powders with much thinner oxide surfaces. The elastic modulus values of these composites, in both versions, are very close to the theoretical upper bound value from the rule of mixtures for 30 vol.% loading. These results suggested that potential reinforcement phases for PRA materials should be broadened from refractory ceramics to include, e.g., intermetallic compounds that also can form a strong bond with the Al matrix by solid state sintering. Such composites made from powders with a thinner oxide surface can achieve significant improvements in tensile properties over the same composites made from commercial powders with thick oxide and impurity surfaces [11]. The unusually pronounced strengthening in this simple metal matrix composite system also prompted the study of residual stress and load partitioning effects in these samples to understand their possible role in the composites strengthening behavior.

In this paper, the above mentioned elemental Al matrix composite system, which was made from elemental Al and spherical $Al_{63}Cu_{25}Fe_{12}$ quasicrystal alloy powders by powder metallurgy techniques, was used to investigate the effects of consolidation and reinforcement volume fraction on the residual stresses and load partitioning between phases.

2. Materials and Experimental Procedure

2.1 Sample constituents and P/M consolidation methods

Table 1 identifies the metal powders that were used to fabricate the composite samples in this study. Two kinds of composite material samples (AFF and GFF) were consolidated by vacuum hot pressing (VHP). Quasi-isostatic forging was used to produce the 30 vol.% loading AFF and GFF composite materials. Gas atomization reaction synthesis (GARS) is a technique patented by Ames Lab, U.S. DOE [12]. The metal powders made by this technique have a much thinner oxide surface layer and less chemisorbed water on the powder surfaces than commercial metal powders. Therefore, GARS metal powder can exhibit better sintering kinetics, relatively clean interfaces, and higher bonding strength between particles. Detailed descriptions of this technique and studies on the GARS powder can be found in other references [11, 13]. A typical x-ray diffraction pattern of the as-atomized structure of both CIGA and GARS Al-Cu-Fe quasicrystal powders is shown in Figure 1. The results reveal that there are two phases in the Al-Cu-Fe reinforcement powder which include the major $Al_{63}Cu_{25}Fe_{12}$ quasicrystal phase and some β-Al(Cu, Fe) phase.

Table 1. Powders used for pure Al and Al matrix composite samples.

	Sample name	Powders used
Composite materials	AFF-15 AFF-20 AFF-30	CIGA Al powder (<10μm) + (15, 20, 30 vol.%) CIGA AlCuFe powder (<10μm)
	GFF-15 GFF-20-L GFF-20-H GFF-30	GARS Al powder (< 10μm) + (15, 20, 30 vol.%) GARS AlCuFe powder (<10μm)

Note: CIGA – commercial inert gas atomization, 99.7% purity,
GARS – gas atomization reaction synthesis, 99.99% purity.

The processing parameters for forging and VHP processes are shown in table 2 and table 3, respectively. The consolidation temperature of both processes was 550°C. The samples were held at this temperature under pressure for 10 minutes for forging and 5 hours for VHP. The pressure used in the forging process was 635 MPa, which is much higher than the 175 MPa pressure used in the VHP process.

Table 2. Quasi-isostatic forging parameters.

Pre-heat Atmosphere	Forge Temp.	Soak at Temp.	Forge Pressure	Dwell at Pressure
99.999% Argon	550°C	10 min	635 MPa	5 second

Table 3. Vacuum hot pressing parameters.

Temperature	Soak at Temp.	Pressure (MPa)	Dwell at Pressure	Cooling Rate to Room Temp.
550°C	6 hour	175	5 hour	250°C/hr.

Note: GFF-20-H sample was vacuum hot pressed at 245 MPa.

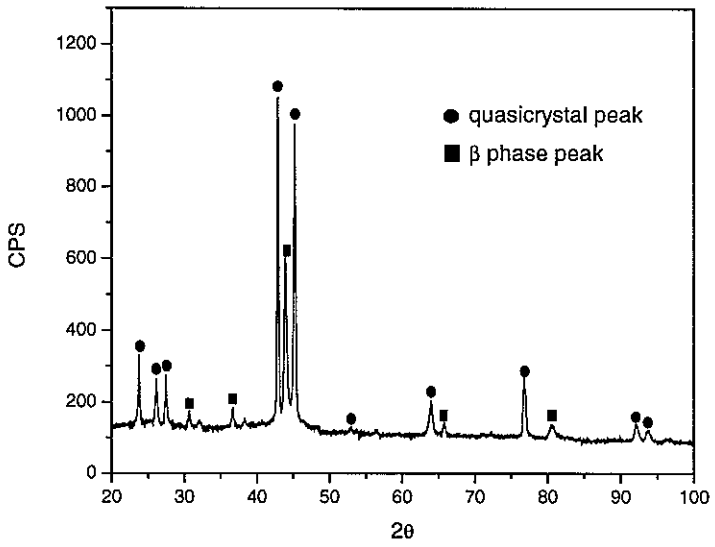

Figure 1. X-ray diffraction of Al-Cu-Fe quasicrystal metal powders.

2.2 Neutron diffraction

Determination of internal stresses in the material phases by neutron diffraction was accomplished in a similar manner as x-ray diffraction. Using a monochromatic neutron beam, the lattice spacing of a particular phase can be determined by Bragg's law of diffraction,

$$2d_{hkl}\sin\theta_{hkl} = \lambda \qquad (1)$$

where d_{hkl} is the lattice spacing of (hkl) planes, $2\theta_{hkl}$ is the diffraction angle and λ is the neutron wavelength. With the value of d_{hkl}, the strain can be determined from,

$$\varepsilon = \frac{d_{hkl} - d_0}{d_0} = \frac{\Delta d}{d_0} \qquad (2)$$

where d_0 the lattice spacing measured from the stress-free standard material. For the internal stresses measurements in this paper, high purity or commercial purity Al powders were used as stress-free standard materials. The hydrostatic stress state was assumed for all the residual stress measurements. Thus, the residual stresses determined from the above standard materials were calculated by using following equation,

$$\sigma = \varepsilon \frac{E}{1-2\upsilon} \qquad (3)$$

where E is the Young's moludus of Al(111) lattice plane. Poisson's ratio of Al (111), υ, is equal to 0.3516. The residual stress in the reinforcement particles was calculated by the stress balance relationship, as follows,

$$V_r \sigma_r + V_m \sigma_m = 0 \qquad (4)$$

where V_r and V_m are the volume fraction of reinforcement and Al matrix phases, and σ_r and σ_m are the internal stresses inside the reinforcement particles and Al matrix, respectively.

The neutron studies were conducted with the neutron spectrometer at the NIST (National Institute of Standards and Technology) Center for Neutron Research, Gaithersburg, MD. For phase residual stress measurement, the composite samples were made by VHP as disks, 5mm thick, 19mm diameter. The monochromator used for neutron diffraction was silicon (311) with a d-spacing of 1.6374 $\mathring{A}$. The neutron wavelength was 2.4337 $\mathring{A}$. A gauge volume of $5\times5\times5$ mm was used for all stress-free standard Al powders and residual stress measurements.

A fully computer controlled load frame with a 10 kN load cell was used for the in-situ load sharing measurements in composite samples. The gauge length of the cylindrical tensile samples was 12.7 mm and the diameter was 3.78 mm. The stress-free standards (d_0) for the Al matrix and reinforcement particles were the lattice parameters measured from load free tensile samples. A gauge volume of $2\times2\times7$ mm was used for the tensile samples without load, in which the longitudinal direction of the tensile samples is the z direction. A gauge volume of $5\times5\times5$ mm was used for the tensile samples with applied load. Al (111) and ω phase (214) peaks were chosen for all the residual stress and load partitioning measurements because these peaks have relatively high intensities and do not overlap with other peaks. The elastic modulus of the Al_7Cu_2Fe (ω) phase was measured by in-situ compression tests, using neutron diffraction to measure the lattice strains. The compression test bar of ω phase had a dimension of $4\times4\times15$ mm.

2.3 Other tests

The Archimedes technique was used to measure the density of the composite material samples. Microstructures of the as-received composite materials were mechanically polished without any etching and examined on an AMRAY 1845 field emission scanning electron microscope. X-ray diffraction characterization of composite samples was performed using a Philips PW1830 generator with Cu K_α radiation.

3. Results

3.1 Microstructures and x-ray diffraction of composite materials

Figure 3 shows a cross-section microstructure of an AFF forged composite material with 30 vol.% of reinforcement particles, which represents a typical microstructure of all the composite materials. The bright phase is the Al-Cu-Fe alloy particles and the dark phase is the Al matrix. Micrographs of all the other composite materials can be found in another paper [14]. The density measurements of the composite materials are shown in tables 5 and 6. The density of the GFF-20-L sample is obviously not fully dense and lower than the density of the GFF-20-H sample. As reported in reference [14], the GFF-20-L sample's tensile properties and load transfer capability, measured by neutron diffraction are also inferior to the GFF-20-H sample. The residual stress data of the GFF-20 sample reported in this paper is from GFF-20-L, which was the only sample of this type available for this measurement, but was consolidated with the same VHP processing parameters as all other GFF type samples, while the load partitioning measurement result is from GFF-20-H. The density of all other composite samples is very close to the theoretical density calculated from the rule of mixtures equation. Macroscopically, the distribution of reinforcement particles in the Al matrix is very homogeneous, although there is some local clustering of fine particles due to the high volume fraction of the reinforcement particles.

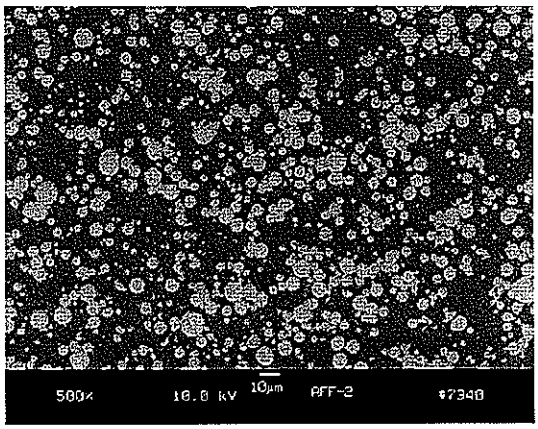

Figure 3. Typical general microstructures of the composite material sample, AFF forging composite material with 30 vol. % of reinforcement particles.

Table 5. Density of all VHP composite material samples.

Samples	AFF-15	GFF-15	AFF-20	GFF-20-L	GFF-20-H	AFF-30	GFF-30
Density (g/cm^3)	3.0	3.0	3.09	3.06	3.09	3.28	3.28
Theoretical density (g/cm^3)	3.0		3.1			3.3	

Table 6. Density of quasi-isostatic forging composite material samples.

Samples	AFF-30 forging	GFF-30 forging
Density (g/cm^3)	3.28	3.28

X-ray diffraction patterns of the AFF-30 and GFF-30 forged composite materials are shown in Figure 4. These two forged composite materials were used to measure the load partitioning in matrix and reinforcement phases and their residual stress measurement results were reported elsewhere [15]. The x-ray diffraction results of all the other VHP composite materials can be found in one other report [14] and their x-ray diffraction patterns are similar to that of the GFF-30 forged sample. Thus, all of the composites are composed of Al phase and Al_7Cu_2Fe crystalline phase (ω phase). The initial Al-Cu- Fe quasicrystal phase particles reacted with the Al matrix and transformed into ω phase. The only exception is the x-ray pattern from the AFF-30 forged sample, shown in Figure 4, which contains a small peak from $Al_{63}Cu_{25}Fe_{12}$ quasicrystal phase, indicating that there was some amount of residual quasicrystal phase.

During high temperature processing, such as quasi-isostatic forging and the VHP procedure, the Al can diffuse into quasicrystal particles and produce a more Al-rich ω phase [12]. For the composite samples made from VHP, almost all the quasicrystal phases transformed into ω phase because there was a relatively long dwelling time (5 hours) at high temperature and

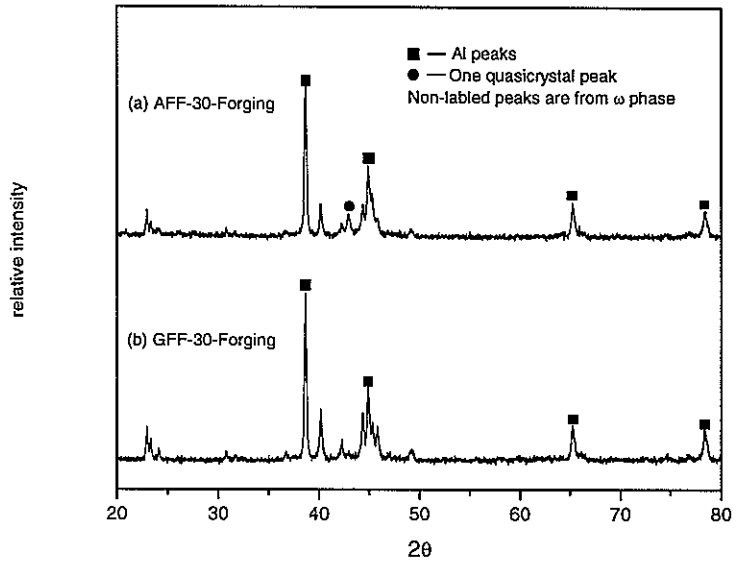

Figure 4. X-ray diffraction of forged composite materials (a) AFF-30 and (b) GFF-30.

also a slow cooling rate in the furnace, which appears to be quite sufficient for the phase transformation [14]. For the composite materials made by the forging process, the CIGA powders have a relatively thick oxide and impurity layer on the powder surfaces. Since this layer which can act as a strong obstacle for Al diffusion [11, 16] and the forging processing time is short (10 minutes), it is reasonable that the AFF forging sample still has some amount of residual quasicrystal phase. The GFF samples were made from high purity GARS powders with much thinner oxide and impurity surfaces, in which Al diffusion from matrix to reinforcement particles is faster and easier. Therefore, all of the quasicrystal phases in the GFF forging sample appeared to transform into ω phase and no x-ray diffraction peak from quasicrystal phase can be observed. More detailed characterization and comparison of the effect of powder surface chemistry on elemental inter-diffusion and sintering behavior of CIGA and GARS metal powders can be found in previous reports [11, 16]. The significant effect of this phase transformation on the residual stresses in the VHP processed composite materials will be discussed later.

3.2 Residual stresses in composite materials

The residual stresses in Al matrix calculated from d-spacing and elastic modulus measurements are shown in Figure 5. The elastic modulus of the Al (111) lattice plane used for calculation of residual stresses is 72.4 GPa, according to a study by Gnäupel-Herold [17]. The uncertainties of the residual stress data in Figure 5 are from the Al (111) lattice spacing measurement. Almost all of the VHP composite materials show compressive residual stresses in Al matrix except the AFF-30 VHP sample, which shows a low tensile type residual stress. It seems that there is a decreasing compressive stress with increased reinforcement volume fraction, which appears to be linear in the results for AFF VHP samples. Another observation is that the GFF VHP samples exhibit relatively higher compressive stresses in the matrix than the AFF VHP samples for all three volume fraction loading cases.

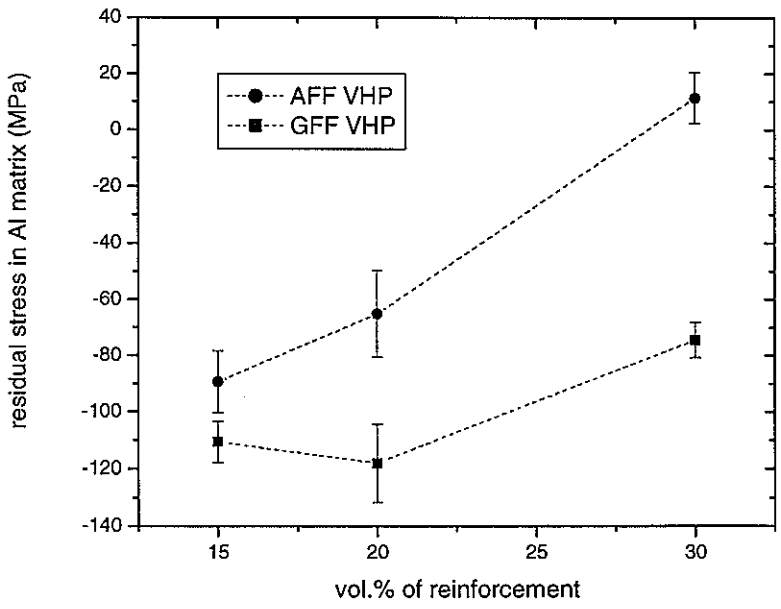

Figure 5. Residual stresses in the Al matrix of VHP composite materials.

3.3 In-situ load sharing stresses measurement

Using an in-situ tensile strain frame during neutron diffraction measurement, lattice strains of Al (111) and ω (214) planes of VHP and forged composite samples were measured while applying uniaxial tensile load. The load sharing of the phases was only measured in the elastic deformation range of the composite materials. Applied stresses during the tensile tests ranged from 0 to 90 MPa. For composite samples with 15 and 20 vol.% loading, the applied stress was from about 0 to 50 MPa. The load sharing stresses of Al matrix and ω phase reinforcement phases were calculated from measured lattice strains and the elastic modulus of corresponding lattice planes. Figure 6 shows the lattice strain and applied stress relationship from a compressive test of the ω phase sample. Linear regression of the data shows that the elastic modulus of the ω (214) plane is about 204.5 GPa, which was used to calculate the ω phase stresses.

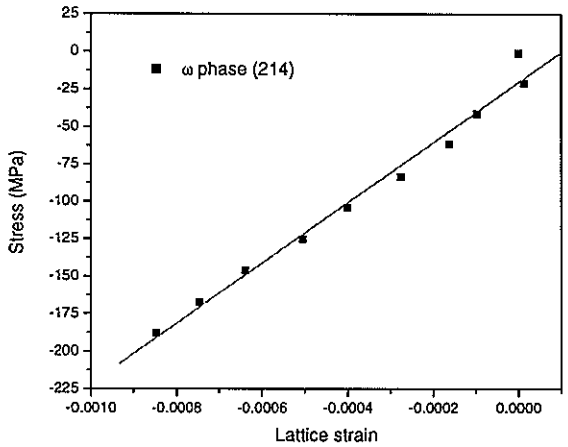

Figure 6. Neutron diffraction measurement of ω phase (214) plane lattice strain under compressive stresses.

Using the Al and ω phase stresses as x and y axes, respectively, the phase stress results are plotted in Figure 7. The "bearing stress ratio" of reinforcement phases, σ_r, and Al matrix

stress, σ_{Al}, for all composite materials can be obtained from a linear fit of the data points in the plots in Figure 7. The bearing stress ratios are all above one, which means that the reinforcement phase shared higher internal stresses than the Al matrix. The higher the bearing stress ratio, the more is the portion of the external load that is transferred to the reinforcement phase. Because of a lack of available sample material, the load sharing stresses of the phases in the AFF-30 VHP and GFF-30 VHP composite materials were not measured by the in-situ tensile test. Instead, the load partitioning of the AFF-30 and GFF-30 forged samples were measured.

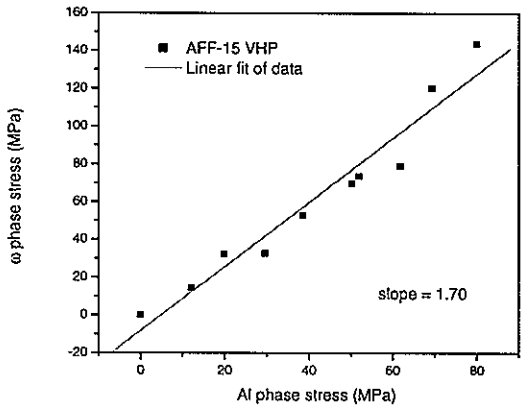

(a)

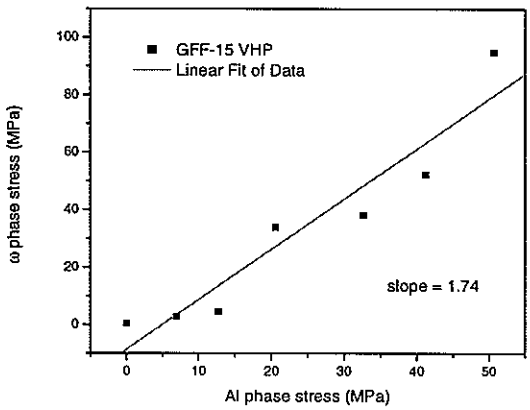

(b)

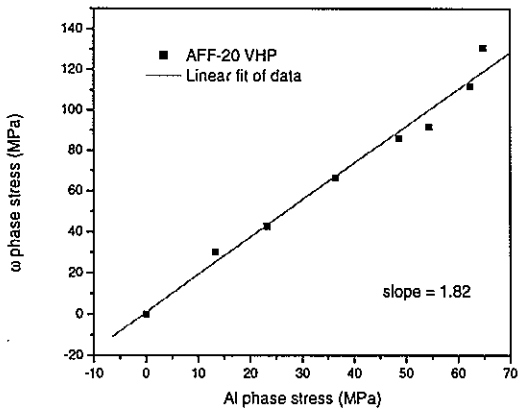

(c)

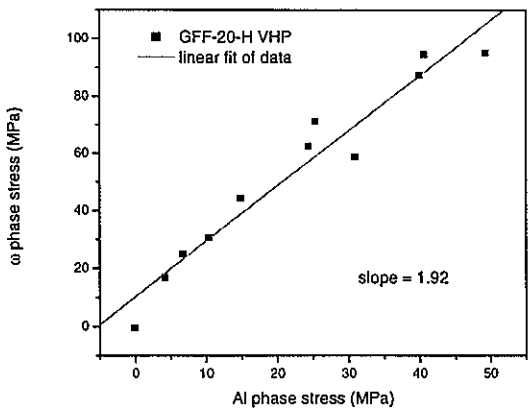

(d)

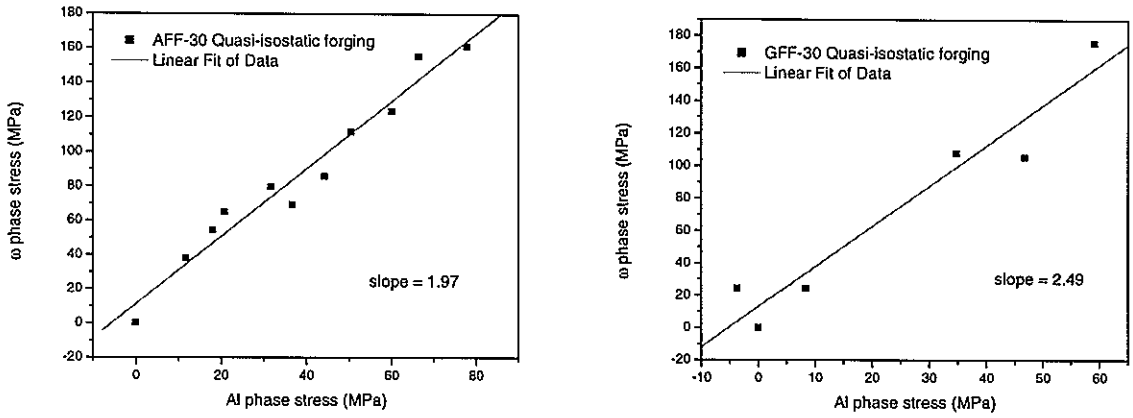

(e) (f)

Figure 7. Bearing stresses ratio (σ_r/σ_{Al}) of Al matrix and ω phase calculated by linear regression of the neutron diffraction measurement results of (a) AFF-15 VHP, (b) GFF-15 VHP, (c) AFF-20 VHP, (d) GFF-20 VHP, (e) AFF-30 forged and (f) GFF-30 forged samples.

4. Discussion

4.1 Residual stresses in Al matrix and reinforcement particles

There are several factors that affected the residual stress formation in the composites. The first one is most likely the phase transformation of $Al_{63}Cu_{25}Fe_{12}$ quasicrystal phase to Al_7Cu_2Fe (ω) phase during composite consolidation. Because the quasicrystal phase has a higher density than ω phase, as shown in Table 7, there is a volume expansion of the reinforcement particles after the phase transformation into ω phase. This internal source of volume expansion should produce a compressive stress state in both Al matrix and reinforcement particles when the external VHP or forging pressure resists the volume expansion of the composite sample in the VHP die or forging "can." At this stage (within a constraint) in the analysis, it seems that an increased volume fraction of ω phase will produce

a higher compressive stress in both phases. However, if the volume fraction of ω phase is increased, it is not clear what trend in the stress state of the Al matrix to expect after the constraint is removed.

Table 7. Properties of $Al_{63}Cu_{25}Fe_{12}$ quasicrystal phase and Al_7Cu_2Fe (ω) phase.

	Density (g/cm^3)	CTE ($\times 10^{-6}K^{-1}$)
$Al_{63}Cu_{25}Fe_{12}$	4.7	12.6 [18]
Al_7Cu_2Fe	4.18	15.45

During cooling of the composites from high temperature to room temperature, the other prominent factor, the mismatch of the CTE properties of the Al matrix and ω phase, should also affect the residual stress, regardless of any external constraint. The CTE of the elemental Al matrix is $23.6\times10^{-6}K^{-1}$ and the CTE of the ω phase is only $15.45\times10^{-6}K^{-1}$, which was measured by a TMA method, as shown in Figure 8. Therefore, there is more thermal shrinkage in the Al matrix than there is in the reinforcement particles and, hence, the Al matrix may accumulate residual tensile stress during cooling of the composite material. Just like the source of residual tensile stress in Al/SiC composite material [1, 2], this type of ΔCTE should make the residual stress in the Al matrix more positive. In other words, any compressive residual stresses remaining in the Al matrix will be reduced by the ΔCTE effect.

When the external applied VHP or forging pressure is released after consolidation of the composites, the stiffness mismatch of Al and ω phase should alter the stress balance of matrix and reinforcement phases initially constrained in the die, and should increase the compressive stress in the Al matrix, which has a lower stiffness than the reinforcement particles. From the data in Figure 5, it seems that at low ω phase volume fraction, phase transformation and stiffness mismatch effects dominate and the residual stress is more negative, and at high ω phase volume fraction ΔCTE effect dominates, which make the residual stress more positive.

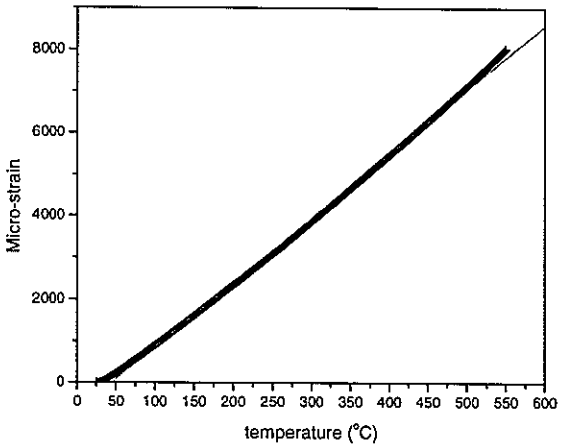

Figure 8. CTE measurement of ω phase

Because the Al atoms must diffuse into reinforcement particles for the transformation of the quasicrystal phase into ω phase, the diffusion of Al, which affects the phase transformation kinetics and transformed volume, may also have a secondary effect on the residual stress evolution. This transport of Al atoms from matrix to reinforcement phase may reduce slightly the compressive stress state during the transformation. The interface chemistry between Al matrix and reinforcement particles, which shows a significant effect on metal powder sintering [9-12], may also affect the Al diffusion rate and alter the transformation reaction kinetics. Thus, a complex combination of the above factors seems to be the cause of the net compressive residual stresses in the Al matrix of essentially all of the composite materials. Therefore, based on the above discussion of the complexity of residual stress formation in the Al matrix, it appears that in-situ X-ray or neutron diffraction measurements of the icosahedral (quasicrystal) to tetragonal (ω) phase transformation and the evolution of residual stresses during composite consolidation are needed to gain insight on the unresolved issues.

Another experimental question is raised by Figure 5, which shows that the GFF VHP samples exhibit consistently larger compressive stresses than the AFF VHP samples. The differences between these residual stress values increase when the reinforcement volume

fraction becomes higher. As stated previously, the powder surface chemistry between AFF and GFF samples may affect the Al diffusion and phase transformation kinetics, and also influence the residual stresses. Because of the differences in interface oxide and impurity layer thickness between the initial powders used for producing AFF and GFF samples [9-12], the kinetics of the Al diffusion into the quasicrystal particles and, hence, the kinetics of phase transformation of AFF and GFF samples were expected to be different. The thinner oxide layer associated with the GARS powders may promote a more rapid phase transformation in GFF samples than in AFF samples. In other words, there may be more ω phase formed in GFF samples. The experimentally measured residual stresses in Figure 5 reveal that the volume expansion of the particles may have been more significant in GFF samples than in AFF samples, resulting in higher compressive residual stresses in GFF samples. For the quasi-isostatic forging process, which was performed at high temperature for only about 10 minutes, the x-ray patterns of produced AFF and GFF composites in Figure 4 showed that there is still a quasicrystal peak from the AFF sample, while there is no obvious quasicrystal peak appear in the GFF sample. This observation suggests that the phase transformation kinetics are reduced in AFF, compared to composite materials, but in-situ neutron or X-ray diffraction measurements would be useful again to provide direct evidence.

4.2 Load sharing in Al matrix and reinforcement particles

Figure 9 presents a comparison of load bearing ratios of both AFF and GFF composites with different reinforcement volume fractions. For both AFF and GFF composites, the bearing stress ratios can be seen as increasing monotonically with the reinforcement volume fraction up to 30 vol. %. A linear fit of the bearing stress ratio data shows a slope of 0.051 for the GFF type composites, while the AFF type of composites only shows a slope of 0.018, which means the bearing stress ratio of GFF composites increases at a rate of almost 3 times higher than that of the AFF composites. Because the bearing stress ratio is a measurement of load

transfer capability from matrix to reinforcement phase, the higher the bearing stress ratio, the higher the load transfer capability of the composites and, hence, the more load transfer strengthening can be obtained. The more significant increase of the bearing stress ratio of the GFF composites, compared to the AFF composites, implies that the external load on the composites can be much more efficiently transferred to the reinforcement phase in GFF composites. This is most likely the reason why the strengthening effect of the GFF composites is always higher than AFF composites, which can be seen in other reports on the tensile properties of these two kinds of composite materials [9, 10, 14].

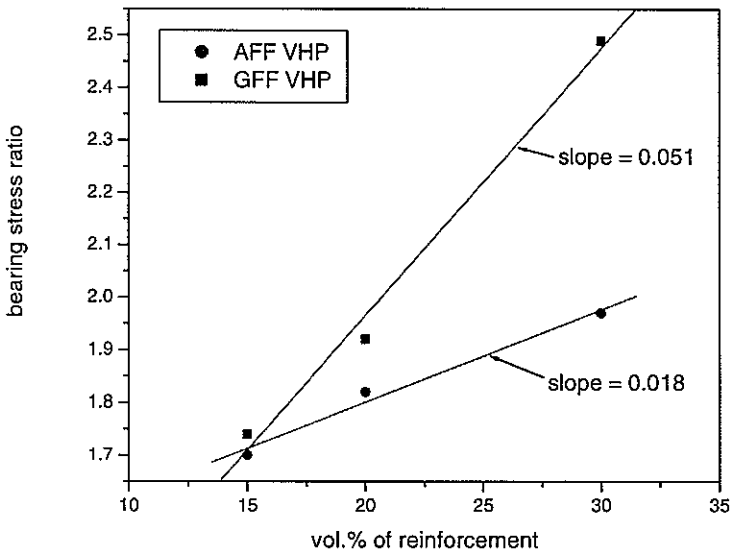

Figure 9. Relationship between bearing stress ratio σ_{Al}/σ_r of composite materials and reinforcement volume fraction.

In our previous studies, many observations were reported of the effect of the metal powder surface chemistry on the sintering kinetics and interface microstructures of sintered powders or consolidated composites [9-12, 14, 15]. These results consistently show that a metal powder with thinner oxide layer and less chemisorbed water on the surface will remarkably

enhance the solid state sintering kinetics and tensile properties of the consolidated materials [9-12, 14, 15]. Therefore, we can also attribute the higher load transfer efficiency of the GFF sample to the initial high purity Al and reinforcement alloy powders with thinner oxide surface layers, which promotes increased bonding strength between the matrix and reinforcement particles.

5. Conclusion

1. Neutron diffraction measurements show that composites consolidated from Al and $Al_{63}Cu_{25}Fe_{12}$ quasicrystal alloy powders have compressive residual stress in the Al matrix. This compressive residual stress may be promoted by the combination of several factors, such as the volume expansion of the reinforcement particles caused by phase transformation of the quasicrystal phase to a lower density crystalline phase and the stiffness mismatch of the matrix and reinforcement phases. The compressive stresses are likely reduced by effects including the ΔCTE between matrix and reinforcement phases and Al diffusion from matrix into the reinforcement particles. Further in-situ neutron diffraction measurement during a consolidation process, e.g. VHP, should be done to resolve the mechanisms of residual stress evolution in the composites.

2. The load partitioning measurements by neutron diffraction show that there is a linear relationship between load bearing stress ratio and particle volume fraction. The GFF composite samples made from "clean" GARS powders with a thin oxide surface layer show significantly higher load transfer efficiency than the composites made from commercially atomized powders. The higher load transfer efficiency in GFF type composites may result from the enhanced inter-particle bonding strength, promoted by the clean interfaces between particles.

Acknowledgements

The authors greatly appreciate the assistance of the Materials Preparation Center of the Ames Laboratory for the CIP and VHP, performed by Mr. Paul Wheelock and SEM studies performed by Mr. Fran Laabs. Also, the assistance the NIST neutron research center is acknowledged for doing the neutron diffraction measurements. Dr. Dan Sordelet provided HIP consolidated bulk $Al_{63}Cu_{25}Fe_{12}$ quasicrystal and Al_7Cu_2Fe alloy samples for density and CTE measurements. The discussions with Dr. S.B.Biner, Dr. Vinay Dayal and Mr. Junfeng Mei are also greatly appreciated. The funding of this project from DOE Basic Energy Sciences under contract number W-7405-Eng-82 is gratefully acknowledged.

References

1. R. J. Arsenault, M. Taya, Acta Metallurgica et Materialia, 35 (1987) 651-659.
2. Z. M. Sun, J. B. Li, Z. G. Wang, W. J. Li, Acta Metallurgica et Materialia, Vol. 40, 1992, p. 2961-2966.
3. N. Shi, B. Wilner, R. J. Arsenault, Acta Metallurgica et Materialia, 40 (1992) 2841-2854.
4. P. J. Withers, Key Engineering Materials, 108-110 (1995) 291-314.
5. G. Albertini, G. Bruno, A. Carrado, F. Fiori, M. Rogante, F. Rustichelli, Measurement Science and Technology, 10 (1999) R56-R73.
6. A. D. Krawitz, Neutron stress measurements in composites, Residual Stresses in Composites, Measurement, Modeling & Effects on Thermo-Mechanical Behavior, Proceedings of a symposium sponsored by the SMD of TMS, Edited by E.V.Barrera and I.Dutta, Denver, Colorado, February 21-25, 1993, p. 161-176.
7. P. J. Withers, A. P. Clarke, Acta Materialia, 46 (1998) 6585-6598.

8. A. J. Allen, M. A. M. Bourke, S. Dawes, M. T. Hutchings, P. J. Withers, Acta Matallurgica et Materialia, 40 (1992) 2361-2373.

9. F. Tang, I. E. Anderson, S. B. Biner, Materials Science and Engineering A, A363 (2003) 20-29.

10. F. Tang, I. E. Anderson, S. B. Biner, J. C. Foley, Tensile properties of pure Al based Al-Cu-Fe quasicrystal reinforced model MMC, Advance in Powder Metallurgy & Particulate Materials 2001, ed. by W. B. Eisen and S. Kassam, Proceedings of the 2001 International Conference on Powder Metallurgy & Particulate Materials, May 13-17, New Orleans, LA, Sponsored by APMI/MPIF, Part 9, p. 12 -25.

11. I. E. Anderson and J.C.Foley, Surface and Interface Analysis, 31 (2001) 599-608.

12. I. E. Anderson, B. K. Lograsso, T. W. Ellis, (Ames Lab, Iowa State University), US Patent No. 5,368,657, Nov. 29, 1994.

13. J. F. Flumerfelt, Aluminum Powder Metallurgy Processing, Ph.D. Thesis, Iowa State University, 1998.

14. F. Tang, I. E. Anderson, Pure Al matrix Composites Produced by Vacuum Hot Pressing: Tensile Properties and Strengthening Mechanisms, submitted to Materials Science and Engineering A.

15. F. Tang, H. Meeks, J. Spowart, I. E. Anderson, Consolidation Effects on Tensile Properties of a Pure Al Matrix Composites, in preparation and to be submitted to Metallurgical and Materials Transaction A.

16. F. Tang, I. E. Anderson, S. B. Biner, Journal of Light Metals, 2 (4) (2002) 201-214.

17. T. Gnäupel-Herold, H. J. Prask, Diffraction Elastic Constants for Arbitrary Specimen and crystal Symmetries: Theory and Practical Consequences, Proceedings of the 6th International Conference on Residual Stresses (ICRS-6), Oxford, July 10-12, 2000, p 243-250.

18. A. M. Korsunsky, A. I. Salimon, I. Pape, A. M. Polyakov, A. N. Fitch, Scripta Materialia, 44 (2001) 217-222.

CHAPTER 7. GENERAL CONCLUSIONS

1. Solid state vacuum sintering was studied in tap densified Al powder and in hot quasi-isostatically forged samples composed of commercial inert gas atomized or high purity Al powder, generated by a gas atomization reaction synthesis technique. The GARS process results in spherical Al powder with a far thinner surface oxide. After vacuum sintering at 525°C for up to 100 hours, SEM results showed that the GARS Al powder achieved significantly advanced sintering stages, compared to the CIGA Al powder. Tensile results from forged samples of the two powder types also showed that although its UTS is lower, 95MPa vs. 147MPa, the ductility of the GARS pure Al sample is higher than that of the CIGA Al sample. The overall results indicated the enhanced ability of GARS-processed Al and Al alloy powders for solid state sintering, which may lead to simplification of current Al powder consolidation processing methods.

2. Elemental Al-based composites reinforced with spherical Al-Cu-Fe alloy powders were produced by quasi-isostatic forging and VHP processing methods. It was proved that spherical Al-Cu-Fe alloy powders can serve as an effective reinforcement particulate for elemental Al-based composites, because of their high hardness and a preferred type of matrix/reinforcement interfacial bonding, with reduced strain concentration around the particles.

3. Microstructures and tensile properties of Al/Al-Cu-Fe composites were characterized. It was found that the quasicrystal phase in the Al-Cu-Fe reinforced particle transformed to ω phase which has a lower density, but similar elastic modulus, CTE and hardness properties as quasicrystalline $Al_{63}Cu_{25}Fe_{12}$. Ultimate tensile strength and yield strength of the composites were increased over the corresponding Al matrix values far beyond typical

observations, probably promoted by a fine reinforcement particle size that matched the matrix powders, an improved spatial distribution of the reinforcements, and an improved interface bond strength between matrix and reinforcement particles. This reinforcement effectiveness is further evidenced by elastic modulus measurements of the composites that are very close to the upper bound predictions of the rule of mixtures.

4. Particle cracking of the reinforcement particulate was a dominant failure mechanism for the composites under tensile loading, implying that there is sufficient interfacial bonding between the reinforcement particles and Al matrix to achieve the full benefit from the reinforcement. It was also observed that Al-Cu-Fe reinforcement particles can be sintered together to form strong agglomerates, unlike typical SiC reinforcement particles

5. Composite samples made from high purity powders show a higher strengthening effect and ductility than the samples made from commercial purity powders, which may result from improved bonding between the high purity powders. Auger surface analysis detected evidence of increased matrix/reinforcement interfacial bonding in the composite sample made from GARS powder by alloy inter-diffusion layer measurements, consistent with the tensile property measurements.

6. By measuring the load partitioning of matrix and reinforcement phases in the composites, using neutron diffraction, and combining this direct strengthening contribution with calculation of the two dislocation strengthening mechanisms, the Y.S. increase of both AFF and GFF composite samples can be predicted quite accurately. This predictive capability is probably aided by our simplified case of elemental Al matrix composite samples without precipitation strengthening and severe strain hardening during consolidation. It appears that a summation of direct and indirect strengthening mechanisms is sufficient to predict accurately the strength of the composites. In a non-

ideal case, porosity in the composites was found to reduce significantly the load transfer capability from reinforcement particles to Al matrix, reducing the strength of the composite material.

7. Neutron diffraction measurements also showed that the composites consolidated from Al and $Al_{63}Cu_{25}Fe_{12}$ quasicrystal alloy powders have compressive residual stress in the Al matrix. However, the composites made by the quasi-isostatic forging process exhibited much higher compressive residual stresses in the Al matrix than the composites made by the VHP process. This compressive residual stress resulted from the combination of several factors, including the volume expansion of the reinforcement particles caused by phase transformation of the quasicrystal phase to a lower density crystalline ω phase and the CTE and stiffness mismatch of the matrix and reinforcement phases. Further in-situ neutron diffraction measurement during consolidation process should be done to resolve the mechanisms of residual stress evolution in the composites.

8. The load partitioning measurements by neutron diffraction show that there is a linear relationship between load bearing stress ratio and reinforcement particle volume fraction. The GFF composite samples made from "clean" GARS powders with a thin oxide surface layer show significantly higher load transfer efficiency than the composites made from commercially atomized powders. The higher load transfer efficiency in GFF type composites may result from the enhanced inter-particle bonding strength, promoted by the clean interfaces between particles.

9. The effect of consolidation techniques, including quasi-isostatic forging and VHP, was studied. As shown by quantitative analysis of the reinforcement particle spatial distribution in all composite material samples for a wide range of length scales, the high level of reinforcement particle dispersion was almost the same in the forged and VHP

samples. Therefore, the significant tensile strength differences between forged and VHP composite samples may not result from any minor particle spatial distribution differences. Compressive residual stresses formed in the Al/Al-Cu-Fe alloy composite materials during consolidation can be very beneficial to the tensile properties. The high strain rate and short processing time of quasi-isostatic forging probably were responsible for higher compressive residual stresses in the Al matrix and, presumably, a higher dislocation density than VHP processed materials. After annealing for about the same time as the duration of the VHP process, the tensile strengths of a forged composite sample were reduced to the same strength level as that of the VHP composite samples. Relief of the compressive residual stresses was verified after annealing in the forged samples. The compressive residual stresses in the Al matrix may be beneficial to the fatigue behavior of the composites, which should be studied in further experiments.

ACKNOWLEDGMENTS

I would like to thank my wife and family for their encouragement and support during my study at Iowa State University. I also want to express my sincere thanks to my major professor, Dr. Iver Anderson, whose wisdom, advice, discussion and encouragement helps me all along my research and study. Dr. Bulent Biner, my associate major professor, and Dr. James Foley are also thanked for their valuable insight and discussions.

I would also like to give my special thanks to Mr. Henry Meeks at Ceracon Inc., Dr. Jonathan Spowart at UES Inc. and Air Force Research Lab, Dr. Thomas Gnaupel-Herold and Dr. Henry (Hank) Prask at NIST Neutron Research Center for their kind help and discussion during my research.

I would also like to thank lots of the staff members and scientists at Ames Lab, who helped me in all aspects of my research. To just name a few, I am grateful to Bob Terpestra, Fran Laabs, Hal Sailsbury, Lanny Lincoln, Paul Wheelock, Arne Swanson, Dan Barnard, Jim Anderegg, the machine shop crew, Kevin Dennis, Joel Harringa, Matt Besser, Dr. Dan Sordelet, Stacy Scott, Alexandria Percharsky, Dennis Sailsbury, Ann Coffman, Susan Elsner, and Larry Jones.

The research project was funded by the Materials Science Division of DOE-BES under the contract number W-7405-Eng-82. The United States Government has assigned DOE report number IS-T-1983 to this thesis.